An Electrochemical Neutralization Cell to Harvest the Water Formation Energy

विद्या वाचस्पति की

उपाधि की अपेक्षाओं की आंशिक पूर्ति में प्रस्तुत शोध प्रबंध

A thesis submitted in partial fulfillment of the requirements of the degree of Doctor of Philosophy

द्वारा / By

ऋत्विक मंडल / Ritwik Mondal

पंजीकरण सं. / Registration No.:

20182012

शोध प्रबंध पर्यवेक्षक / Thesis Supervisor:

Prof. Muhammed Musthafa O. T.

भारतीय विज्ञान शिक्षा एवं अनुसंधान संस्थान पुणे

INDIAN INSTITUTE OF SCIENCE EDUCATION AND RESEARCH PUNE

2024

Dedicated to my

beloved parents

& animes

INDIAN INSTITUTE OF SCIENCE EDUCATION AND RESEARCH, PUNE
[An Autonomous Institution under MHRD, Government of India]

Prof. Musthafa Ottakam Thotiyl
Associate Professor
Chemistry Division and
Centre for Energy Science

Tel: +91-20-25908261
E-mail: musthafa@iiserpune.ac.in/
musthafa@acads.iiserpune.ac.in
Web: http://www.iiserpune.ac.in/~musthafa/

IISER PUNE

Main Academic Building,
Dr Homi Bhabha Road
Pashan, Pune- 411008
www.iiserpune.ac.in

CERTIFICATE

Certified that the work incorporated in the thesis entitled "**An Electrochemical Neutralization Cell to Harvest the Water Formation Energy**" Submitted by **Mr. Ritwik Mondal** was carried out by the candidate, under my supervision. The work presented here or any part of it has not been included in any other thesis submitted previously for the award of any degree or diploma from any other University or institution.

Dr. Muhammed Musthafa O. T.
Department of Chemistry,
IISER Pune

Date: 20th December 2024

Declaration by Student

Name of Student: **Ritwik Mondal**

Reg. No.: **20182012**

Thesis Supervisor(s): **Muhammed Musthafa O. T.**

Department: **Chemistry**

Date of joining program: **01/08/2018**

Date of Pre-Synopsis Seminar: **29/07/2024**

Title of Thesis: **An Electrochemical Neutralization Cell to Harvest the Water Formation Energy**

I declare that this written submission represents my idea in my own words and where others' ideas have been included; I have adequately cited and referenced the original sources. I declare that I have acknowledged collaborative work and discussions wherever such work has been included. I also declare that I have adhered to all principles of academic honesty and integrity and have not misrepresented or fabricated or falsified any idea/data/fact/source in my submission. I understand that violation of the above will be cause for disciplinary action by the Institute and can also evoke penal action from the sources which have thus not been properly cited or from whom proper permission has not been taken when needed.

The work reported in this thesis is the original work done by me under the guidance of

Prof. **Muhammed Musthafa O. T.**

Date: **20/12/2024**

Signature of the student

ACKNOWLEDGEMENTS

The long journey of my doctoral thesis was made possible through the invaluable guidance and support extended by many individuals. While my deepest gratitude extends to everyone who contributed to this achievement, I would like to express special thanks to a select group who played key roles in making this vision a reality**.**

Firstly, I extend my heartfelt gratitude to my supervisor, Prof. Muhammed Musthafa O. T., for his continuous support and guidance throughout my Ph.D. journey. His excellent lab facilities and intellectual work environment, coupled with the freedom to pursue various projects, have been invaluable. I deeply appreciate his scientific insights, patient mentorship, and constructive feedback, all of which have shaped me into an independent thinker. His emphasis on technical expertise and scientific integrity, conveyed through personal and group meetings and informal discussions, has played a crucial role in my growth as a researcher and a responsible individual.

I also express my deepest gratitude and respect to my RAC members, Prof. Partha Hazra from IISER Pune and Prof S.B. Sukumaran from NCL Pune, for their continuous support and scientific inputs during my PhD journey, particularly in RAC meetings.

I express my deepest gratitude to the previous Director, Prof. Jayant Udgaonkar, and present Director, Prof. Sunil Bhagwat, for fostering a vibrant academic environment and offering upgraded facilities and a strong research infrastructure at the institute. I sincerely thank the past chair, Prof. H. N. Gopi, and the present chair, Prof. Nirmalya Ballav, of the chemistry department. I am also thankful to IISER Pune MHRD for awarding me the Ph.D. fellowship over my long journey. I am deeply moved by the support of the faculty members of the chemistry and physics departments for providing access to various instrument facilities in their labs.

This journey would not have been possible without the steadfast support and intellectual interactions of my past and present lab mates. I cherish the scientific and non-scientific discussions (especially at teatime or group dinners) with them. Firstly, I want to thank my seniors, Dr. Alagar, Dr. Manu, Dr. Zahid, Dr. Soumodip, Dr. Neethu and Dr. Sanchayita. Special notes go to my labmates Bhoj, Hemanga, Shyaam, Rahul, Muskan, Shifali, Hitesh, Suhail, Akshay, and Abhishek for producing a healthy and enjoyable lab environment. I want to express deep gratitude to Dr. Ravikumar Thimmappa for experimentally supporting my research. I am truly grateful to the technical, academic, library, housekeeping, and IT staff for their commendable services.

The constant presence of my college friends brought vibrant color and joy to this research journey. I also want to cordially thank my loving parents (Baba and Maa) and close family members (my cousins Riju and Apurba) for their unwavering love and encouragement throughout my integrated PhD career. Though some friends and colleagues may have been unintentionally left out, I sincerely acknowledge their collective contributions throughout my time at IISER Pune.

Table of Contents

Synopsis of the thesis entitled "An Electrochemical Neutralization Cell to Harvest the Water Formation Energy"

A clean transition towards the hydrogen economy from the carbon economy is inevitable due to the current state of the global energy landscape, which is grappling with a severe crisis due to growing energy demands driven by exponential population and economic growth. The widespread of a sustainable hydrogen economy is facing hurdles like high energy requirements in the major stages of hydrogen economy like hydrogen production, hydrogen purification, hydrogen utilization etc. In this scenario, harvesting the electrochemical water formation energy in an acid-alkali decoupled system provides significant energy and voltage benefits in driving electrochemical reactions in various electrochemical energy conversion devices. Although the water formation energy has substantial thermodynamic and technological prospects, the non-redox nature of this water formation reaction is barricading the electrochemical harnessing of this energy for several purposes. In this regard, the principal aim of this thesis is the electrochemical harvesting of water formation energy as an electromotive force in an acid-alkali decoupled architecture for electrochemical process modulations.

The first chapter focuses on the need for innovative green energy solutions to advance the hydrogen economy. The shift towards a robust hydrogen economy is significantly challenged because most of the industrially produced H_2 fuel streams contain carbonaceous and non-carbonaceous impurities beyond the tolerance level of a fuel cell. Often, state-of-the-art purification methods are extremely energy-intensive, requiring extreme temperatures and pressures. To address these critical energy issues, this chapter highlights the possibilities of directly harnessing the energy released during water formation as an electrochemical driving force. This naturally non-redox and exothermic reaction, with a reaction voltage of approximately 0.82 V, can be harvested as an EMF through hydrogen redox. This offers a thermodynamically and technologically viable solution for hydrogen fuel purification, spontaneous heavy hydrogen production, low-grade heat harvesting, etc.

The second chapter explores a method to extract this energy of water formation by utilizing hydrogen redox reactions using a decoupled acid-alkali configuration. The process involves the pH-dependent hydrogen redox at the alkaline anode and the acidic

cathode, respectively, enabling the harnessing of water formation energy as electrical potential. The electrochemical performance metrics of the water formation cell heavily depends on the pH gradient and the amount of hydrogen supply to the anolyte. Furthermore, employing a temperature gradient in this acid-alkali decoupled architecture makes it a thermogalvanic device, due to its positive entropy change of the neutralization pathway. The electrical power output can be enhanced by introducing a temperature

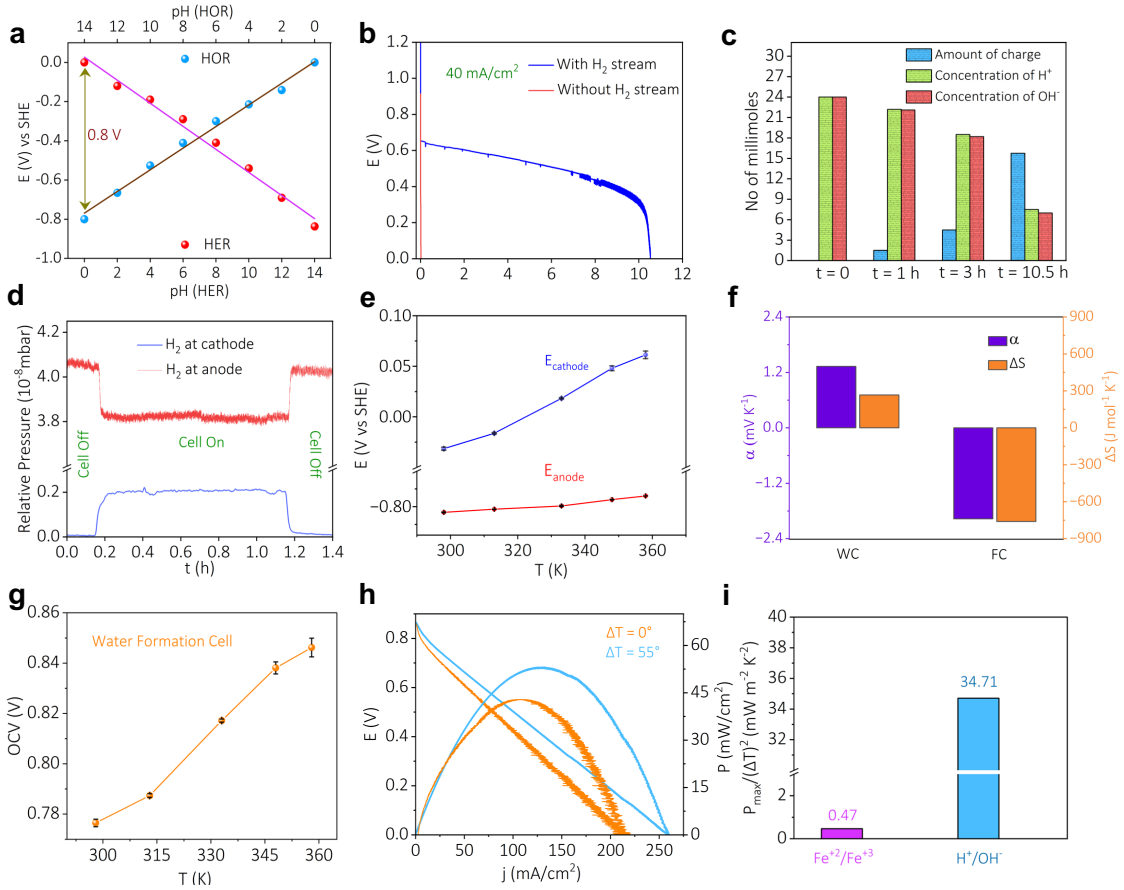

Figure 1: (a) Pourbaix diagrams for HER and HOR reactions. (b) Galvanostatic polarizations at a constant current density of 40 mA/cm^2 with and without H_2 gas as an anodic feed stream. (c) Correlation between the charge passed and the remaining amount of H^+/OH^- dual ion concentration in the half cells during the long-term discharge without H_2 as feed gas stream (10 mL/min). (d) In situ electrochemical mass spectrometry of cathodic half and anodic half of the water formation cell. (e) The variation of the potential of hydrogen redox in acidic (blue trace) and alkaline half-cells (red trace) with respect to surrounding temperature. The temperature dependency of open circuit voltage for (f) the water formation cell (g) The comparison of the Seebeck coefficient and partial molar entropy change between the water formation cell (WC) and the H_2-O_2 fuel cell (FC).(h) Polarisation curves with and without temperature gradient ($\Delta T = 55^0$) between the two half cells of the water formation cell. (i) Comparison of the temperature-insensitive maximum power density between the water formation-based (H^+/OH^-) and ferrocyanide/ferricyanide (Fe^{2+}/Fe^{3+}) redox-based thermogalvanic system.

gradient as well as a pH gradient between the two half cells of the water formation energy harvesting device, as shown in Figure 1.

The third chapter showcases the purification of impure hydrogen fuel streams during electricity generation under ambient conditions by harnessing water-formation energy. Unlike conventional energy-intensive hydrogen purification techniques, this approach purifies impure hydrogen fuel streams from binary and quaternary impure mixtures in a single step during electricity generation, and the purification is affected under ambient weather conditions. In situ electrochemical mass spectrometry substantiates the consumption of hydrogen from the impure stream at the anode and the production of extremely pure hydrogen fuel at the cathode of the fuel purifier. Electrochemical polarisation, chronopotentiometry, and quantification of pure hydrogen confirm the viability of the hydrogen fuel purifier, Figure 2. This device achieves hydrogen purity of approximately 99.9% in a single step, requiring around 24 kJ of energy input while delivering about 90 kJ of electrical energy output per mole of purified hydrogen.

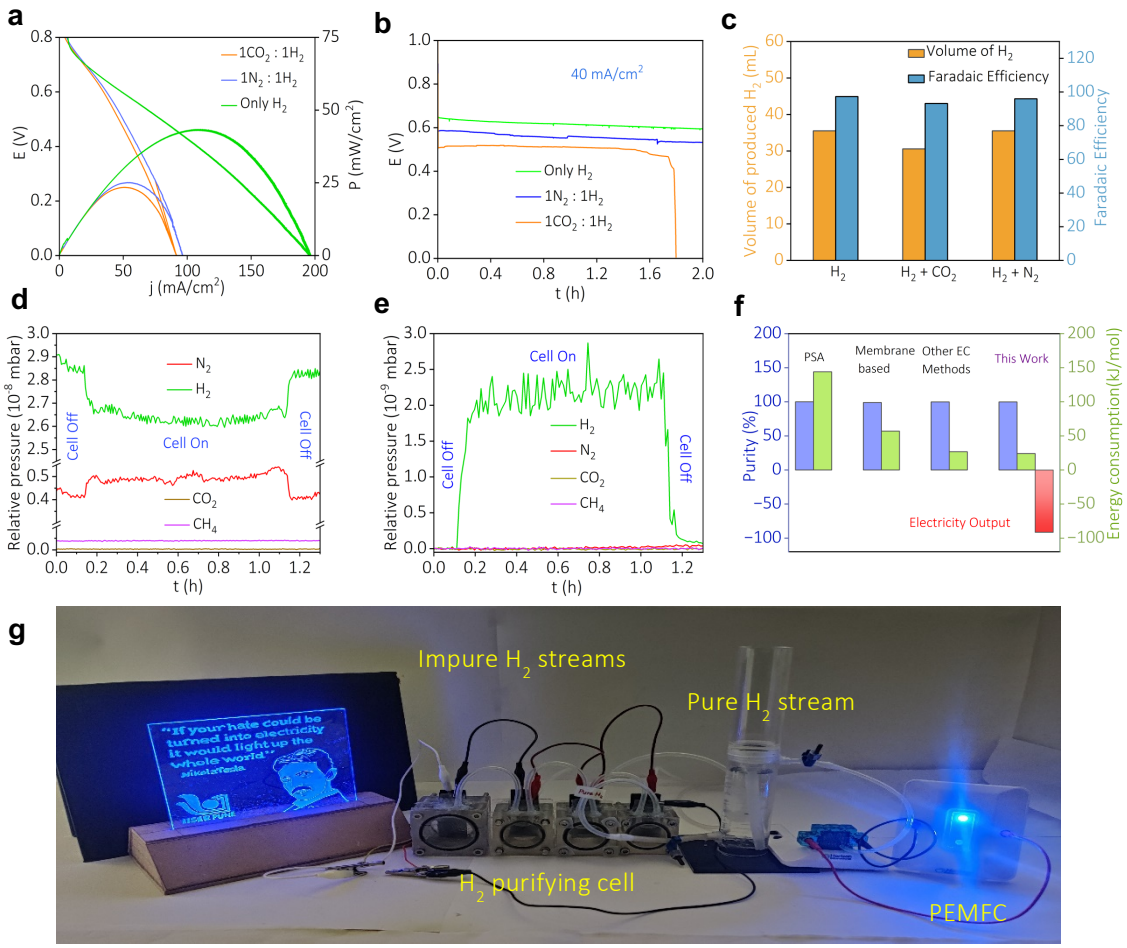

Figure 2: (a) Polarization curves for H_2 purifier with pure and impure H_2 gas feed streams (10 mL/min). (b) Galvanostatic polarizations at a constant current density of 40 mA/cm^2 with pure and impure H_2 gas feed streams. The impure gas streams were H_2-CO_2 (1:1) gas mixture and H_2-N_2 (1:1) gas mixture. (c) Volume of H_2 and Faradaic efficiency with pure and impure hydrogen gas feed streams. In-situ electrochemical mass spectra for (d) the anodic half-cell and (e) the cathodic half-cell with crude H_2 gas mixture as anodic feed gas stream (CO_2: CH_4: N_2: H_2 = 20: 1: 4: 75). (f) The energy consumption and the purity of produced H_2 for the spontaneous fuel purifier compared with the state-of-the-art fuel purification processes. (g) Photograph demonstrating spontaneous fuel purifier directly serving as a fuel reservoir for a commercial PEMFC.

The fourth chapter emphasizes the removal of electrocatalyst-poisoning impurities such as carbon monoxide and hydrogen sulfide from impure hydrogen fuel streams under ambient conditions. By harnessing water formation energy as electrical power, these impurities can be removed in a single step at room temperature and pressure using non-precious and poison-tolerant electrocatalysts, which in turn enhances the durability of the fuel purifier and lowers the overall cost of hydrogen purification. This chapter also

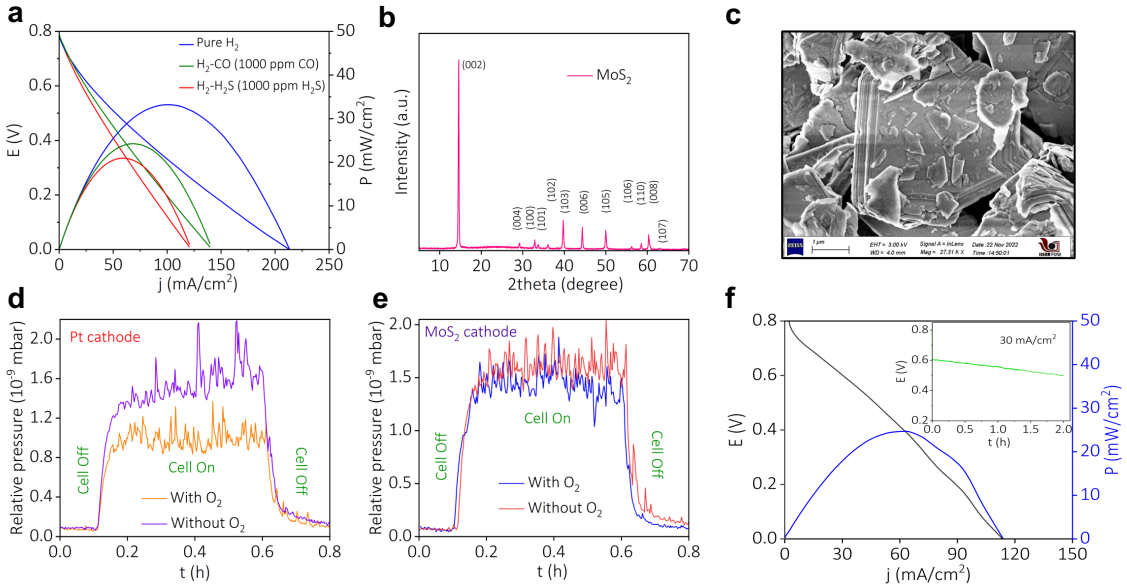

Figure 3: (a) Polarization curves for fuel purifier with Pt-Ru/C as anodic electrocatalyst. Pure H_2, H_2-H_2S (1000 ppm H_2S), and H_2-CO (1000 ppm CO) binary mixtures are used as anodic feed gas streams. (b) XRD, (c) SEM image of as-synthesized MoS_2. In-situ electrochemical mass spectra of the cathodic half-cell of the fuel purifier with (d) Pt (e) MoS_2 as the cathodic electrocatalyst in the presence and absence of oxygen. (f) The polarization curve of the Pt-free fuel purifier equipped with Ni/C as anodic electrocatalyst and MoS_2/rGO as the cathodic electrocatalyst. The inset shows the galvanostatic polarization when a current of 30 mA/cm^2 is drawn from the Pt-free fuel purifier.

discusses the viability of this fuel purifier under open-air conditions in a precious metal-free architecture, Figure 3.

The fifth chapter illustrates a method for spontaneous electrochemical heavy hydrogen generation by utilizing the energy of heavy water formation under ambient temperature and pressure. The decoupled heavy acid-alkali configuration provides an electrochemical driving force for the evolution of heavy hydrogen (D_2) in a thermodynamically downhill manner. This chapter discusses the electrochemical isotopic effect between the heavy hydrogen and light hydrogen redox reactions. In situ electrochemical mass spectra corroborate the heavy hydrogen production at the cost of light hydrogen, Figure 4. This exergonic electrochemical process produces approximately 357 mL of D_2 over nearly 85 hours of continuous electrolysis, yielding an electrical energy output of 122 kJ per mole of D_2.

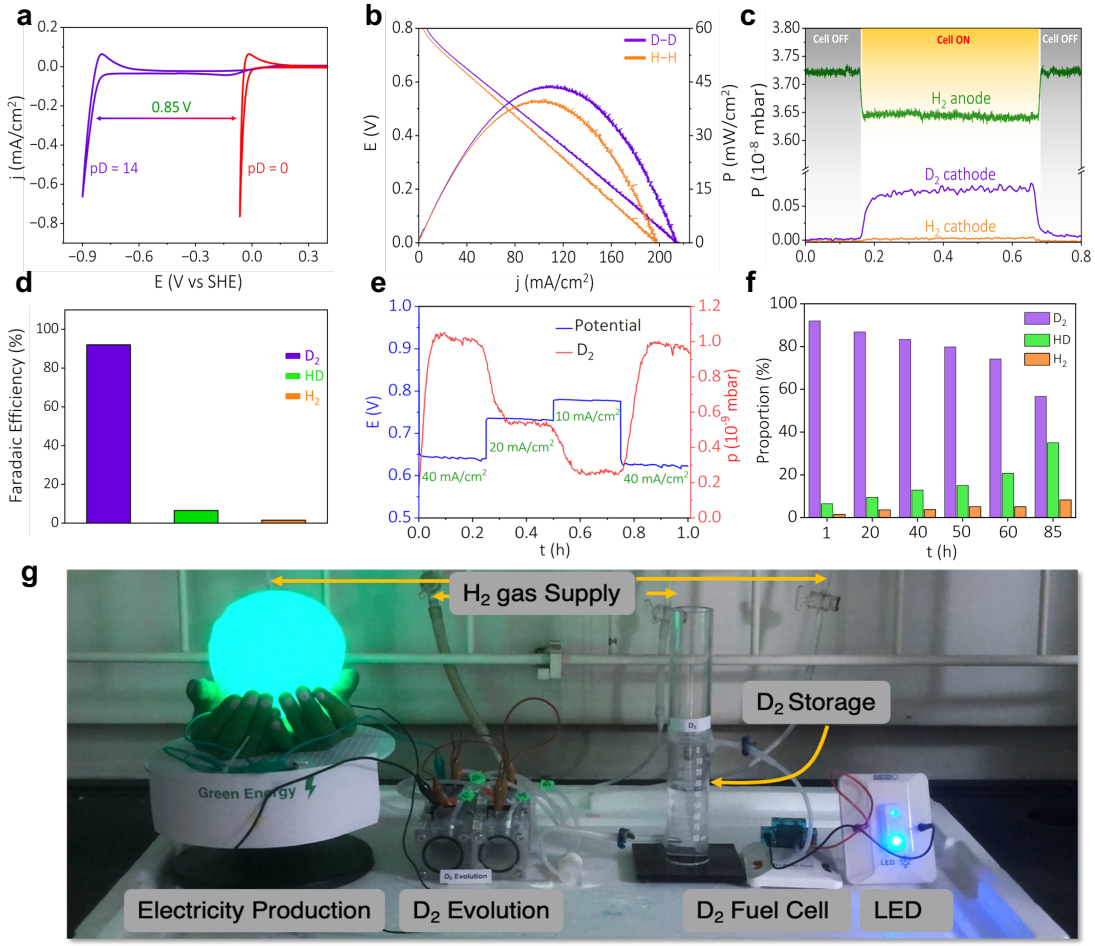

Figure 4: (a) The accessible potential difference available based on the gradients in dual ions concentration (pD gradients) between the electrolytes. (b) Polarisation curves for the two-compartment device with NaOH-H_2SO_4 (orange trace) and NaOD-D_2SO_4 (violet trace) dual electrolyte systems. (c) In-situ electrochemical mass spectra for the device NaOD-D_2SO_4 dual electrolytes. (d) In-situ electrochemical mass spectra for the device with a) NaOH-H_2SO_4 dual electrolytes and b) NaOD-D_2SO_4 dual electrolytes. (e) In situ electrochemical mass spectrum during chronopotentiometry staircase test of the spontaneous heavy hydrogen generator. (f) The proportions of D_2, HD, and H_2 in the cathodic exhaust of the heavy hydrogen generator at various stages of the long-term operation. (g) Photograph demonstrating spontaneous electrochemical deuterium generator directly serving as a D_2 reservoir for a D_2 air fuel generator.

The sixth chapter provides a summary (Figure 5) and a future outlook of the thesis.

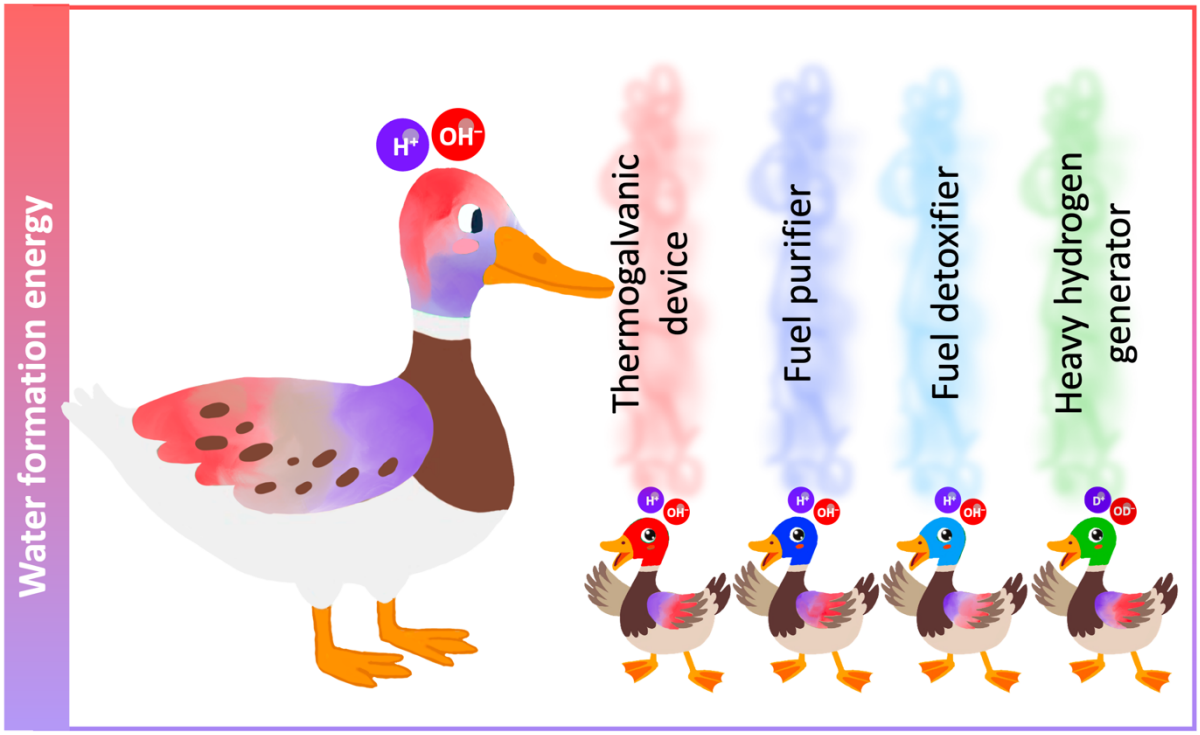

Figure 5: Water formation energy for electrochemical process modulation.

Chapter 1

Introduction

1.1 Current Energy Scenario

The global energy landscape is defined by a blend of challenges and transitions and the need to balance energy sustainability and affordability.[1-4] The energy scenario has a strong -and direct connection with the worldwide economy, population, and their various requirements for several forms of energy.[5,6] With the exponential increment in the global population and economic growth, the current global energy scenario faces a severe crisis towards these growing energy demands.[7-10] The daily average energy consumption is around 57.6 kWh per person (2022). With approximately 8.2 billion people around the globe, the cumulative energy demand or energy consumption will be a scary and gigantic figure.[11,12] This energy economy is predominantly governed (around 80 %) by fossil fuels or non-renewable energy sources (petroleum, oils, coal, and natural gases).[13,14] The rapid depletion of fossil fuel sources and the environmental pollution caused by it leads to a transition towards renewable energies to fulfill the ongoing energy demands.[15-17] Renewable energies have the upper hand over fossil fuels with adequate resources and green nature.[18] These energy dynamics lead to a carbon-neutral, eco-friendly energy economy due to zero-emission technology.[19] Renewable energy stocks can be sustainable alternatives like solar, wind, biomass, geothermal, hydroelectric energy, etc.[20-22] These renewable sources offer cleaner and eco-friendly energy but harnessing them efficiently presents challenges.[18-22] For example, the Earth receives an immense amount of solar energy, but developing materials to fully capture it remains a complex issue.[23] All these energy stocks are more likely converted to electrical energy, the most flexible form of energy, which can be used to drive electrical utilities or electrochemical energy storage and conversion devices.[24-26] However, these renewable energies have drawbacks like intermittency, lack of mobility and storage, etc.[27,28] In the current world, we are covered by a blanket of utilities and equipment run via electricity, so the demand for electricity is soaring very high. In these aspects, fuel cells are one of the significant energy conversion devices that can convert chemical energy from fuel to electrical energy.[29,30] Hydrogen fuel cells have drawn a lot of attention in the current energy scenario because of their easy conversion, storage, and transportation, which leads to a robust hydrogen economy.[31-35]

1.2 Hydrogen

Hydrogen (H) is the most abundant element in the universe.[36,37] Hydrogen (Protium, ^{1}H) consists of one proton at the core nucleus, surrounded by one electron. Hydrogen (H) has a total of three isotopes: protium or light hydrogen (^{1}H), deuterium or heavy hydrogen (^{2}H or D), and tritium (^{3}H or T), Figure 1.1.[38]

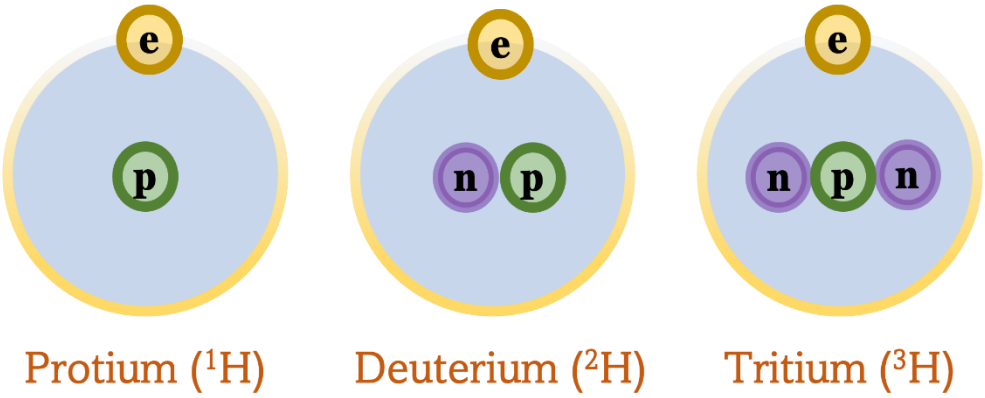

Figure 1.1: Isotopes of hydrogen.

Deuterium has one extra neutron at its nucleus as compared to protium. Tritium, the radioactive isotope of hydrogen with a lifetime of around 12 years, has two neutrons, one proton, and one electron.[39] Hydrogen (^{1}H) is a colorless, odorless, and tasteless gas found as a diatomic molecule at room temperature.[40,41] At 25°C, hydrogen's solubility in water is about 7.79×10^{-4} mol/L. Hydrogen (^{1}H) has a very low density of 0.08988 g/L, which makes it 14 times lighter than air.[42,43] Apart from these physical properties, hydrogen can act as an excellent energy carrier or fuel because it will form only water (H_2O) upon oxidation instead of greenhouse gases.[44] Hydrogen (^{1}H) offers a very high gravimetric energy density of 120 MJ/kg at 25°C, which is even 3 times higher than gasoline.[45] To address the growing energy crisis and inconsiderate pollution, the hydrogen economy becomes a crucial alternative with a near-zero carbon footprint.[46] It is to be noted that hydrogen redox, like hydrogen evolution and hydrogen oxidation, are quintessential aspects of a robust hydrogen economy.[47]

1.3 Hydrogen Economy

The hydrogen (H_2) economy mainly consists of the utilization, production, purification, storage, and transportation of hydrogen (H_2), with the most important steps being production, purification, and utilization.[48-51] This vision evolves as H_2 becomes a clean energy carrier involved in technological growth and innovative infrastructures in various

sectors like industry, transportation, etc.[52-54] With a substantial gravimetric energy density value, H_2 has the potential to be an ideal green energy carrier.[45,55] It is often called the fuel of the future due to its high conversion rate and long-term storage options.[53] Renewable energies can also be integrated into the hydrogen economy to produce green hydrogen.[56] Due to the limited options for fossil fuels, hydrogen is directing the energy economy for the near-future energy landscape.[50-53]

1.3.1 Hydrogen Utilization

One of the key portions of the hydrogen (H_2) economy is hydrogen utilization or the demand for hydrogen in various sectors.[52] Hydrogen can be utilized in hydrogen fuel cells, transportation (fuel cell electric vehicles), energy storage, chemical sectors, industrial heating, etc.[51-54] Intermittent renewable energies can be stored as H_2 for future utilization or transportation. H_2 can power the electric motor of fuel cell electric vehicles (FCEV) by producing electricity in an $H_2 - O_2$ fuel cell.[35]

1.3.2 Fuel Cells

Fuel cells are electrochemical energy conversion devices that directly convert the chemical energy of fuels into electrical energy.[31-33] Sir William Robert Grove, a Welsh inventor and physicist, invented the first fuel cell around the year 1839.[57] He termed his device a "gas battery" because it was propelled by combining hydrogen and oxygen gases in the presence of an electrolyte to produce electricity.[58,59] Ludwig Mond and Charles Langer, in 1889, attempted to create a functional fuel cell, followed by William White Jaques.[50] In 1959, Francis T. Bacon demonstrated a five-kilowatt fuel cell known as the "Bacon Cell".[60,61] There are various types of fuel cells like alkaline fuel cells (AFC), solid oxide fuel cells, polymer electrolyte membrane fuel cells (PEMFC), direct alcohol fuel cells (DAFC), and molten carbonate fuel cells, etc, which are differentiated based on their electrolyte type and operating conditions.[62] Fuel cells have two half-cells connected with an external circuit and separated via an ion exchange membrane.[32] Among them, hydrogen fuel cells (HFC) hold significant promise in decarbonizing the industrial energy and transportation sector.[33]

1.3.3 Hydrogen Fuel Cells

A commercial hydrogen fuel cell (HFC) is a type of polymer electrolyte membrane fuel cell (PEMFC), which is also known as a proton exchange membrane fuel cell.[63,64] It mainly consists of a hydrogen anode, an oxygen cathode, and a proton exchange membrane to separate them, Figure 1.2.[65]

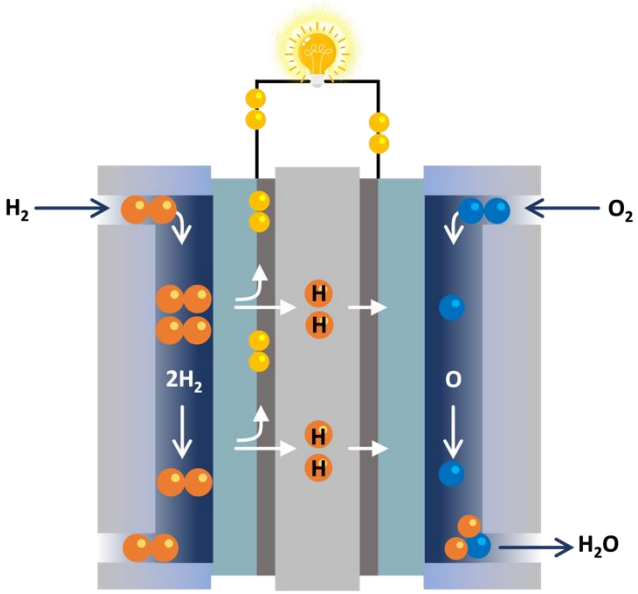

Figure 1.2: Schematic of hydrogen fuel cell.

Hydrogen gas and oxygen gas are used as the fuels for HFC.[66] On the anodic electrocatalyst, hydrogen oxidation occurs (eq 1.1) to form protons (H^+) by releasing electrons.[33] These electrons pass through the external circuit by powering the external load to the cathodic half of the fuel cell. In the cathodic electrocatalyst, these electrons are accepted by oxygen to form water (eq 1.2). These two half-cells are separated by a proton-exchange membrane, which conducts protons during the redox reactions. This device exhausts heat and water molecules, which is evident from the overall cell reaction (eq 1.3).[33]

Anodic half-cell reaction:

$$4H^+ + 4e^- \leftrightarrow 2H_2 \qquad E^0 = 0\ V \qquad \text{(eq 1.1)}$$

Cathodic half-cell reaction:

$$O_2 + 4H^+ + 4e^- \leftrightarrow 2H_2O \qquad E^0 = 1.23\ V \qquad \text{(eq 1.2)}$$

Overall cell reaction:

$$2H_2 + O_2 \leftrightarrow 2H_2O \qquad E^0_{cell} = 1.23\ V \qquad \text{(eq 1.3)}$$

The open circuit potential of a commercial hydrogen fuel cell is around 1.23 V, which can generate kilowatt-level power density along with current density in the ampere range.[67,68] The benchmark electrocatalysts for hydrogen fuel cells are platinum-based electrocatalysts, capable of catalyzing hydrogen oxidation reaction (HOR) and oxygen reduction reaction (ORR).[69-71] Despite being a clean and portable energy source, it has some drawbacks, like precious electrocatalysts and a supply of very pure hydrogen.[72] The anodic feed impurities should not exceed the tolerance level (5 ppb to 1 ppm) of commercial hydrogen fuel cells.[73-76] If the impurity exceeds the tolerance level of an HFC, the electrocatalysts can be poisoned, and overall performance efficiency will be drastically hampered.[74,75] In order to maintain the electrical power delivery of a hydrogen fuel cell, around 99.99% of pure hydrogen fuel is required as the anodic feed for a commercial hydrogen fuel cell.[78] For the long-term operational durability of an HFC, the industrially produced hydrogen must be purified to match the tolerance level of the hydrogen fuel cell.

1.3.4 Hydrogen Production

To maintain a robust hydrogen economy, there must be secured production or supply of hydrogen to meet the growing demand for hydrogen.[49,50] Hydrogen is the most abundant element in the universe but does not exist in its pure form on Earth.[36]

Industrially, steam-reforming of methane gas produces H_2 with a carbon dioxide byproduct.[79,80] The natural gas (methane, CH_4) reacts with steam at high temperatures (700°C–1,000°C) in the presence of a catalyst (nickel or platinum) to produce hydrogen (H_2), carbon monoxide, and a small amount of carbon dioxide (eq 1.4).[79-81] The carbon monoxide is then reacted with steam in a second step, called the water-gas shift reaction (eq 1.5), to produce additional hydrogen and carbon dioxide.[82] Blue or grey hydrogen can be produced via this method.

Steam methane reformation

$$CH_4 + H_2O \rightarrow CO + 3H_2 \qquad \text{(eq 1.4)}$$

Water-gas shift reaction

$$CO + H_2O \rightarrow CO_2 + H_2 \qquad \text{(eq 1.5)}$$

Coal gasification is one of the methods to produce H_2, where coal reacts with oxygen and steam at high temperatures to produce a gas mixture called syngas.[83-85] Syngas is a mixture of hydrogen, carbon monoxide, methane, and carbon dioxide when the proportion of H_2 is around 30 %.[86] Black or brown hydrogen is generated at the end of this method.

Biomass gasification involves breaking down biomass such as agricultural waste, forest waste, or other bio-bodies at very high temperatures with oxygen or steam.[87,88] This also produces syngas, which can be purified to extract hydrogen.[89] This method leads to grey or blue hydrogen.

Thermochemical water splitting is one of the processes that generate hydrogen. This process uses high-temperature heat to perform chemical reactions that cause water splitting to form hydrogen and oxygen.[90] If the driving force for the chemical reaction is driven by nuclear reaction, then the produced hydrogen is called pink hydrogen.[91]

In the partial oxidation method, several types of hydrocarbons, such as natural gas, petroleum, etc, are reacted with oxygen to produce hydrogen and carbon monoxide. High temperature is not required.[92,93] The hydrogen produced by this method is called blue hydrogen.

In the methane pyrolysis method, methane is heated at around 1,500°C in the absence of oxygen, producing hydrogen gas and solid carbon (typically in the form of carbon black).[94,95] This process does not emit any greenhouse gases. This type of hydrogen is called turquoise hydrogen.[96]

Electrochemical water splitting is one of the green methods to produce hydrogen and oxygen.[97-99] This hydrogen is also called green if the electrical driving force is derived from renewable resources.[41,100] It utilizes electricity to split the water into fuel. This electricity can be generated via renewable energy (solar energy, wind energy, etc) stocks.[101] Hydrogen is classified into various colors based on its production process, as illustrated in Figure 1.3. As noted before, hydrogen redox, including hydrogen evolution reaction and hydrogen oxidation reaction, are essential reactions involved during the hydrogen production stage and utilization stage, respectively, in corresponding electrochemical devices.[102]

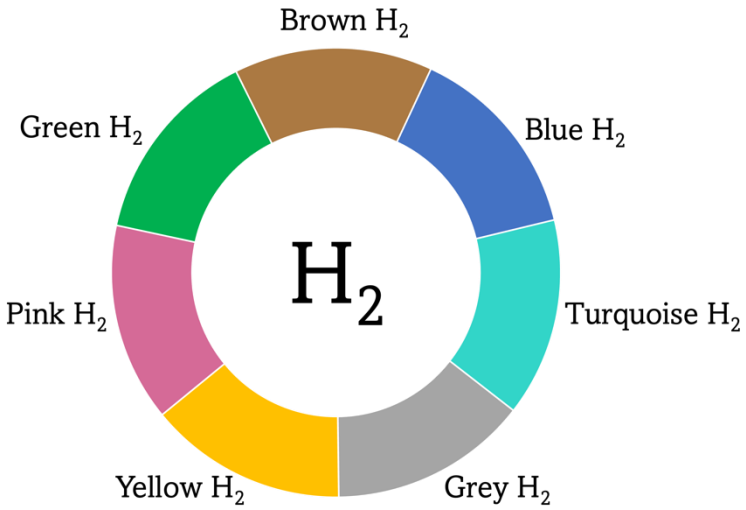

Figure 1.3: Hydrogen color spectrum.

1.4 Hydrogen Redox

Hydrogen redox mainly consists of hydrogen oxidation reaction (HOR) and hydrogen evolution reaction (HER). Hydrogen redox is the pillar of the hydrogen economy.

1.4.1 Hydrogen Oxidation Reaction

Hydrogen oxidation reaction (HOR) is one of the main pillars of a robust hydrogen economy. This reaction leads to the release of electrons, which is essential for power generation in a fuel cell.[103] Hydrogen fuel is oxidized at the anode of a hydrogen fuel cell to form protons, leading to the liberation of electrons (eq 1.6), which will be accepted by oxygen molecules at the cathode.[104]

$$H_2 \leftrightarrow 2H^+ + 2e^- \qquad \text{(eq 1.6)}$$

This HOR is a pH-dependent reaction, and the hydrogen oxidation reaction is more facile in acidic electrolytes.[105] The benchmark electrocatalysts for hydrogen oxidation reaction are majorly precious metal-based electrocatalysts.[106-111] Platinum (Pt) is the most widely used and highly efficient electrocatalyst for the hydrogen oxidation reaction, known for its exceptional catalytic performance, especially in acidic conditions.[112,113] It effectively adsorbs hydrogen molecules, aiding their breakdown into protons and electrons. However, platinum is both scarce and costly, and its efficiency can be compromised by impurities like carbon monoxide (CO), which can poison the catalyst by occupying its

active sites.[114,115] There are other metals like palladium (Pd), ruthenium (Ru), nickel (Ni), and Pt-Ru alloys, etc which can be utilized as electrocatalysts for hydrogen oxidation reactions.[106-111] The reaction mechanism of the HOR is defined by the adsorption and dissociation of hydrogen molecules on the surface of the electrocatalyst.[116] A highly efficient commercial hydrogen fuel cell is governed by how quickly and efficiently the catalyst can adsorb, dissociate, and oxidize hydrogen molecules to release electrons. In this respect, platinum stands out as a benchmark electrocatalyst for HOR as it has a strong hydrogen atom binding, as well as a rapid dissociation of hydrogen atoms from the surface.[110,112,113] Very strong hydrogen binding and a sluggish rate of dissociation of hydrogen from the surface of the electrocatalyst can hinder the hydrogen oxidation reaction kinetics.[116,117] The required potential for the hydrogen oxidation reaction is approximately 0 V with respect to the reversible hydrogen electrode (RHE) under standard conditions and pH = 0. From a pragmatic point of view, overpotentials are required, such as extra voltage, to run the reaction. For a certain electrocatalyst, the magnitude of overpotential for a reaction is different, and lower overpotentials are desirable to improve the overall efficiency of the fuel cell.

1.4.2 Hydrogen Evolution Reaction

Hydrogen evolution reaction (HER) is one of the pivotal electrochemical reactions in principle. The green hydrogen is mainly produced by an electrochemical hydrogen evolution reaction in an electrolyzer.[97,98] In a renewable energy economy, hydrogen gas is the means to store renewable energy for future utilization. Proton (H^+) or water molecules get reduced to form hydrogen (H_2) gas via accepting electrons, (eq 1.7,1.8). This reaction heavily depends on the pH of the electrolyte or the concentration of protons in the solution.[105]

Acidic media

$$2H^+ + 2e^- \leftrightarrow H_2 \qquad \text{(eq 1.7)}$$

Alkaline media

$$2H_2O + 2e^- \leftrightarrow H_2 + 2OH^- \qquad \text{(eq 1.8)}$$

Hydrogen evolution reactions can be catalyzed by various electrocatalysts. The benchmark electrocatalysts are majorly platinum-based due to their exceptional catalytic properties, including their ability to rapid proton reduction and hydrogen gas generation at very low overpotentials.[111, 118-120] Platinum exhibits ideal hydrogen binding energy, meaning it can effectively adsorb and desorb hydrogen atoms during the HER in both acidic and alkaline media.[121-124] Nickel, cobalt, and iron-based electrocatalysts are also capable of catalyzing hydrogen evolution reactions but with relatively higher overpotential than platinum.[125-127] HER can also be performed on some transition metal chalcogenides due to their electronic properties.[125,128] Majorly, the HER mechanism proceeds via two pathways: Volmer-Heyrovsky and Volmer-Tafel mechanism.[129-132] The thermodynamic potential of HER is approximately 0 V (vs standard hydrogen electrode) in acidic media and − 0.83 V (vs standard hydrogen electrode) in alkaline media. Some electrocatalysts are active in acidic media, and some show facile HER in alkaline media.[118-124] Robust and sustainable electrocatalysts with low overpotentials are the need of the hour to make the hydrogen economy a viable alternative.

Deuterium (^{2}H or D) is the heavier isotope of protium or light hydrogen (^{1}H).[133] Deuterium is also known as heavy hydrogen.[134] It has one extra neutron in the nucleus as compared to light hydrogen. Due to an extra neutron in the nucleus of deuterium, the mass of D is double the mass of H. Deuterium is the third most abundant element in the whole universe, but the natural occurrence on Earth is very low, only 0.015%.[133-135] Deuterium has slightly different physical and electrochemical behavior due to the mass difference.[136] Heavy hydrogen has several applications in nuclear reactors, nuclear fusion reactions, the chemical industry, the pharmaceutical sector, medicinal drug development, etc.[137-142] Deuterium or heavy hydrogen mostly exists as deuterium oxide (D_2O) in Earth's water bodies (30 ppm D_2O in seawater). D does not exist in its gaseous form on the earth, it exists as heavy water, D_2O. Deuterium separation from protium or light hydrogen is mainly called the deuterium production process. There are several ways to produce deuterium in industry.[143] Fractional distillation is a way to separate D and H, as D and H have different boiling points.[143,144] Laser isotope separation is a method to separate deuterium from hydrogen, based on differences between energy levels.[145,146] Thermal diffusion and chemical isotope exchange are some other methods to separate deuterium from a mixture of isotopes.[147] Mostly this separated deuterium is in liquid state as

deuterium oxide. Electrolysis or electrochemical splitting of this heavy water is the primary and major method to produce deuterium on an industrial scale.[148,149] By applying a potential (more than 1.23 V), Liquid D_2O or acidified D_2O (D_2O + D_2SO_4) can be electrolyzed at the precious metal-based electrode (Pt, Pd, Ir, etc.) to form oxygen (O_2) and deuterium (D_2) gas, (eq 1.9).[150-152]

$$2D_2O \rightarrow 2D_2 + O_2 \qquad \text{(eq 1.9)}$$

Electrochemical heavy water (D_2O) splitting requires slightly more potential as compared to electrochemical light water (H_2O) splitting. Photocatalytic heavy water splitting is an alternative technique to produce deuterium by applying light into the system.[153] Often these methods are energy intensive with substantial cost implications in the deuterium industry.

1.4.3 Impurities in a Fuel Stream

It is a major concern that most of the methods for hydrogen production led to impure streams of hydrogen (H_2), which is majorly contaminated by carbon monoxide (CO), carbon dioxide (CO_2), hydrogen sulfide (H_2S), and methane (CH_4), etc.[154-156] Around 95% of overall produced H_2 (blue, black, brown, and grey hydrogen, etc) is in the impure form with carbonaceous and non-carbonaceous impurities.[157] To address these concerns, these impure fuel streams are purified via several techniques (as detailed below) before utilizing in commercial hydrogen fuel cells. Therefore, industrially produced H_2 needs to be purified before feeding to commercial hydrogen fuel cells; otherwise, it can pose a threat to the architectural components of the fuel cells.

There are various gaseous and non-gaseous impurities in the hydrogen fuel streams.[154] These impurities can contaminate the fuels mainly during hydrogen production, storage, or distribution. Impurities in hydrogen fuel streams can greatly affect the electrocatalysts, performance, durability, and safety of fuel cells and other hydrogen-oriented technologies.[73-75,114] Some of these contaminants can be poisonous to the electrocatalysts of the fuel cell, which can severely damage the expensive electrodes and decay the fuel cell performance in the long run.[74-76] Often, they can irreversibly bind to the electrocatalyst and decrease the fuel cell performance.[73-76]

1.4.3.1 Poisonous Impurities

Carbon monoxide (CO) is often incorporated during hydrogen production via processes like steam methane reforming (SMR) or partial oxidation of hydrocarbons.[79,80] CO strongly adsorbs to the platinum catalysts used in commercial hydrogen fuel cells, thereby "poisoning" the catalyst and reducing the fuel cell's efficiency.[75,76,114,115] CO can form a linear or bridge bonding to the platinum metal and block the active electrocatalytic sites of platinum as follows (eq 1.10, 1.11).[158,159]

Linear bonding

$$Pt + CO \rightarrow Pt- C\equiv O^{+} \qquad \text{(eq 1.10)}$$

Bridge bonding

$$2Pt + CO \rightarrow Pt_2C=O \qquad \text{(eq 1.11)}$$

This will decrease the extent of the hydrogen oxidation reaction in the fuel cell and drastically degrade the fuel cell's performance or efficiency.[160,161] Even concentrations as low as a few parts per million (ppm) can significantly affect the performance of a hydrogen fuel cell.[73,159]

Hydrogen sulfide (H_2S) is another poisonous impurity that spoils the platinum electrocatalyst of the hydrogen fuel cell.[73] Sulfur can irreversibly bind with platinum, leading to severe degradation of both performance and durability (eq 1.12,1.13).[162] If the hydrogen is produced from fossil fuels or biomass, H_2S can be present in the hydrogen fuel streams. Few parts per billion (ppb) can cause severe damage to the electrocatalyst.[73,74,162]

$$Pt + H_2S \rightarrow Pt{-}S_{ads} + H_2 \qquad \text{(eq 1.12)}$$

$$Pt{-}H + H_2S \rightarrow Pt{-}S_{ads} + 1.5\ H_2 \qquad \text{(eq 1.13)}$$

1.4.3.2 Non-poisonous Impurities

Carbon dioxide (CO_2) is the major carbonaceous, non-poisonous impurity that can be present in the fuel stream.[154] It can be incorporated into the fuel stream through the production of hydrogen via steam methane reforming, coal gasification, etc.[80-83] Carbon dioxide in the fuel stream can reduce the partial pressure of hydrogen in the stream, which in turn can decrease the cell voltage of the device. Further, this can decrease the extent

of hydrogen oxidation reaction at the anode, followed by fuel cell energy output. Carbon dioxide can also deteriorate the electrolyte of commercial fuel cells when the used electrolyte is alkaline.[163]

Nitrogen (N_2) can be present in the hydrogen fuel stream when the fuel is produced via partial oxidation technique. The presence of nitrogen in the fuel stream reduces the partial pressure of hydrogen fuel, leading to a reduced fuel cell performance. Ammonia (NH_3) may be introduced in hydrogen fuel streams when hydrogen is produced via processes like ammonia reforming, or it may contaminate the hydrogen streams when the reforming is carried out in nitrogen-rich environments.[164,165] Ammonia can directly degrade the electrolyte by reacting with the proton present in the acidic electrolyte, which reduces fuel cell efficiency, particularly in PEM fuel cells.[166,167]

Moisture or water vapor (H_2O) can infiltrate the fuel stream during any of the hydrogen fuel production, storage, or transportation phases, especially when hydrogen is kept in environments with high humidity. Excess water or moisture in the fuel stream can lead to fuel cell flooding, deteriorating hydrogen fuel cells and their efficiency.[168-171]

Methane and other hydrocarbons may remain in the hydrogen stream as the residue of steam methane reforming (SMR) or other hydrocarbon reforming.[79,81] Methane does not react with the components of the fuel cells at room temperature, but it decreases the hydrogen concentration in the fuel stream, lowering the fuel's energy density.

All these warrant the purification of hydrogen fuel streams to the tolerance level (Table 1.1) of hydrogen based device before feeding them to hydrogen utilization devices like hydrogen-oxygen fuel cells.

Table 1.1: The permissible quantities of impurities in an ultra-high pure (UHP) hydrogen fuel.

Impurity	Permissible Quantity (ppm)
Nitrogen (N_2)	100
Carbon dioxide (CO_2)	2
Methane (CH_4)	2
Carbon monoxide (CO)	0.2
Hydrogen sulfide (H_2S)	0.004

1.4.4 Hydrogen Purification

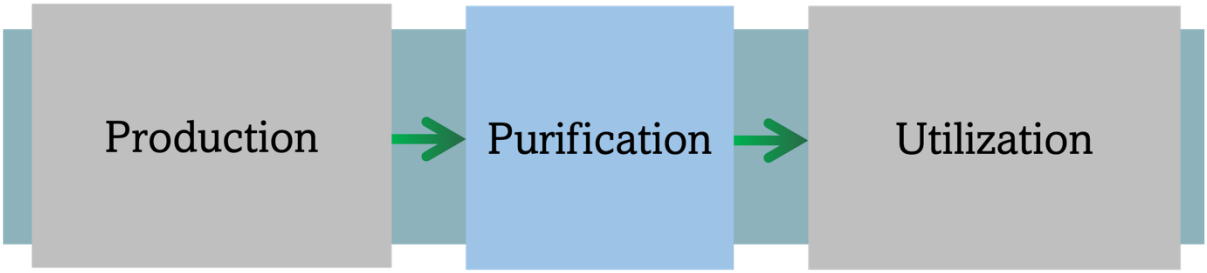

Figure 1.4: Various stages of hydrogen economy.

There must be a step of hydrogen purification between the production and utilization of hydrogen (Figure 1.4) for a sustainable hydrogen economy. Impure hydrogen streams can be purified via various techniques mentioned below.

Pressure swing adsorption (PSA) is a technique where H_2 is purified by varying the pressure, which leads to gas adsorption on materials like zeolites or activated carbon.[172] At high pressure, impurities are selectively adsorbed onto the adsorbent material.[173] The adsorbed gases are released from the material by reducing pressure.[173] Though this method results in 99.9% fuel purity, it is energy intensive as it requires around 100 to 400°C and a high pressure of 5 to 25 bars.[174-176]

The membrane separation technique requires a porous membrane where gases can pass selectively through the membrane based on the sizes of the gas molecules and pour sizes of the membrane.[177-179] The membranes used in these cases are polymeric or metallic in nature.[178] When an impure fuel stream is passed through these membranes, some gases can pass through, and some are stuck on one side of the membrane. Being very small in size, hydrogen gas molecules can diffuse through the membrane swiftly and get purified on the other side of the membrane.[177,179] This method produces a very high purity of 99.99% fuel but requires extreme conditions like high pressure and high temperate (200-400°C) and expensive membranes.[177-181]

Cryogenic distillation purifies hydrogen from impurities based on their different boiling points. The impure fuel mixture is cooled at around -85°C until the contaminants liquefy or solidify, resulting in highly pure hydrogen gas.[182,183] This process is highly energy intensive due to the cryogenic temperature requirements and the need for costly and sophisticated infrastructure.[182-184]

Metal hydride separation is a method of fuel purification that mainly depends on the capability of some metals (magnesium or palladium) to form metal hydrides by absorbing hydrogen at specific temperatures and pressures.[185] After the adsorption of hydrogen into the metals, it is separated from impurities, which do not get specifically adsorbed like hydrogen.[186] This purified hydrogen can be regenerated by heating the metal hydride.

Electrochemical purification occurs in an electrochemical cell where an impure hydrogen (H_2) stream is oxidized to form protons at the anodic half-cell by applying an electric field.[187-189] The protons pass through the ion exchange membrane towards the cathodic half and get reduced to form hydrogen (H_2) at the cathode. Under an applied potential, the impure mixture is fed at the anode, and pure hydrogen will be evolved at the cathode.[188-190] This purification method requires high applied potential and external energy to purify impure hydrogen fuel. Other than these purification methods, chemical purification, scrubbing, etc., are mild-scale purifying processes.[191] All these purification techniques are no doubt essential, but these methods require extreme pressures and temperatures, high energy input, and sophisticated equipment, which stand as barriers in the future of the hydrogen economy. The fact that more energy/cost is required to produce hydrogen than that it can be recovered during its utilization stage derails the journey toward the implementation of a robust hydrogen economy. It is the need of the hour to explore novel methodologies and pathways to make the hydrogen economy a viable alternative to fossil fuel based energy economy.

1.5 Aim and Scope of the Thesis

The major aim of this thesis is to directly harness water formation reaction energy for hydrogen fuel purification, spontaneous heavy hydrogen production, and low-grade heat harvesting. Water formation energy refers to the energy released during the formation of water molecules (eq 1.14) via combining proton (H^+) and hydroxyl (OH^-) ions. This water formation reaction releases a huge amount of energy in the form of heat, and harvesting this energy has huge technological implications. Annually, around 100 million tons of global acidic waste are being dumped into water bodies after neutralizing the waste acids. This huge amount of wasted energy corresponds to 44 TWh of electrical energy. Being non-redox in nature, the water formation reaction lacks electron transfer, which makes

the water formation energy harvesting extremely challenging. The major focus of this thesis is to directly interconvert this heat energy as an electrochemical driving force for several electrochemical reactions via a hydrogen redox in a decoupled acid-alkali device.

Water formation is an exothermic and spontaneous process with a standard molar enthalpy change (ΔH^0) of − 55.84 kJ mol^{-1} and a standard entropy change (ΔS^0) of 80.66 J mol^{-1} K^{-1}, Calculation 1.1. Therefore, this water formation reaction has a standard molar Gibbs free energy change (ΔG^0) of − 79.9 kJ mol^{-1}. Based on this, 0.82 V of electromotive force can be harvested from the water formation energy, Calculation 1.1. As the entropy changes for this water formation energy is positive in nature, it can extract energy from the surroundings during operation. This leads to a thermodynamic efficiency value greater than 1. The energy generated by water formation heavily depends on the pH of both half-cells of an electrochemical energy conversion device, Calculation 1.2. In other words, the Gibbs free energy of the water formation energy directly correlates to the concentration of acid and alkali in two specific half-cells of the device.

Calculation 1.1

Water formation reaction from H^+ and OH^- dual ions

$$H^+ + OH^- \leftrightarrow H_2O \qquad \text{(eq 1.14)}$$

Enthalpy changes for the reaction.

$\Delta H^0 = H^0 (H_2O) – H^0 (H^+) – H^0 (OH^-)$

$= – 285.8 – 0 – (– 230)$

$=$ **$– 55.8$ kJ/mol**

Entropy changes for the reaction

$\Delta S^0 = S^0 (H_2O) – S^0 (H^+) – S^0 (OH^-)$

$= 69.91 – 0 – (– 10.75)$

$=$ **0.08066 kJ/K mol**

Gibbs free energy of the reaction

$\Delta G^0 = \Delta H^0 – T\Delta S^0$

= – 55.8 – (298 * 0.08066)

= **– 79.875 kJ/mol**

Thermodynamic efficiency (ξ) = $\Delta G^0/\Delta H^0$ = 1.43

$\Delta G^0 = -nFE^0$

$E^0 = -\Delta G^0/nF$

$E^0 = -(-79875)/1*96500$

E^0 = **0.82 V**

Calculation 1.2

The total cell reaction for the water formation cell is:

$H^+(aq) + OH^-(aq) \rightarrow H_2O(l)$ (eq 1.14)

The free energy change for that reaction can be written as follows:

$\Delta G = \Delta G^o + RT \ln \left(^{product}/_{reactant}\right)$

$\Delta G = \Delta G^o + RT \ln \left(^{[H_2O]}/_{[H^+][OH^-]}\right)$

$\Delta G = \Delta G^o - RT \ln [H^+] - RT \ln [OH^-]$

$\Delta G = \Delta G^o - RT\ 2.303 (\log[H^+] + \log [OH^-])$

$\Delta G = \Delta G^o - RT\ 2.303 (-pH - pOH)$

$\Delta G = \Delta G^o + RT\ 2.303 (pH + pOH)$

$\Delta G = \Delta G^o + RT\ 2.303 (pH_A + 14 - pH_B)$,

where pH_A = pH of acidic electrolyte and pH_B = pH of alkaline electrolyte

$\Delta G = \Delta G^o + RT\ 2.303 (pH_A - pH_B) + RT\ 2.303*14$

$\Delta G = \Delta G^o - RT\ 2.303\ \Delta pH + RT\ 2.303*14$ ($pH_B > pH_A$)

$\Delta G = -79.8 - 5.7\Delta pH + 79.8$

$\Delta G = -5.7\ \Delta pH$

$$E = {}^{-\Delta G}/_{nF} = 0.059\ \Delta pH \qquad \text{(eq 1.15)}$$

From eq 1.15, it is obvious that the Gibbs free energy of the water formation reaction is proportional to the pH gradient between two half-cells of the electrochemical energy device. If the pH gradient is higher, the energy output is also higher. It is necessary to have a pH gradient to avail the water formation energy as potential output.

Anodic half-cell reaction:

$$2H_2O + 2e^- \leftrightarrow H_2 + 2OH^- \qquad \text{(eq 1.16)}$$

Cathodic half-cell reaction:

$$2H^+ + 2e^- \leftrightarrow H_2 \qquad \text{(eq 1.17)}$$

Overall cell reaction:

$$2H^+ + 2OH^- \leftrightarrow 2H_2O \qquad \text{(eq 1.18)}$$

Being a thermodynamically exciting reaction with huge industrial relevance, direct harnessing of water formation energy as electromotive force offers new avenues and possibilities for electrochemical process modulations. As noted before, the major challenge involved in their interconversion as EMF is the non-redox nature of the water formation reaction. In the work outlined in this thesis, this challenge is overcome via a hydrogen redox (eq 1.16, 1.17, and 1.18) in a decoupled acid-alkali device with tremendous possibilities for hydrogen fuel purification, spontaneous heavy hydrogen production, and low-grade heat harvesting during electricity production. The thesis is organized into the following chapters.

1.5.1 Chapter 1

This chapter rationalizes the requirement of innovative green energy stocks to maintain the current energy scenario and hydrogen economy. For a carbon-free, eco-friendly future, the world is transitioning from fossil fuel to a hydrogen-based energy economy, where H_2 acts as a green fuel to be utilized in fuel cells to generate electrical energy for multiple purposes. This H_2 economy is majorly hindered by impure H_2 fuel streams and highly energy-intensive fuel purification techniques. To resolve these severe energy concerns, direct harvesting of water formation energy as an electrochemical driving force

is proposed from a thermodynamic and technological standpoint. This reaction is naturally non-redox and exothermic, and the reaction voltage (around 0.82 V) can be directly harvested as EMF by utilizing hydrogen redox. In the upcoming chapters, the application prospects of this water formation during electricity production are elucidated for various electrochemical process modulations.

1.5.2 Chapter 2

Being a non-redox reaction, capturing the water formation energy in a redox cell holds challenges due to the absence of electron flow in the system. This chapter sheds light on the method for extracting the energy of the water formation reaction by performing hydrogen redox in a decoupled acid-alkali configuration. The employment of hydrogen oxidation reaction at the alkaline anode and hydrogen evolution reaction at the acidic cathode assist in harvesting the water formation energy as electrical potential. This electrical power output can be maximized by introducing a temperature gradient between the two electrodes of this device due to its positive entropy change.

1.5.3 Chapter 3

This chapter deals with the purification of impure hydrogen fuel streams during electric power production under ambient weather conditions by utilizing water-formation energy. Unlike energy-intensive conventional hydrogen purification methods, the fuel purifier based on water formation energy purifies the impure hydrogen fuel streams during electricity production. This spontaneous hydrogen purifier can continuously release pure hydrogen as long as an acid-base gradient is maintained within the device. Fuel mixtures with various impurities can be purified to ~99.9 % purity in a single step, requiring ~24 kJ of energy input and yielding ~90 kJ of electrical energy output per mole of pure hydrogen.

1.5.4 Chapter 4

This chapter deals with separating electrocatalyst poisoning impurities from impure hydrogen fuel streams under ambient conditions. Impurities like carbon monoxide and hydrogen sulfide can irreversibly bind with the platinum electrocatalyst of a hydrogen fuel cell and drastically decrease the performance in the long run. By harvesting the water formation energy as electrical power, these poisonous impure

streams can be purified in a single step at room temperature and pressure. The employment of non-precious and poison-tolerant electrocatalysts in the anode of the fuel purifier further leads to improvement in the durability of the device further reduces the cost of fuel purification using this approach.

1.5.5 Chapter 5

This chapter explores a way toward spontaneous electrochemical heavy hydrogen evolution by harnessing the heavy water formation energy under ambient temperature and pressure. Exploiting the pD gradient in a heavy water formation cell provides an electrochemical driving force for heavy hydrogen (D_2) evolution in a thermodynamically downhill manner. This exergonic electrochemical process produces approximately 357 mL of D_2 over nearly 85 hours of continuous electrolysis, delivering a corresponding electrical energy output of 122 kJ per mole of D_2.

1.5.6 Chapter 6

This chapter offers a concise summary and presents future perspectives for the research discussed in this thesis.

1.6 References

1. E. Aramendia, P. E. Brockway, P. G. Taylor, J. B. Norman, M. K. Heun and Z. Marshall, Nat. Energy, 2024, **9**, 803–816.
2. M. Jayachandran, R. K. Gatla, K. P. Rao, G. S. Rao, S. Mohammed, A. H. Milyani, A. A. Azhari, C. Kalaiarasy and S. Geetha, Sustain. Energy Technol. Assessments, 2022, **53**, 102692.
3. C. Verma, D. S. Chauhan, R. Aslam, P. Banerjee, J. Aslam, T. W. Quadri, S. Zehra, D. K. Verma, M. A. Quraishi, S. Dubey, A. AlFantazi and T. Rasheed, Green Chem., 2024, **26**, 4270–4357.
4. F. Fuso Nerini, J. Tomei, L. S. To, I. Bisaga, P. Parikh, M. Black, A. Borrion, C. Spataru, V. Castán Broto, G. Anandarajah, B. Milligan and Y. Mulugetta, *Nat. Energy*, 2018, **3**, 10–15.
5. M. Büchs, N. Cass, C. Mullen, K. Lucas and D. Ivanova, Nat. Energy, 2023, **8**, 758–769.
6. I. Staffell, D. Scamman, A. Velazquez Abad, P. Balcombe, P. E. Dodds, P. Ekins, N. Shah and K. R. Ward, Energy Environ. Sci., 2019, **12**, 463–491.
7. F. J. Gomes da Silva and R. M. Gouveia, eds. F. J. Gomes da Silva and R. M. Gouveia, Springer International Publishing, Cham, 2020, pp. 33–75.
8. K.-E. Norrman, World, 2023, **4**, 684–697.

9. I. Khan, F. Hou, M. Irfan, A. Zakari and H. P. Le, Renew. Sustain. Energy Rev., 2021, **146**, 111157.
10. T. Ahmad and D. Zhang, Energy Reports, 2020, **6**, 1973–1991.
11. M. Santamouris and K. Vasilakopoulou, e-Prime - Adv. Electr. Eng. Electron. Energy, 2021, **1**, 100002.
12. D. Adam, Nature, 2021, **597**, 462–465.
13. B. Freedman, W. Dorsey, A. Frazier, M. Kambhampati, J. Galiotos and S. Mukherjee, Environ. Sci., 2024.1
14. C. Yu, M. Moslehpour, T. K. Tran, L. M. Trung, J. P. Ou and N. H. Tien, Resour. Policy, 2023, **80**, 103221.
15. D. Welsby, J. Price, S. Pye and P. Ekins, Nature, 2021, **597**, 230–234.
16. K. N. Rather, M. K. Mahalik and H. Mallick, Environ. Sci. Pollut. Res., 2024, **31**, 25706–25720.
17. J. L. Holechek, H. M. E. Geli, M. N. Sawalhah and R. Valdez, Sustain., 2022, **14**, 1–22.
18. M. Mohsin, F. Taghizadeh-Hesary, N. Iqbal and H. B. Saydaliev, Renew. Energy, 2022, **190**, 777–787.
19. X. Yuan, C.-W. Su, M. Umar, X. Shao and O.-R. LOBONŢ, J. Environ. Manage., 2022, **308**, 114648.
20. A. Rahman, O. Farrok and M. M. Haque, Renew. Sustain. Energy Rev., 2022, **161**, 112279.
21. W. Strielkowski, E. Tarkhanova, M. Tvaronavi˘ and Y. Petrenko, Energies, 2021, **14**, 1–24.
22. E. T. Sayed, T. Wilberforce, K. Elsaid, M. K. H. Rabaia, M. A. Abdelkareem, K.-J. Chae and A. G. Olabi, Sci. Total Environ., 2021, **766**, 144505.
23. A. O. M. Maka and J. M. Alabid, Clean Energy, 2022, **6**, 476–483.
24. W. P. Schill, Joule, 2020, **4**, 2059–2064.
25. S. V. Venkatesan, A. Nandy, K. Karan, S. R. Larter and V. Thangadurai, Electrochem. Energy Rev., 2022, **5**, 16.
26. G. R. Timilsina, Renew. Energy, 2021, **180**, 658–672.
27. G. E. Halkos and E. C. Gkampoura, Energies, 2020, **13**, 2906.
28. D. Maradin, Int. J. Energy Econ. Policy, 2021, **11**, 176–183.
29. Y. Luo, Y. Wu, B. Li, T. Mo, Y. Li, S.-P. Feng, J. Qu and P. K. Chu, J. Energy Storage, 2021, **42**, 103124.
30. D. A. Cullen, K. C. Neyerlin, R. K. Ahluwalia, R. Mukundan, K. L. More, R. L. Borup, A. Z. Weber, D. J. Myers and A. Kusoglu, Nat. Energy, 2021, **6**, 462–474.
31. P. Halder, M. Babaie, F. Salek, N. Haque, R. Savage, S. Stevanovic, T. A. Bodisco and A. Zare, Int. J. Hydrogen Energy, 2024, **52**, 973–1004.
32. M. A. Aminudin, S. K. Kamarudin, B. H. Lim, E. H. Majilan, M. S. Masdar and N. Shaari, Int. J. Hydrogen Energy, 2023, **48**, 4371–4388.
33. M. K. Singla, P. Nijhawan and A. S. Oberoi, Environ. Sci. Pollut. Res., 2021, **28**, 15607–15626.

34. L. Shi, Y. Zhao, S. Matz, S. Gottesfeld, B. P. Setzler and Y. Yan, Nat. Energy, 2022, **7**, 238–247.
35. R. F. Service, Science., 2009, **324**, 1257–1259.
36. T. Yusaf, A. S. Faisal Mahamude, K. Kadirgama, D. Ramasamy, K. Farhana, H. A. Dhahad and A. R. Abu Talib, Int. J. Hydrogen Energy, 2024, **52**, 1026–1045.
37. V. Zgonnik, Earth-Science Rev., 2020, **203**, 103140.
38. S. Kopf, F. Bourriquen, W. Li, H. Neumann, K. Junge and M. Beller, Chem. Rev., 2022, **122**, 6634–6718.
39. A. Mamun, HydroResearch, 2025, **8**, 41–48.
40. A. S. Mahmudovich, Int. J. Orange Technol., 2021, **3**, 173–175.
41. B. A. Nicolin and I. Nicolin, Incas Bull., 2023, **15**, 141–147.
42. P. O. Longe, D. K. Danso, G. Gyamfi, J. S. Tsau, M. M. Alhajeri, M. Rasoulzadeh, X. Li and R. G. Barati, Energies, 2024, **17**, 5723.
43. C. Wei, S. M. Jafari Raad, Y. Leonenko and H. Hassanzadeh, Int. J. Hydrogen Energy, 2023, **48**, 34930–34944.
44. M. Newborough and G. Cooley, Fuel Cells Bull., 2021, **2021**, 16–19.
45. M. D. Allendorf, V. Stavila, J. L. Snider, M. Witman, M. E. Bowden, K. Brooks, B. L. Tran and T. Autrey, Nat. Chem., 2022, **14**, 1214–1223.
46. P. M. Falcone, M. Hiete and A. Sapio, Curr. Opin. Green Sustain. Chem., 2021, **31**, 100506.
47. D. Guan, B. Wang, J. Zhang, R. Shi, K. Jiao, L. Li, Y. Wang, B. Xie, Q. Zhang, J. Yu, Y. Zhu, Z. Shao and M. Ni, Energy Environ. Sci., 2023, **16**, 4926–4943.
48. P. Zhang, Y.-J. Guo, J. Chen, Y.-R. Zhao, J. Chang, H. Junge, M. Beller and Y. Li, *Nat. Catal.*, 2018, **1**, 332–338.
49. D. Hauglustaine, F. Paulot, W. Collins, R. Derwent, M. Sand and O. Boucher, Commun. Earth Environ., 2022, **3**, 1–14.
50. J. O. M. Bockris, Int. J. Hydrogen Energy, 2013, **38**, 2579–2588.
51. A. M. Oliveira, R. R. Beswick and Y. Yan, Curr. Opin. Chem. Eng., 2021, **33**, 100701.
52. G. Marbán and T. Valdés-Solís, Int. J. Hydrogen Energy, 2007, **32**, 1625–1637.
53. M. van der Spek, C. Banet, C. Bauer, P. Gabrielli, W. Goldthorpe, M. Mazzotti, S. T. Munkejord, N. A. Røkke, N. Shah, N. Sunny, D. Sutter, J. M. Trusler and M. Gazzani, Energy Environ. Sci., 2022, **15**, 1034–1077.
54. J. N. Tiwari, N. K. Dang, S. Sultan, P. Thangavel, H. Y. Jeong and K. S. Kim, Nat. Sustain., 2020, **3**, 556–563.
55. K. T. Møller, T. R. Jensen, E. Akiba and H. wen Li, Prog. Nat. Sci. Mater. Int., 2017, **27**, 34–40.
56. T. S. Uyar and D. Beşikci, Int. J. Hydrogen Energy, 2017, **42**, 2453–2456.
57. A. J. Appleby, J. Power Sources, 1990, **29**, 3–11.
58. Grove, W.R. On Voltaic Series and the Combination of Gases by Platinum. Lond. Edinb. Philos. Mag. J. Sci. 1839**,** **14**, 127–130.

59. Grove, W.R. On a Gaseius Voltaic Battery. Lond. Edinb. Philos. Mag. J. Sci. 1842, **21**, 417–420
60. M. Eisler, Overpotential, 2019.
61. Eisler, Matthew N. Technology and Culture 50, no. 2, 2009, 345-36.
62. B. Viswanathan and M. A. Scibioh, Chemphyschem, 2000, **1**, 162-193.
63. Y. Wang, K. S. Chen, J. Mishler, S. C. Cho and X. C. Adroher, Appl. Energy, 2011, **88**, 981–1007.
64. K. Jiao, J. Xuan, Q. Du, Z. Bao, B. Xie, B. Wang, Y. Zhao, L. Fan, H. Wang, Z. Hou, S. Huo, N. P. Brandon, Y. Yin and M. D. Guiver, Nature, 2021, **595**, 361–369.
65. M. Cheng, M. Liu, Y. Feng, Y. Guo, H. Xu, L. Luo, J. Yin, X. Yan, S. Shen and J. Zhang, Energy Convers. Manag., 2024, **311**, 118525.
66. R. A. Felseghi, E. Carcadea, M. S. Raboaca, C. N. Trufin and C. Filote, Energies, 2019, **12**, 4593.
67. S. A. Vilekar and R. Datta, J. Power Sources, 2010, **195**, 2241–2247.
68. J. Zhang, Y. Tang, C. Song, J. Zhang and H. Wang, J. Power Sources, 2006, **163**, 532–537.
69. K. Ehelebe, N. Schmitt, G. Sievers, A. W. Jensen, A. Hrnjić, P. Collantes Jiménez, P. Kaiser, M. Geuß, Y. P. Ku, P. Jovanovič, K. J. J. Mayrhofer, B. Etzold, N. Hodnik, M. Escudero-Escribano, M. Arenz and S. Cherevko, ACS Energy Lett., 2022, **7**, 816–826.
70. C. Wei, R. R. Rao, J. Peng, B. Huang, I. E. L. Stephens, M. Risch, Z. J. Xu and Y. Shao-Horn, Adv. Mater., 2019, **31**, 1–24.
71. R. Riasse, C. Lafforgue, F. Vandenberghe, F. Micoud, A. Morin, M. Arenz, J. Durst and M. Chatenet, J. Power Sources, 2023, **556,** 232491.
72. A. Król, M. Gajec, J. Holewa-Rataj, E. Kukulska-Zając and M. Rataj, Energies, 2024, **17**, 3794.
73. T. Lopes, V. A. Paganin and E. R. Gonzalez, J. Power Sources, 2011, **196**, 6256–6263.
74. W. Dong, C. Xu, W. Zhao, M. Xin, Y. Xiang, A. Zheng, M. Dou, S. Ke, J. Dong, L. Qiu and G. Xu, ACS Appl. Energy Mater., 2022, **5**, 12640–12650.
75. W. Luo, Y. Jiang, M. Wang, D. Lu, X. Sun and H. Zhang, RSC Adv., 2023, **13**, 4803–4822.
76. D. Long, X. Ping, J. Ni, F. Chen, S. Chen, Z. Wei, L. Guo and J. Zheng, Chem. Commun., 2023, **59**, 13583–13586.
77. Z. Li, Y. Wang, Y. Mu, B. Wu, Y. Jiang, L. Zeng and T. Zhao, Renew. Sustain. Energy Rev., 2023, **176**, 113182.
78. A. Murugan, M. de Huu, T. Bacquart, J. van Wijk, K. Arrhenius, I. te Ronde and D. Hemfrey, Int. J. Hydrogen Energy, 2019, **44**, 19326–19333.
79. R. Kumar, A. Kumar and A. Pal, Fuel, 2024, **362**, 130742.
80. H. Zhang, Z. Sun and Y. H. Hu, Renew. Sustain. Energy Rev., 2021, **149**, 111330.
81. J. O. Ighalo and P. B. Amama, Int. J. Hydrogen Energy, 2024, **51**, 688–700.
82. E. Baraj, K. Ciahotný and T. Hlinčík, Fuel, 2021, **288**, 119817.

83. A. Midilli, H. Kucuk, M. E. Topal, U. Akbulut and I. Dincer, Int. J. Hydrogen Energy, 2021, **46**, 25385–25412.
84. L. Jiang, D. Xue, Z. Wei, Z. Chen, M. Mirzayev, Y. Chen and S. Chen, Energy Rev., 2022, **1**, 100004.
85. S. Kumar Rajput, S. Verma, A. Gupta, A. Ranjan Paul, A. Jain and N. Haque, IOP Conf. Ser. Earth Environ. Sci., 2021, **795**, 012029.
86. T. Matamba, S. Iglauer and A. Keshavarz, J. Energy Inst., 2022, **105**, 81–102.
87. H. Song, G. Yang, P. Xue, Y. Li, J. Zou, S. Wang, H. Yang and H. Chen, Appl. Energy Combust. Sci., 2022, **10**, 100059.
88. Y. Gao, M. Wang, A. Raheem, F. Wang, J. Wei, D. Xu, X. Song, W. Bao, A. Huang, S. Zhang and H. Zhang, ACS Omega, 2023, **8**, 31620–31631.
89. K. Kundu, A. Kumar, H. Kodamana and K. K. Pant, Fuel, 2024, **378**, 132931.
90. B. Ghorbani, S. Zendehboudi, Y. Zhang, H. Zarrin and I. Chatzis, Energy Convers. Manag., 2023, **297**, 117599.
91. P. Fernández-Arias, Á. Antón-Sancho, G. Lampropoulos and D. Vergara, Energies., 2024, **17**, 2291.
92. A. Blankenship, M. Artsiusheuski, V. Sushkevich and J. A. van Bokhoven, Nat. Catal., 2023, **6**, 748–762.
93. F. Xu, Y. Wang, F. Li, X. Nie and L. Zhu, J. Fuel Chem. Technol., 2021, **49**, 367–373.
94. M. R. G. Pangestu, Z. Malaibari, A. Muhammad, F. N. Al-Rowaili and U. Zahid, Energy and Fuels, 2024, **38**, 13514–13538.
95. S. R. Patlolla, K. Katsu, A. Sharafian, K. Wei, O. E. Herrera and W. Mérida, Renew. Sustain. Energy Rev., 2023, **181**, 113323.
96. A. Boretti, Clean. Chem. Eng., 2024, 100139.
97. A. Raveendran, M. Chandran and R. Dhanusuraman, RSC Adv., 2023, **13**, 3843–3876.
98. U. Shahzad, M. Saeed, H. M. Marwani, J. Y. Al-Humaidi, S. ur Rehman, R. H. Althomali and M. M. Rahman, Int. J. Hydrogen Energy, 2024, **65**, 215–224.
99. J. Wei, Y. Shao, J. Xu, F. Yin, Z. Li, H. Qian, Y. Wei, L. Chang, Y. Han, J. Li and L. Gan, Nat. Commun., 2024, **15**, 9012.
100. Q. Hassan, A. M. Abdulateef, S. A. Hafedh, A. Al-samari, J. Abdulateef, A. Z. Sameen, H. M. Salman, A. K. Al-Jiboory, S. Wieteska and M. Jaszczur, Int. J. Hydrogen Energy, 2023, **48**, 17383–17408.
101. X. Li, C. J. Raorane, C. Xia, Y. Wu, T. K. N. Tran and T. Khademi, Fuel, 2023, **334**, 126684.
102. S. O. Jeje, T. Marazani, J. O. Obiko and M. B. Shongwe, Int. J. Hydrogen Energy, 2024, **78**, 642–661.
103. X. Zhang, Y. Xie and L. Wang, Nano Res., 2024, **17**, 960–981.
104. Q. Wang, H. Wang, H. Cao, C.-W. Tung, W. Liu, S.-F. Hung, W. Wang, C. Zhu, Z. Zhang, W. Cai, Y. Cheng, H. B. Tao, H. M. Chen, Y.-G. Wang, Y. Li, H. Bin Yang, Y. Huang, J. Li and B. Liu, Nat. Catal., 2023, **6**, 916–926.

105. L. Su, J. Chen, F. Yang, P. Li, Y. Jin, W. Luo and S. Chen, J. Am. Chem. Soc., 2023, **145**, 12051–12058.
106. A. Munir, J. Abdul Nasir, T. ul Haq, J. Iqbal, I. Hussain and A. Qurashi, Coord. Chem. Rev., 2024, **521**, 216112.
107. J. T. Ren, L. Chen, H. Y. Wang, Y. Feng and Z. Y. Yuan, Energy Environ. Sci., 2024, **17**, 3960–4009.
108. Y. Chen, Y. Yang, Z. Liang, Z. Tao and Q. Ni, J. Mater. Chem. A, 2025, DOI:10.1039/d4ta07777f.
109. F. Yang, X. Tian, W. Luo and L. Feng, Coord. Chem. Rev., 2023, **478**, 214980.
110. A. Heinritz, T. Binninger, J. Herranz and T. J. Schmidt, Journal of The Electrochemical Society, 2024, **171**, 114511.
111. J. Kim and J. Lee, Energy and Fuels, 2023, **37**, 17765–17781.
112. T. Zhao, M. Li, D. Xiao, X. Yang, Q. Li, L. An, Z. Deng, T. Shen, M. Gong, Y. Chen, G. Wang, X. Zhao, L. Xiao, X. Yang, L. Li and D. Wang, J. Am. Chem. Soc., 2023, **145**, 4088-4097.
113. S. Zhang, X. He, Y. Ding, Z. Shi and B. Wu, Renew. Sustain. Energy Rev., 2024, **204**, 114821.
114. Z. Yang, C. Chen, Y. Zhao, Q. Wang, J. Zhao, G. I. N. Waterhouse, Y. Qin, L. Shang and T. Zhang, Adv. Mater., 2023, **35**, 1–9.
115. Z. Yang, W. Lai, B. He, J. Wang, F. Yu, Q. Liu, M. Liu, S. Zhang, W. Ding, Z. Lin and H. Huang, Adv. Energy Mater., 2023, **13**, 1–10.
116. X. Mu, S. Liu, L. Chen and S. Mu, Small Struct., 2023, **4**, 2200281.
117. L. Wu, L. Su, Q. Liang, W. Zhang, Y. Men and W. Luo, ACS Catal., 2023, **13**, 4127–4133.
118. J. Zhang, C. Ma, S. Jia, Y. Gu, D. Sun, Y. Tang and H. Sun, Adv. Energy Mater., 2023, **13**, 1–19.
119. Y. Zhu, M. Klingenhof, C. Gao, T. Koketsu, G. Weiser, Y. Pi, S. Liu, L. Sui, J. Hou, J. Li, H. Jiang, L. Xu, W. H. Huang, C. W. Pao, M. Yang, Z. Hu, P. Strasser and J. Ma, Nat. Commun., 2024, **15**, 1447.
120. H. G. Xu, X. Y. Zhang, Y. Ding, H. Q. Fu, R. Wang, F. Mao, P. F. Liu and H. G. Yang, Small Struct., 2023, **4**. 2200404.
121. Y. Xu, X. Zhang, Y. Liu, R. Wang, Y. Yang and J. Chen, Environ. Sci. Pollut. Res., 2023, **30**, 11302–11320.
122. H. Yang, Y. Ji, Q. Shao, W. Zhu, M. Fang, M. Ma, F. Liao, H. Huang, Y. Zhang, J. Yang, Z. Fan, Y. Li, Y. Liu, M. Shao and Z. Kang, Energy Environ. Sci., 2023, **16**, 574–583.
123. W. Ma, X. Zhang, W. Li, M. Jiao, L. Zhang, R. Ma and Z. Zhou, Nanoscale, 2023, **15**, 11759–11776.
124. Z. Li, R. Ge, J. Su and L. Chen, Adv. Mater. Interfaces, 2020, **7**, 1–13.
125. S. Anantharaj, S. Kundu and S. Noda, J. Mater. Chem. A, 2020, **8**, 4174–4192.
126. R. Zahra, E. Pervaiz, M. Yang, O. Rabi, Z. Saleem, M. Ali and S. Farrukh, Int. J. Hydrogen Energy, 2020, **45**, 24518–24543.

127. S. Xu, H. Zhao, T. Li, J. Liang, S. Lu, G. Chen, S. Gao, A. M. Asiri, Q. Wu and X. Sun, J. Mater. Chem. A, 2020, **8**, 19729–19745.
128. Y. Wang, Y. Zhao, X. Ding and L. Qiao, J. Energy Chem., 2021, **60**, 451–479.1
129. E. E. Siddharthan, S. Ghosh and R. Thapa, ACS Appl. Energy Mater., 2023, **6**, 8941–8948.
130. H. Q. Fu, M. Zhou, P. F. Liu, P. Liu, H. Yin, K. Z. Sun, H. G. Yang, M. Al-Mamun, P. Hu, H. F. Wang and H. Zhao, J. Am. Chem. Soc., 2022, **144**, 6028–6039.
131. W. Xu, X. Q. Tang, Z. Zhang, Y. R. Wang, J. L. Luo, I. Bulugu, W. J. Yin, X. Tang and Y. Shen, Fuel, 2024, **358**, 130174.
132. A. Hanan, M. Nazim Lakhan, R. Walvekar, M. Khalid and C. Prakash, Chem. Eng. J., 2024, **483**, 149107.
133. Liu, M.; Zhang, L.; Little, M. A.; Kapil, V.; Ceriotti, M.; Yang, S.; Ding, L.; Holden, D. L.; Balderas-Xicohténcatl, R.; He, D.; Clowes, R.; Chong, S. Y.; Schütz, G.; Chen, L.; Hirscher, M.; Cooper, A. I. Science. 2019, **366**, 613–620.
134. Miller, A. I. Can. Nucl. Soc. Bull. 2001, **22**, 1–14.
135. Hartogh, P.; Lis, D. C.; Bockelée-Morvan, D.; De Val-Borro, M.; Biver, N.; Küppers, M.; Emprechtinger, M.; Bergin, E. A.; Crovisier, J.; Rengel, M.; Moreno, R.; Szutowicz, S.; Blake, G. A. Nature 2011, **478**, 218–220.
136. Qiu, Y.; Ren, H.; Edwards, M. A.; Gao, R.; Barman, K.; White, H. S. Langmuir 2020, **36**, 6073–6078.
137. Atzrodt, J.; Derdau, V.; Kerr, W. J.; Reid, M. Angew. Chemie - Int. Ed. 2018, **57**, 3022–3047.
138. Harbeson, S. L.; Tung, R. D. Elsevier Inc., 2011; Vol. 46.
139. Ditmire, T.; Zweiback, J.; Yanovsky, V. P.; Cowan, T. E.; Hays, G. Nature 1999, **398**, 489–492.
140. Di Martino, R. M. C.; Maxwell, B. D.; Pirali, T. Nat. Rev. Drug Discov. 2023, **22**, 562–584.
141. Lu, L.; Li, H.; Zheng, Y.; Bu, F.; Lei, A. CCS Chem. 2021, **3**, 2669–2675.
142. Pirali, T.; Serafini, M.; Cargnin, S.; Genazzani, A. A. J. Med. Chem. 2019, **62**, 5276–5297.
143. J. R. Bartlit, R. H. Sherman, R. A. Stutz and W. H. Denton, *Cryogenics (Guildf).*, 1979, **19**, 275–279.
144. I. Alekseev, E. Arkhipov, S. Bondarenko, O. Fedorchenko, V. Ganzha, K. Ivshin, P. Kammel, P. Kravtsov, C. Petitjean, V. Trofimov, A. Vasilyev, T. Vasyanina, A. Vorobyov and M. Vznuzdaev, *Rev. Sci. Instrum.*, 2015, **86**, 125102.
145. J. C. Vanderleeden, J. Appl. Phys., 1980, **51**, 1273–1285.
146. C. B. Moore, Acc. Chem. Res., 1973, **6**, 323–328.
147. G. Huang, D. Wang, L. Hu, J. Bao, Y. Song, X. Yan, R. Xiong, T. Tang and W. Luo, Int. J. Hydrogen Energy, 2024, **57**, 8–25.
148. N. Zeng, C. Hu, C. Lv, A. Liu, L. Hu, Y. An, P. Li, M. Chen, X. Zhang, M. Wen, K. Chen, Y. Yao, J. Cai and T. Tang, Sep. Purif. Technol., 2023, **310**, 123148.

149. H. Sato, H. Matsushima, M. Ueda and H. Ito, Int. J. Hydrogen Energy, 2021, **46**, 33689–33695.
150. J. Liu, Z. Chen, M. J. Koh and K. P. Loh, Energy Mater., 2022, **1**, 100016.
151. Ogawa, R.; Tanii, R.; Dawson, R.; Matsushima, H.; Ueda, M. Energy 2018, **149**, 98–104.
152. Fleischmann, M.; Pons, S.; Anderson, M. W.; Li, L. J.; Hawkins, M. J. Electroanal. Chem. 1990, **287**, 293–348.
153. Zeng, G.; Zeng, H.; Niu, L.; Chen, J.; Song, T.; Zhang, P.; Wu, Y.; Xiao, X.; Zhang, Y.; Huang, S. ChemSusChem 2020, **13**, 2935–2939.
154. Z. Du, C. Liu, J. Zhai, X. Guo, Y. Xiong, W. Su and G. He, Catalysts, 2021, **11**, 1–19.
155. K. M. K. Yu, W. Tong, A. West, K. Cheung, T. Li, G. Smith, Y. Guo and S. C. E. Tsang, Nat. Commun., 2012, **3**, 1-7.
156. M. Onozaki, K. Watanabe, T. Hashimoto, H. Saegusa and Y. Katayama, Fuel, 2006, **85**, 143–149.1
157. B. M. Besancon, V. Hasanov, R. Imbault-Lastapis, R. Benesch, M. Barrio and M. J. Mølnvik, Int. J. Hydrogen Energy, 2009, **34**, 2350–2360.
158. Z. Dong, Y. Nan, T. Tang, X. Z. Liu, J. Fu, H. R. Pan, Z. Jiang, L. Ding, X. Cheng, L. R. Zheng, J. Zhang, X. Chang, B. Xu and J. S. Hu, ACS Catal., 2023, **13**, 7822–7830.
159. W. Chen, J. Cao, W. Fu, J. Zhang, G. Qian, J. Yang, D. Chen, X. Zhou, W. Yuan and X. Duan, Angew. Chemie - Int. Ed., 2022, **61**, e202200190.
160. V. B. K.P, G. Varghese, T. V. Joseph and P. Chippar, Int. J. Hydrogen Energy, 2021, **46**, 8179–8196.
161. V. F. Valdés-López, T. Mason, P. R. Shearing and D. J. L. Brett, Prog. Energy Combust. Sci., 2020, **79**, 100842.
162. S. Ke, B. Cui, C. Sun, Y. Qin, J. Zhang and M. Dou, ACS Appl. Mater. Interfaces, 2022, **14**, 47765–47774.
163. F. Lucile, J. Serin, D. Houssin and P. Arpentinier, J. Chem. Eng. data, 2012, **57**, 784–789.
164. Y. Yi, X. Wang, A. Jafarzadeh, L. Wang, P. Liu, B. He, J. Yan, R. Zhang, H. Zhang, X. Liu, H. Guo, E. C. Neyts and A. Bogaerts, ACS Catal., 2021, **11**, 1765–1773.
165. V. Cechetto, L. Di Felice, J. A. Medrano, C. Makhloufi, J. Zuniga and F. Gallucci, Fuel Process. Technol., 2021, **216**, 106772.
166. D. Schonvogel, J. Büsselmann, H. Schmies, H. Langnickel, P. Wagner and A. Dyck, J. Power Sources, 2021, **502**, 229993.
167. R. Lin, J. Tian, Y. Jing, L. Chen and S. Hua, Int. J. Hydrogen Energy, 2023, **48**, 31366–31376.
168. B. Xiao, J. Zhao, L. Fan, Y. Liu, S. H. Chan and Z. Tu, Energy, 2022, **245**, 123298.
169. M. B. Yousefkhani, H. Ghadamian, K. Daneshvar, N. Alizadeh and B. C. R. Troconis, Energies, 2020, **13**, 1–11.

170. J. Fu, G. Zhang, D. Xu, X. Sun, T. He and H. Li, Int. J. Hydrogen Energy, 2024, **86**, 823–834.
171. J. Zhao, Z. Tu and S. H. Chan, Energy, 2022, **239**, 122270.
172. S. Sircar and T. C. Golden, Sep. Sci. Technol., 2000, **35**, 667–687.
173. M. Yáñez, F. Relvas, A. Ortiz, D. Gorri, A. Mendes and I. Ortiz, Sep. Purif. Technol., 2020, **240**, 116334.
174. M. Mondal and A. Datta, Int. J. energy Res., 2017, **41**, 448–458.
175. M. Luberti and H. Ahn, Int. J. Hydrogen Energy, 2022, **47**, 10911–10933.
176. V. Kalman, J. Voigt, C. Jordan and M. Harasek, Sustain., 2022, **14**, 14037.
177. L. Schorer, S. Schmitz and A. Weber, Int. J. Hydrogen Energy, 2019, **44**, 12708–12714.
178. G. Venugopalan, D. Bhattacharya, E. Andrews, L. Briceno-Mena, J. Romagnoli, J. Flake and C. G. Arges, ACS Energy Lett., 2022, **7**, 1322–1329.
179. L. Vermaak, H. W. J. P. Neomagus and D. G. Bessarabov, Membranes (Basel)., 2021, **11**, 1–32.
180. P. L. Mores, A. M. Arias, N. J. Scenna, J. A. Caballero, S. F. Mussati and M. C. Mussati, Processes, 2018, **6**, 221.
181. N. Sazali, Int. J. Hydrogen Energy, 2020, **45**, 18753–18771.
182. M. Chen, P. Li, C. Hu, J. Luo, M. Wen, B. Yu, F. Jiang, Y. An, Y. Shi, J. Song and W. Luo, Int. J. Hydrogen Energy, 2022, **47**, 11955–11961.
183. J. J. Urm, D. Park, J.-U. Lee, M. H. Chang and J. M. Lee, Fusion Eng. Des., 2021, **172**, 112736.
184. Y. Wang, S. B. Peh and D. Zhao, Small, 2019, **15**, 1–38.
185. D. Dunikov and D. Blinov, Int. J. Hydrogen Energy, 2020, **45**, 9914–9926.
186. M. Amin, A. S. Butt, J. Ahmad, C. Lee, S. U. Azam, H. A. Mannan, A. B. Naveed, Z. U. R. Farooqi, E. Chung and A. Iqbal, Energy Reports, 2023, **9**, 894–911.
187. G. N. B. Durmus, C. O. Colpan and Y. Devrim, J. Power Sources, 2021, **494**, 229743.
188. Y. Aykut and A. Bayrakçeken Yurtcan, Int. J. Hydrogen Energy, 2022, **47**, 19619–19632.
189. G. Zhang, T. Chen, Z. Guo, G. Zheng, X. Bao, R. Sun, L. Xu, Y. Zhou and S. Wang, Chem. Eng. J., 2024, **495**, 153521.
190. M. Rhandi, M. Trégaro, F. Druart, J. Deseure and M. Chatenet, Chinese J. Catal., 2020, **41**, 756–769.
191. E. Naeiji, A. Noorpoor and H. Ghanavati, Sustain., 2022, **14**, 3686.

Chapter 2

Heat Harvesting via Electrochemical Water Formation

Abstract

Low-grade heat harvesting has emerged as a promising strategy to recover and interconvert waste heat into usable energy. Among various heat harvesting methods, aqueous thermogalvanic systems are a promising alternative with their low cost, safety, and superior ionic conductivity. The water formation energy from H^+ and OH^- ions is explored to enhance the heat harvesting from the surroundings owing to its positive entropy change, leading to the interconversion of entropic heat as an electrical driving force. This proposed approach combines hydrogen redox reactions in a decoupled H^+ and OH^- asymmetric thermogalvanic device with temperature gradients, thereby increasing voltage and power outputs. This water formation-based thermogalvanic device has a high temperature-insensitive maximum power density as high as ~ 34.7 $mWcm^{-2}K^{-2}$, which is around 70 times higher than the state-of-the-art ferrocyanide-ferricyanide-based thermogalvanic devices, thereby paving the way for efficient heat harvesting solutions.

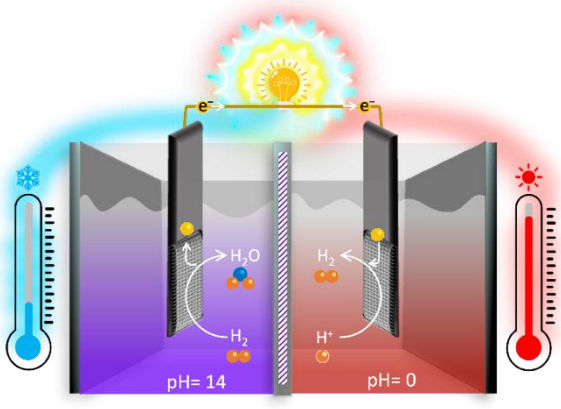

Declaration: The work in this chapter is original and has not yet been published anywhere. (Manuscript under preparation)

2.1 Introduction

The growing global energy requirement, accelerated by population and industrial expansion, has made the need for sustainable and efficient energy solutions inevitable.[1-4] Traditional energy sources, such as fossil fuels, not only have limited reserves but also contribute significantly to environmental challenges like greenhouse gas emissions and climate change.[5,6] Not only limited energy stock but also the wastage of energy in the form of heat drives this energy imbalance to a different level.[7] Due to these factors, heat harvesting has emerged as a promising approach to utilize or store waste heat for energy recovery and conversion.[8,9] Heat harvesting deals with converting dissipated heat from industrial power plants, natural heat gradients, and daily energy dissipation into usable energy forms.[10-12] Electrochemical heat harvesting capitalizes on the thermodynamic properties of electrochemical processes to convert dissipated thermal energy directly into electrical energy in a thermogalvanic cell.[13-15] Based on the Seebeck effect, the thermogalvanic cell mainly focuses on the generation of additional overall cell potential due to a temperature gradient (ΔT) in the presence of temperature-dependent redox half cells.[15-17] When one side of the thermogalvanic cell is raised to a higher temperature than the other half, the temperature gradient drives a difference in the reaction potentials of the two electrodes, which causes the redox couple to generate a voltage.[18] The potential (ΔE) generated due to the temperature difference (ΔT) and the Seebeck coefficient (α), is related to the equation $\Delta E = \alpha . \Delta T$.[17-19] Solid-state thermoelectric devices can show durability at high temperatures but have high costs and limitations of suitable materials.[20] Non-aqueous Li-ion-based thermogalvanic systems have good conversion efficiency, but electrolyte degradation in high temperatures is a barrier for these systems.[21,22] Organic redox electrolytes with high Seebeck effects are also utilized to improve the efficiency of thermogalvanic systems, but they lack conductivity and mass transport and possess non-toxic traits.[23-25] Due to these reasons, aqueous thermogalvanic systems have emerged as a potential electrochemical heat harvesting device due to their low cost, safe, non-toxic electrolytes, superior ionic conductivity, high mass transport, and availability of a variety of redox systems, etc.[14,26,27] The main challenges for electrochemical heat harvesting via thermogalvanic systems are low heat-to-power conversion, low partial molar entropy change, low solubility of redox couple and lower potential output, etc.[13,28-30]

Currently, the water formation energy generated from the combination of H^+ and OH^- ions has been investigated to enhance the electrical proficiency of electrochemical energy storage and conversion devices.[31-35] Water formation reaction can extract heat from the surroundings and convert it into an electrochemical driving force due to positive entropy change and positive Seebeck coefficient, Calculation 2.1. The introduction of hydrogen redox in a water formation cell addresses the issue of electron transfer caused by the non-redox nature of the water formation reaction. Deviating from conventional symmetric thermogalvanic systems, an electrochemical water formation cell is employed to harvest the temperature gradient between two asymmetric half-cells. The alkaline anodic hydrogen oxidation at cold temperatures coupled with hot acidic cathodic hydrogen evolution provides an opportunity to increase the voltage output for the water formation cell. The incorporation of temperature gradient as well as pH gradient in a water formation cell can maximize the overall electrical energy output of the thermogalvanic device.

Calculation 2.1

Water formation reaction from H^+ and OH^- dual ions

$H^+ + OH^- \leftrightarrow H_2O$

Enthalpy changes for the reaction.

$\Delta H^0 = H^0 (H_2O) - H^0 (H^+) - H^0 (OH^-)$

$= -285.8 - 0 - (-230)$

$= \mathbf{-55.8\ kJ/mol}$

Entropy changes for the reaction

$\Delta S^0 = S^0 (H_2O) - S^0 (H^+) - S^0 (OH^-)$

$= 69.91 - 0 - (-10.75)$

$= \mathbf{0.08066\ kJ/K\ mol}$

Gibbs free energy of the reaction

$\Delta G^0 = \Delta H^0 - T\Delta S^0$

$= -55.8 - (298 * 0.08066)$

$= \mathbf{-79.875\ kJ/mol}$

Thermodynamic efficiency (ξ) = $\Delta G^0/\Delta H^0$ = 1.43

$\Delta G^0 = -nFE^0$

$E^0 = -\Delta G^0/nF$

$E^0 = -(-79875)/1*96484$

$E^0 = \mathbf{0.82\ V}$

2.2 Results and Discussion

The overall architecture of the water formation cell consists of an anodic alkaline half-cell and a cathodic acidic half-cell, separated by a Nafion 117 cation-conducting membrane, as illustrated in Scheme 2.1. In the anodic alkaline half-cell, Pt supported on carbon (Pt/C) served as the electrocatalyst, while in the cathodic acidic half-cell, platinum electrodeposited on a titanium mesh (using a constant current of 4 mA/cm² for 5 minutes) was utilized as the electrocatalyst. Since water formation by OH^- and H^+ reaction is non-redox in nature, to directly harvest the energy of water formation as an electrical driving force, hydrogen redox(hydrogen evolution reaction (HER) in acidic half-cell and hydrogen oxidation reaction (HOR) in alkaline half-cell was performed) was conducted in respective half-cells . Since hydrogen redox reactions are pH dependent, this decoupled acid-alkali configuration should allow the direct harvesting of water formation energy as an electrical driving force without a net redox. To demonstrate this direct harvesting of water formation energy, we have performed hydrogen redox reactions as a function of pH. The hydrogen redox reactions have a relatively negative potential in an alkaline medium and a relatively positive potential in an acidic medium (Figures 2.1a and 2.1b). Consequently, their Pourbaix diagram exhibits a negative potential shift with respect to the pH (Figure 2.1c), demonstrating a slope ($\boldsymbol{dE/dpH}$) close to the theoretically expected value of 59 mV/pH for a reaction involving equal numbers of electrons and protons (Figure 2.1c). Therefore, there will be a net positive electromotive force (or a negative free energy change) between the same reactions when the direct acid-alkali chemistry is decoupled (Figure 2.1d) in the configuration as shown in Scheme 2.1. This suggests that if a hydrogen oxidation reaction (HOR) is performed in the alkaline half-cell (equation 2.1), the liberated electrons will flow through the external circuit powering the load with

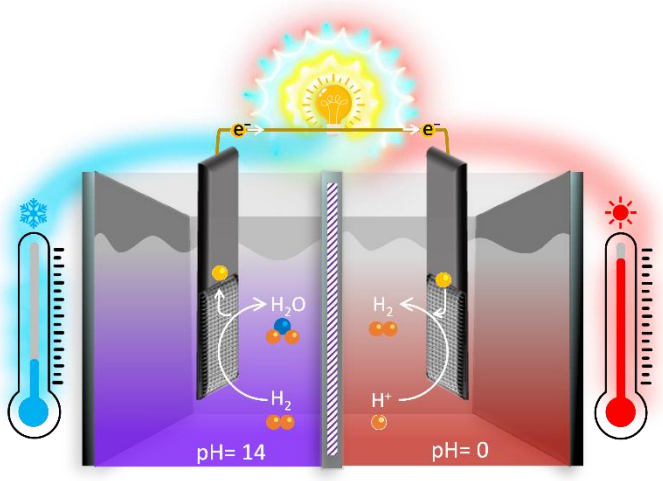

Scheme 2.1: Electrochemical water formation assisted thermogalvanic device.

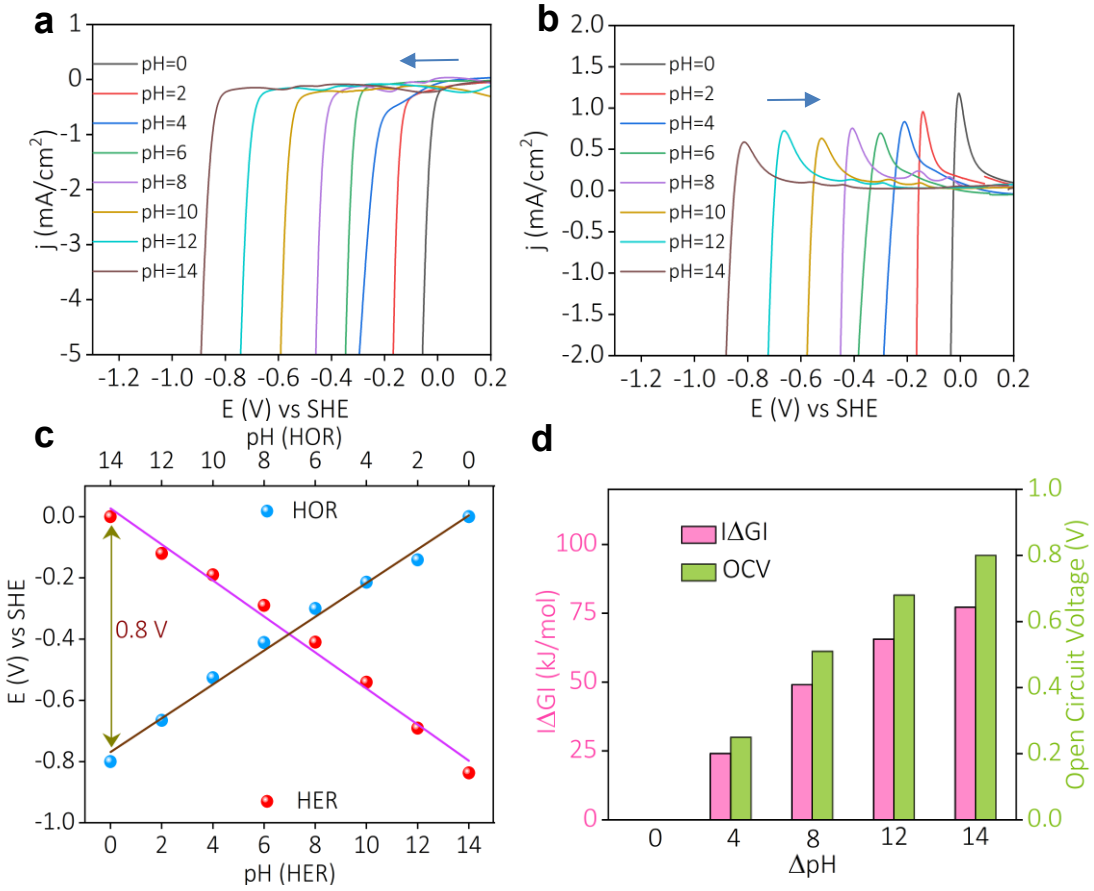

Figure 2.1: (a) Hydrogen evolution reactions (HER) and (b) hydrogen oxidation reactions (HOR) in different pH solutions at a scan rate of 10 mV/s on a platinum electrode. (c) Pourbaix diagrams for HER and HOR reactions. (d) Free energy change and open circuit potential vs. pH gradient plot.

a corresponding hydrogen evolution reaction (HER) occurring in the cathodic half-cell (equation 2.2). The overall reaction (equation 2.3) does not involve any hydrogen consumption, but it involves the formation of water molecules, and consequently, water formation energy is the driving force for the operation of this device (Calculation 2.1).

Anodic half-cell reaction:

$$2H_2O + 2e^- \leftrightarrow H_2 + 2OH^- \quad \text{(equation 2.1)}$$

Cathodic half-cell reaction:

$$2H^+ + 2e^- \leftrightarrow H_2 \quad \text{(equation 2.2)}$$

Overall cell reaction:

$$2H^+ + 2OH^- \leftrightarrow 2H_2O \quad \text{(equation 2.3)}$$

Calculation 2.2

The total cell reaction for the water formation cell is:

$H^+ (aq) + OH^- (aq) \rightarrow H_2O (l)$

The free energy change for that reaction can be written as follows:

$\Delta G = \Delta G^\circ + RT \ln \left({}^{product}/_{reactant}\right)$

$\Delta G = \Delta G^\circ + RT \ln \left({}^{[H_2O]}/_{[H^+][OH^-]}\right)$

$\Delta G = \Delta G^\circ - RT \ln [H^+] - RT \ln [OH^-]$

$\Delta G = \Delta G^\circ - RT\ 2.303 (\log[H^+] + \log [OH^-])$

$\Delta G = \Delta G^\circ - RT\ 2.303 (-pH - pOH)$

$\Delta G = \Delta G^\circ + RT\ 2.303 (pH + pOH)$

$\Delta G = \Delta G^\circ + RT\ 2.303 (pH_A + 14 - pH_B)$,

where pH_A = pH of acidic electrolyte and pH_B = pH of alkaline electrolyte

$\Delta G = \Delta G^\circ + RT\ 2.303 (pH_A - pH_B) + RT\ 2.303*14$

$\Delta G = \Delta G^\circ - RT\ 2.303\ \Delta pH + RT\ 2.303*14 \qquad (pH_B > pH_A)$

$\Delta G = -79.8 - 5.7\Delta pH + 79.8$

$\Delta G = -5.7\ \Delta pH$

$E = {}^{-\Delta G}/_{nF} = 0.059\ \Delta pH$

The device to harvest the water formation energy with the help of hydrogen redox demonstrated a peak power density of ~44 mW/cm^2 at a peak current density of ~110 mA/cm^2, without any temperature gradients (at room temperature and pressure), Figure 2.2a. Without an H_2 stream, there is no significant power in the polarization plot (Figure 2.2b). From galvanostatic polarization at a constant current of 40 mA/cm^2, with and without hydrogen (Figure 2.2c), it can be conveyed that H_2 redox is inevitable for this device, without which the polarization dropped abruptly (red trace in Figure 2.2c). During the galvanostatic discharge, the concentration of H^+ in the catholyte and OH^- in the anolyte are measured with respect to time by acid-base titration, (Figure 2.2d). When current is drawn, H^+ in the catholyte and OH^- in the anolyte get consumed, and hence, the pH gradient (ΔpH) between the two half-cells decreases as a function of time. Consequently, the cell potential should decrease with time as it is related to ΔpH (equation 2.4, Calculation 2.2). This is clearly seen in Figure 2.2d, where the electromotive force tends to zero in nearly 10 hours when a constant current is drawn from the device, signaling the convergence of pH gradients towards zero. This suggests the involvement of H^+ and OH^- ions in the overall reaction. It should be noted that when no current is drawn and when the cell is kept idle, the changes in concentrations of H^+/OH^- dual ions were around 3.5 millimoles for a period of 100 hours, (Figure 2.2e). This corresponds to a self-discharging rate of ~1.2 mV/h under open circuit operations. Which is negligibly small. During electric power delivery for a duration of nearly 10.5 hours (Figure 2.2d), the changes in H^+/OH^- dual ion concentration were nearly 17 mM, which was ~50 times higher than under open circuit conditions, Figure 2.2e. Therefore, during the delivery of electric power, the loss in H^+/OH^- dual ion gradient is majorly due to electrochemical neutralization rather than diffusion-driven self-discharging. Nevertheless, the self-discharging of this hybrid device can be mitigated thanks to the force of electric fields i.e., H^+ tends to migrate to the cathode while OH^- will migrate to the anode, which can, to some extent, prevent the mixing of H^+/OH^-. In addition, a flow cell with continuously freshening catholyte and anolyte can also benefit from maintaining a rather stable pH gradient between anode and cathode. In-situ electrochemical mass spectrometry of the cathodic and anodic half-cells of the device shows H_2 gas evolution in the acidic cathode (blue trace in Figure 2.2f) and H_2 gas consumption in alkaline anode (red trace in Figure 2.2f), respectively, during the device operation. All these indicate that using hydrogen

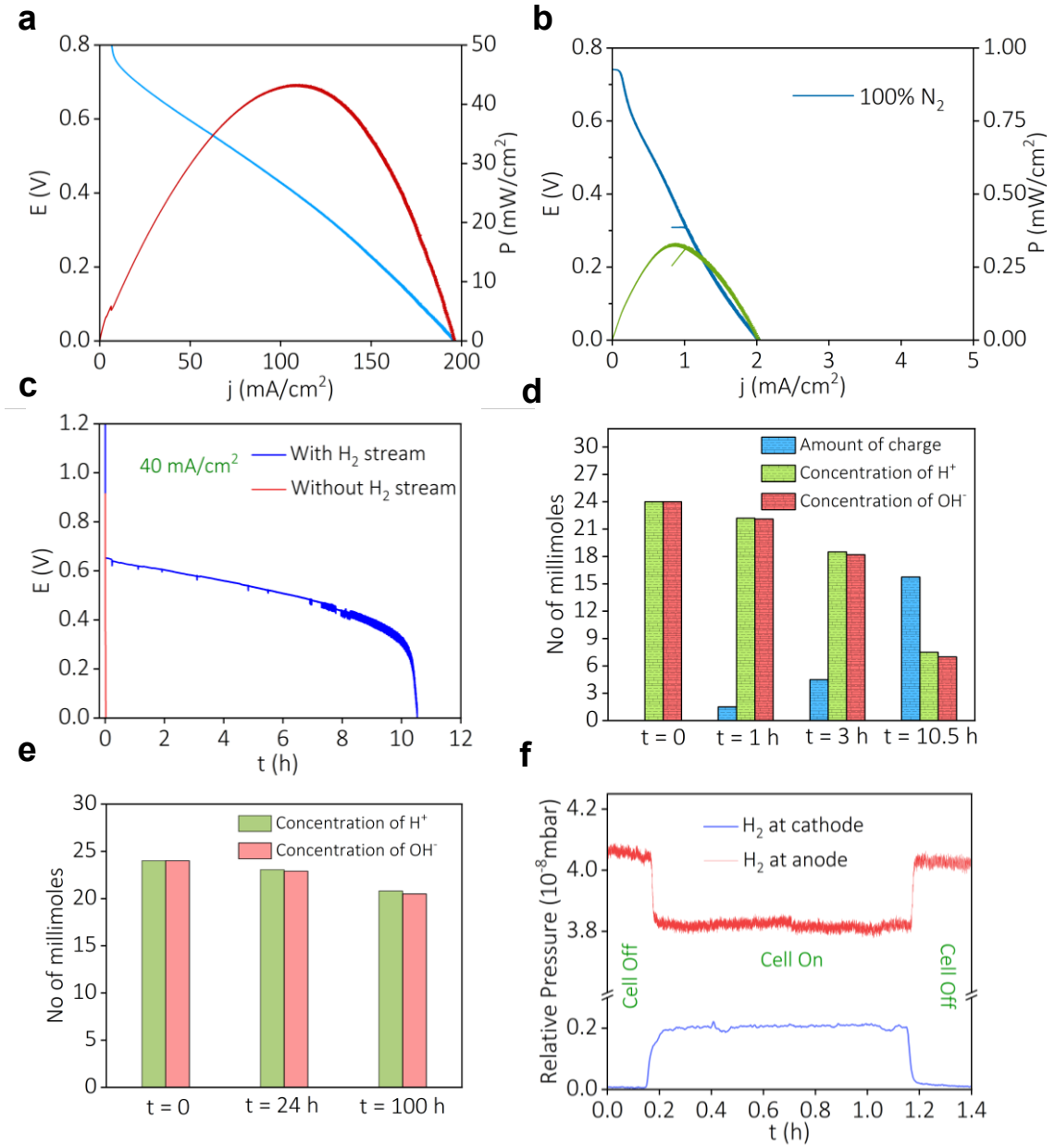

Figure 2.2: Polarization curves for water formation cell (a) with and (b) without H_2 as feed gas stream (10 mL/min). (c) Galvanostatic polarizations at a constant current density of 40 mA/cm^2 with and without H_2 gas as an anodic feed gas stream. (d) Correlation between the charge passed and the remaining amount of H^+/OH^- dual ion concentration in the half cells during the long-term discharge. (e) H^+/OH^- dual ion concentrations before and after keeping the water formation cell under open circuit condition for various time intervals. (f) In situ electrochemical mass spectrometry of cathodic half and anodic half-cells of the water formation cell.

redox, water formation energy can be harvested as an electrical driving force without a net redox, as in equation 2.3. At a surplus concentration of H^+/OH^- dual ion, the amount of H_2 consumed in the anodic half-cell decides the extent of electron release, which in

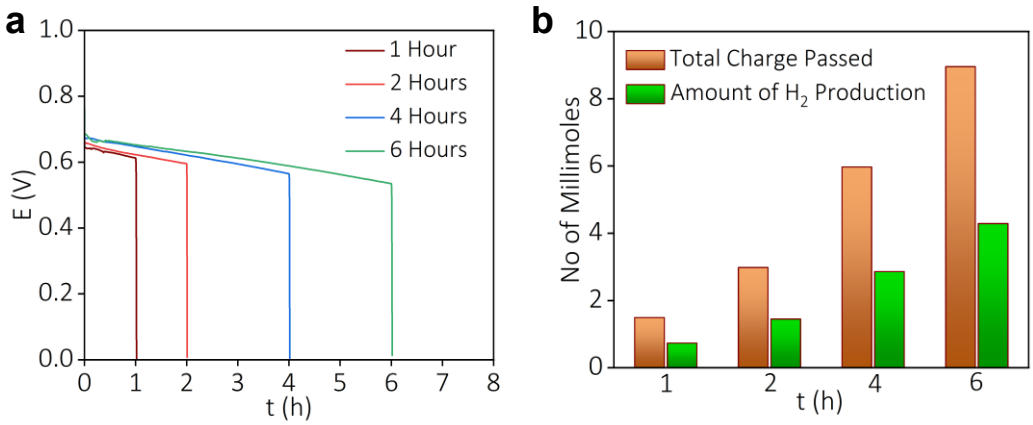

Figure 2.3: (a) Galvanostatic polarizations at 40 mA/cm^2 for different amounts of H_2 as the anodic feed gas streams. and (b) Correlation between the amount of produced hydrogen and the amount of charge passed.

turn decides the amount of H_2 evolved in the cathodic half-cell (Figure 2.3).

In order to investigate the influence of temperature on the water formation reaction, the potential output was measured with the variation in temperature. Firstly, the temperature dependence of each half-cell reaction of the water formation cell is investigated to understand how the half-cell reaction thermodynamics contributes to the device operation. In the case of the acidic cathodic half-cell, it can be observed that the potential of hydrogen redox increases with the rise in temperature, blue trace in Figure 2.4a. This leads to a positive Seebeck coefficient of 1.62 ± 0.11 mV/K, which holds the potential to be utilized in a thermogalvanic cell. The alkaline hydrogen redox also shows a proportional increment of potential with the increase in temperature (red trace in Figure 2.4a), but the magnitude of the increment is quite low, resulting in a Seebeck coefficient of 0.42 ± 0.06 mV/K. The magnitude of potentials for acidic and alkaline hydrogen redox in Figure 2.4a dictates the choice of the hot acidic side as the cathodic half-cell and the cold alkaline side as the anodic half-cell for the water formation-based thermogalvanic system. The open circuit voltage for the water formation cell rises with the increase in temperature of the surroundings (Figure 2.4b), which provides the ability to withdraw energy from the surroundings during the water formation reaction. In the case of a traditional H_2 - O_2 fuel cell, the open circuit voltage drops with the increase in the surrounding temperature (Figure 2.4c), causing a loss of energy from the system to the surroundings as heat during the operation of the fuel cell. The water formation cell has a positive Seebeck coefficient value of 1.38 ± 0.11 mV/K along with partial molar entropy

change of around 266.34 J mol^{-1} K^{-1}(Figure 2.4d), which consolidates the fact of a thermodynamic efficiency value greater than 1, Calculation 2.1, 2.3. On the other hand, the H_2 - O_2 fuel possesses a negative Seebeck coefficient with a magnitude of -1.96 ± 0.06 mV/K with a negative entropy change of - 756 J mol^{-1} K^{-1} (Calculation 2.3), Figure 2.4d. This consolidates the fact that electrical energy output from a water-formation cell will expand with an increment in the temperature, which is not the case for the H_2 - O_2 fuel cell.

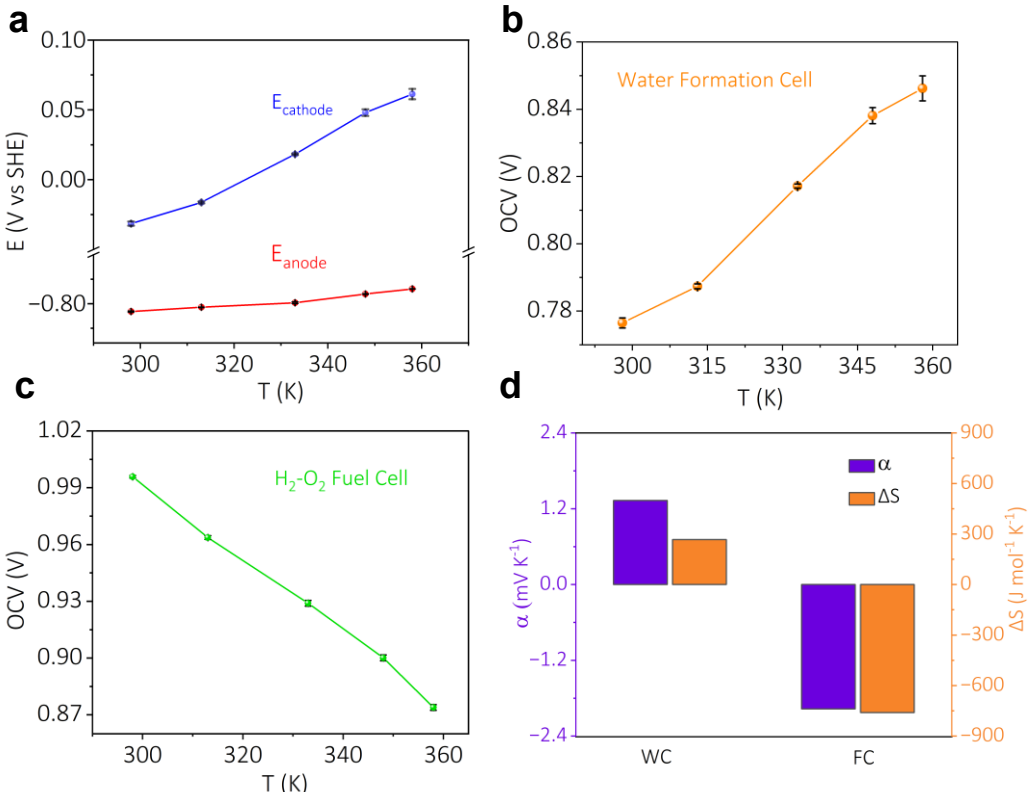

Figure 2.4: (a) The variation of the potential of hydrogen redox in acidic (blue trace) and alkaline half-cells (red trace) with respect to surrounding's temperature. The temperature dependency of open circuit voltage for (b) the water formation cell and (c) the H_2-O_2 fuel cell. (d) The comparison of the Seebeck coefficient and partial molar entropy change between the water formation cell (WC) and the H_2-O_2 fuel cell (FC).

Calculation 2.3

For water formation cell,

The Seebeck coefficient (α) for the water formation cell = 1.38 ± 0.11 mV/K

No. of electrons = 2

Faradaic constant = 96500 C. mol^{-1}

Partial molar entropy change (ΔS) = n. F. α

$= 2 * 96500 * (1.38 \pm 0.11)$

$= 266.34 \pm 21.23$ J mol^{-1} K^{-1}

For the H_2 - O_2 fuel cell,

The Seebeck coefficient (α) for the fuel cell = - 1.96 ± 0.06 mV/K

No. of electrons = 4

Faradaic constant = 96500 C. mol^{-1}

Partial molar entropy change (ΔS) = n. F. α

$= 4 * 96500 * (- 1.96 \pm 0.06)$

$= - 756.56 \pm 24.7$ J mol^{-1} K^{-1}.

From Figure 2.4a, it is obvious that if an acidic half-cell at a high temperature and an alkaline half-cell at a relatively cold temperature are coupled together, a maximum voltage output can be achieved. The open circuit voltage of the water formation cell was measured with and without the temperature gradient between the two half cells, Figure 2.5a. The temperature gradient (ΔT = 55⁰) in the water formation cell leads to a rise in the open circuit voltage of the cell with a magnitude of 67 mV, Figure 2.5a. The polarization performance with a temperature gradient (sky blue trace in Figure 2.5b) exhibits superiority over the isothermal water formation cell, (orange trace in Figure 2.5b). The water formation cell with a temperature gradient (ΔT = 55⁰) achieves a peak power density of 53 mW/cm^2 at a peak current density of 130 mA/cm^2. The peak power density has risen from 43 mW/cm^2 to 53 mW/cm^2 with the inclusion of a temperature gradient of 55⁰. The galvanostatic polarization at a constant current density of 40 mA/cm^2 also reflects a similar performance matrix, Figure 2.5c. The cathodic exhaust of the thermogalvanic cell has been investigated via in-situ electrochemical mass spectrometry at a constant current of 40 mA/cm^2, and in both cases, there is an evolution of pure H_2 in the cathodic exhaust, Figure 2.5d. It should be noted that a similar amount of hydrogen

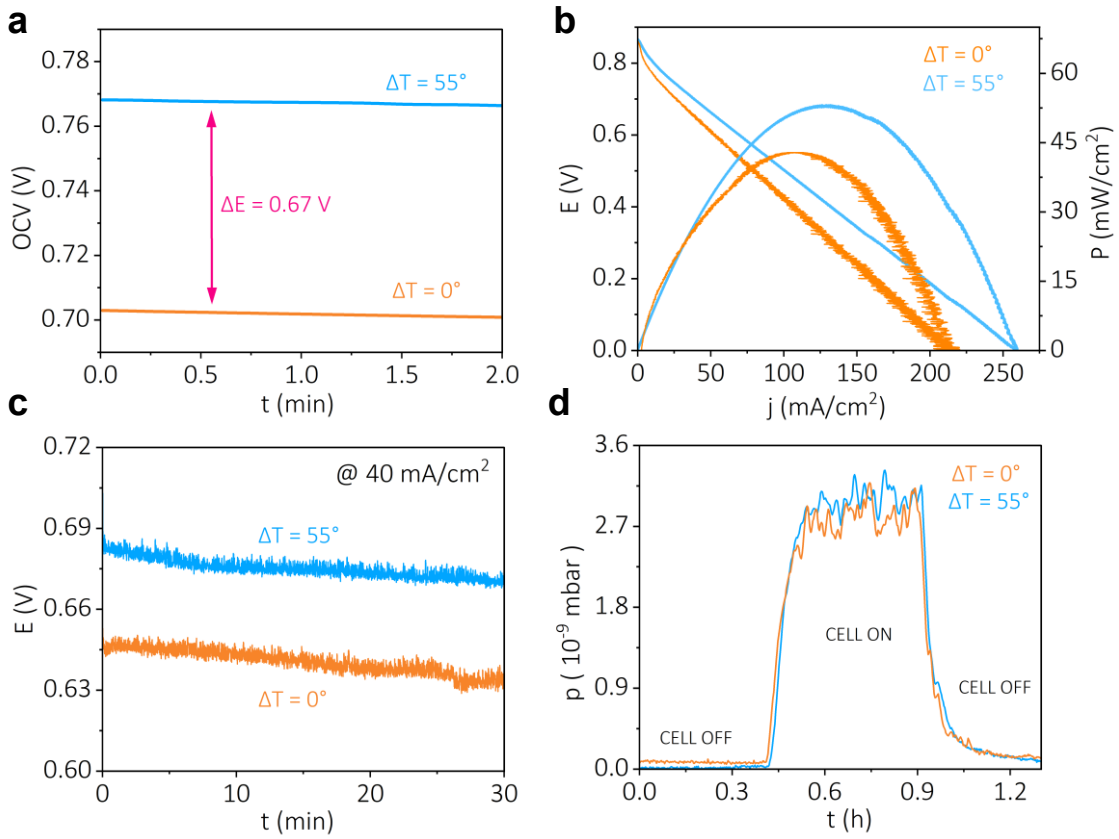

Figure 2.5: (a) Open circuit voltages (b) polarisation curves (c) chronopotentiometry at 40 mA/cm² and (d) constant current (40 mA/cm²) in situ electrochemical mass spectra of the cathodic half-cell of the water formation cell with and without temperature gradient (ΔT = 55⁰) between the two half cells.

gas evolved with a higher potential output for the temperature gradient cell as compared to the isothermal cell, Figure 2.5c and 2.5d.

To know where this water formation reaction-based thermogalvanic cell stands, it is compared with a state-of-the-art aqueous thermogalvanic system based on a ferrocyanide/ferricyanide (Fe^{2+}/Fe^{3+}) redox system. Firstly, the temperature dependence was investigated with the ferrocyanide/ferricyanide (Fe^{2+}/Fe^{3+}) system, which shows a drop in the electromotive force with a rise in temperature, Figure 2.6a. The Seebeck coefficient of this system turns out to be negative in nature with a magnitude of -1.49 ± 0.13 mV/K, which is opposite in nature with respect to the water formation reaction. The device consisting of a ferrocyanide/ferricyanide (Fe^{2+}/Fe^{3+}) system shows no significant open circuit voltage at an isothermal state, green trace in Figure 2.6b. Introduction of a temperature gradient of nearly 55⁰ in this system, the thermogalvanic system provides an

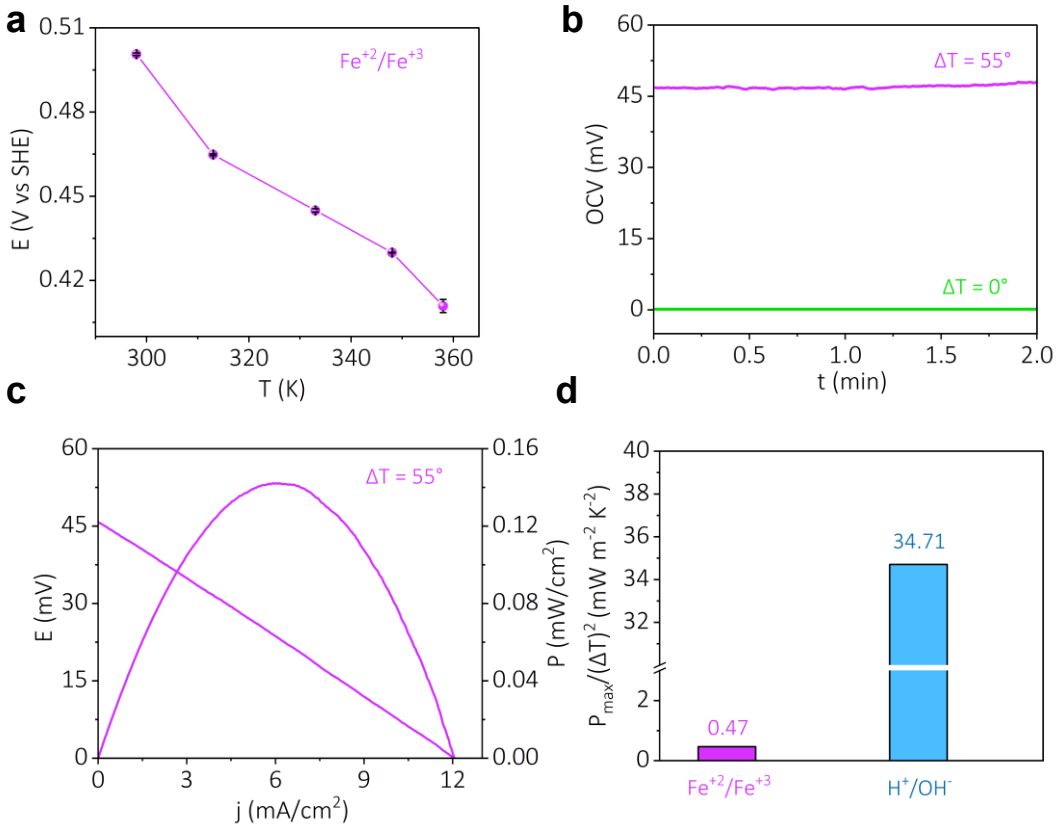

Figure 2.6: (a) The temperature dependency of the potential for the ferrocyanide/ferricyanide (Fe^{2+}/Fe^{3+}) redox system. (b) Open circuit voltages (c) polarisation curves for the ferrocyanide/ferricyanide (Fe^{2+}/Fe^{3+}) redox-based thermogalvanic device. (d) Comparison of the temperature-insensitive maximum power density between the water formation-based and ferrocyanide/ferricyanide (Fe^{2+}/Fe^{3+}) redox-based thermogalvanic system.

open circuit voltage of around 47 mV, violet trace in Figure 2.6b. The polarization curve for this ferrocyanide/ferricyanide-based (Fe^{2+}/Fe^{3+}) thermogalvanic system provides a peak power density of 0.15 mW/cm^2 at a peak current density of 6 mA/cm^2, Figure 2.6c. Upon comparison, it is evident that the thermogalvanic system based on water formation reaction has the upper hand over the ferrocyanide/ferricyanide-based system. This water formation-based thermogalvanic device has a temperature-insensitive maximum power density of ~ 34.7 $mWcm^{-2}K^{-2}$ (Calculation 2.4), which is almost 70 times higher than standard ferrocyanide-ferricyanide based thermogalvanic system, Figure 2.6d. Taken together, the water formation reaction-based thermogalvanic system holds promise for extensive heat harvesting from pH gradient as well as temperature gradient.

Calculation 2.4

For water formation reaction-based thermogalvanic system,

From Figure 2.5b,

Peak power density (P_{max}) ($\Delta T = 55^0$) = 53.5 mW/cm^2

Peak power density (P_{max}) ($\Delta T = 0^0$) = 43 mW/cm^2

ΔP_{max} = 10.5 mW/cm^2 ; ΔT = 55 K

Temperature-insensitive maximum power density ($^{\Delta P_{max}}/_{\Delta T^2}$) = $^{10.5}/_{55^2}$

= 0.003471 $mWcm^{-2}K^{-2}$

= 34.71 $mWm^{-2}K^{-2}$

For ferrocyanide/ferricyanide redox-based thermogalvanic system,

From Figure 2.6c,

Peak power density (P_{max}) ($\Delta T = 55^0$) = 0.143 mW/cm^2

ΔT = 55 K

Temperature-insensitive maximum power density ($^{\Delta P_{max}}/_{\Delta T^2}$) = $^{0.143}/_{55^2}$

= 0.000047 $mWcm^{-2}K^{-2}$

= 0.47 $mWm^{-2}K^{-2}$

2.3 Conclusion

Electrochemical heat harvesting through thermogalvanic cells exploits temperature gradients (ΔT) to generate electrical energy based on the Seebeck effect. The water formation reaction in an electrochemical cell has a positive Seebeck coefficient of nearly 1.38 mV/K, which creates an opportunity for heat harvesting by decoupling the direct acid-alkali chemistry . Alkaline hydrogen oxidation at cold temperatures and acidic hydrogen evolution at hot temperatures significantly boost voltage and electrical energy output. This proposed thermogalvanic device has a high temperature-insensitive power output efficiency of ~ 34.7 $mWcm^{-2}K^{-2}$, which is 70 times higher than state of the art ferricyanide based heat harvesting devices, thereby holding promise for enhanced waste heat recovery.

2.4 Experimental Section

2.4.1 Materials

H_2SO_4 (98%), NaOH (97%), oxalic acid (98%), AgCl (98%), KCl (99%), H_2O_2, CH_3COOH (99%), CH_3COONa (99%), $KHSO_4$ (98%), K_2SO_4 (99%), K_2HPO_4 (98%), KH_2PO_4 (99%), H_3PO_4 (88%), Agar-agar, $K_4[Fe(CN)_6]$ (99.9%), $K_3[Fe(CN)_6]$ (99.9%) and phenolphthalein were purchased from Sigma Aldrich. Pt supported on carbon catalyst (0.5 mg/cm^2 Pt/C), and Nafion117 cation exchange membrane were obtained from Fuel Cell Store (USA).

2.4.2 Electrochemical Study (Single Compartment)

Electrochemical measurements were carried out using a Biologic (VMP-300) electrochemical workstation. A three-electrode system with platinum (0.031 cm^2) as the working electrode and a larger area of platinum mesh as the counter electrode. Ag/AgCl (3.5M KCl) as the reference electrode was utilized for Cyclic voltammetry experiments. 15 mL of electrolyte was used for each measurement. The electrolyte solutions with varying pH like pH = 0 (H_2SO_4), pH = 2 (sulfate buffer), pH = 4 (acetate buffer), pH = 6,8,10,12 (phosphate buffer), pH = 14 (NaOH) were used for pH-dependent study.

2.4.3 In-situ Electrochemical Mass Spectrometry

In-situ electrochemical mass spectrometry was conducted with an HPR-40 (Hiden Analytical) quadruple mass analyzer using a standard QIC inlet. The experiment was carried out with the help of a 'T' shaped connector where three sides are a mass spectrometer inlet, cell outlet, and exhaust to the surroundings. For the cathodic half-cell experiments, Argon (Ar) was used as the carrier gas. The generated gas flow from the cell was supplied to mass the spectrometer inlet via the 'T' connector.

2.4.4 Electrochemical Study (Double compartment)

Polyacrylic sheets were used to construct a two-compartment laboratory prototype for the water formation cell. The electrolytes are pumped inside the two half-cells using two peristaltic pumps at a constant flow rate of 10 ml/min. The device's two half-cells were divided using a Nafion 117 membrane. Before it was utilized in the cell, the Nafion 117 membrane was pretreated with an acidic H_2O_2 solution at 80°C. The membrane was sandwiched between two silicone washer gaskets to prevent intercompartment leakage. The cathodic electrocatalyst for the water formation cell was electrodeposited Pt on Ti mesh (obtained by applying 5 mA/cm^2 continuous current for 10 minutes in chloro-

platinic acid solution), whereas the anodic electrocatalyst for the water formation cell was coated with Pt/C on Toray carbon paper. Table 2.1. Carbon sheets were used as the cathode and anode for the ferrocyanide-ferricyanide redox-based thermogalvanic system.

Table 2.1: Catalyst loading used at the anodic and cathodic half-cells of the electrochemical water formation cell.

	Cathode	Anode
Catalyst	Pt on Ti mesh	Pt/C (Pt:C = 2:3)
Amount	1.5 mg/cm^2	1 mg/cm^2

All the electrochemical experiments were performed under room temperature and pressure. Quantification of generated hydrogen was carried out by water displacement technique. The concentration of anolyte and catholyte was measured by acid-base titration with a phenolphthalein indicator. Oxalic acid was used as the primary standard. Firstly, the prepared NaOH was standardized with oxalic acid. Then, the catholyte from the cell is titrated with the standardized NaOH, and the concentration of the catholyte is determined. The concentration of anolyte is determined by titration with the oxalic acid.

2.4.5 Temperature Dependent Study

Temperature-dependent studies were conducted in both the device mode and three-electrode assembly mode. In the case of the three-electrode assembly mode, the working and counter electrodes were connected to the reference electrode via a salt bridge and the potential values were measured non isothermally (by keeping the temperature of the reference electrode constant while that of the working electrode is scanned). The salt bridge was prepared by mixing agar-agar and Na_2SO_4 in an aqueous solution at 75^{0}C. The chamber with working and counter electrodes was heated to different temperatures, and the reference electrode was kept at room temperature to avoid fluctuations in the reference electrode's potential. The heating mantle was used to heat the working electrode compartment. The potential of the working electrode was measured at a

temperature of 298 K to 358 K. In the device, a temperature gradient of 55 K was maintained between the half-cells.

2.5 References

1. E. Aramendia, P. E. Brockway, P. G. Taylor, J. B. Norman, M. K. Heun and Z. Marshall, Nat. Energy, 2024, **9**, 803–816.
2. M. Büchs, N. Cass, C. Mullen, K. Lucas and D. Ivanova, Nat. Energy, 2023, **8**, 758–769.
3. I. Staffell, D. Scamman, A. Velazquez Abad, P. Balcombe, P. E. Dodds, P. Ekins, N. Shah and K. R. Ward, Energy Environ. Sci., 2019, **12**, 463–491.
4. C. Verma, D. S. Chauhan, R. Aslam, P. Banerjee, J. Aslam, T. W. Quadri, S. Zehra, D. K. Verma, M. A. Quraishi, S. Dubey, A. AlFantazi and T. Rasheed, Green Chem., 2024, **26**, 4270–4357.
5. G. Lopez, D. Keiner, M. Fasihi, T. Koiranen and C. Breyer, Energy Environ. Sci., 2023, **16**, 2879–2909.
6. C. Forman, I. K. Muritala, R. Pardemann and B. Meyer, Renew. Sustain. Energy Rev., 2016, **57**, 1568–1579.
7. Ø. Hodnebrog, G. Myhre, C. Jouan, T. Andrews, P. M. Forster, H. Jia, N. G. Loeb, D. J. L. Olivié, D. Paynter, J. Quaas, S. P. Raghuraman and M. Schulz, Commun. Earth Environ., 2024, **5**, 1–9.
8. A. G. Olabi, K. Elsaid, E. T. Sayed, M. S. Mahmoud, T. Wilberforce, R. J. Hassiba and M. A. Abdelkareem, Nano Energy, 2021, **84**, 105871.
9. P. Simeoni, G. Ciotti, M. Cottes and A. Meneghetti, Energy, 2019, **175**, 941–951.
10. R. Agathokleous, G. Bianchi, G. Panayiotou, L. Aresti, M. C. Argyrou, G. S. Georgiou, S. A. Tassou, H. Jouhara, S. A. Kalogirou, G. A. Florides and P. Christodoulides, Energy Procedia, 2019, **161**, 489–496.
11. C. Gao, S. W. Lee and Y. Yang, ACS Energy Lett., 2017, **2**, 2326–2334.
12. S. Pu, Y. Liao, K. Chen, J. Fu, S. Zhang, L. Ge, G. Conta, S. Bouzarif, T. Cheng, X. Hu, K. Liu and J. Chen, *Nano Lett.*, 2020, **20**, 3791–3797.
13. J. Duan, B. Yu, L. Huang, B. Hu, M. Xu, G. Feng and J. Zhou, Joule, 2021, **5**, 768–779.
14. T. I. Quickenden and Y. Mua, J. Electrochem. *Soc.*, 1995, **142**, 3985–3994.

15. M. A. Buckingham, K. Laws, H. Li, Y. Kuang and L. Aldous, Cell Reports Phys. Sci., 2021, **2**, 100510.
16. H. Zhou, T. Yamada and N. Kimizuka, J. Am. Chem. Soc., 2016, **138**, 10502–10507.
17. J. Duan, G. Feng, B. Yu, J. Li, M. Chen, P. Yang, J. Feng, K. Liu and J. Zhou, Nat. Commun., 2018, **9**, 1–8.
18. T. J. Abraham, D. R. MacFarlane and J. M. Pringle, Energy Environ. Sci., 2013, **6**, 2639–2645.
19. S. W. Lee, Y. Yang, H. W. Lee, H. Ghasemi, D. Kraemer, G. Chen and Y. Cui, Nat. Commun., 2014, **5**, 1–6.
20. L. Yang, H. Sun, S. Wang, L. Jiang and G. Sun, Int. J. Hydrogen Energy, 2017, **42**, 25877–25881.
21. N. S. Hudak and G. G. Amatucci, J. Electrochem. Soc., 2011, **158**, A572.
22. L. B. Hubrechtsen, L. L. De Taeye and P. M. Vereecken, Chem. Mater., 2023, **35**, 5612–5630.
23. W. Fang, H. Luo, I. Mwamburi Mwakitawa, F. Yuan, X. Lin, Y. Wang, H. Yang, T. Shumilova, L. Hu, Y. Zheng, C. Li, J. Ouyang, K. Sun, ChemSusChem 2024, e202401749.
24. H. Chen, H. Zou, F. Zhong, M. Qu, S. Zhao, X. Wei, D. Hong, Y. Song and Z. Liu, Nano Energy, 2024, **129**, 109992.
25. T. Kim, J. S. Lee, G. Lee, H. Yoon, J. Yoon, T. J. Kang and Y. H. Kim, Nano Energy, 2017, **31**, 160–167.
26. C. G. Han, Y. Bin Zhu, L. Yang, J. Chen, S. Liu, H. Wang, Y. Ma, D. Han and L. Niu, Energy Environ. Sci., 2023, **17**, 1559–1569.
27. X. He, H. Sun, Z. Li, X. Chen, Z. Wang, Y. Niu, J. Jiang and C. Wang, J. Mater. Chem. *A*, 2022, **10**, 20730–20755.
28. S. Jia, W. Qian, P. Yu, K. Li, M. Li, J. Lan, Y. H. Lin and X. Yang, Mater. Today Phys., 2024, **42**, 101375.
29. J. Zhang, X. Li, J. Zheng, Z. Hu, Y. Xiao, W. Yang, S. Zhang, Z. Zhou and S. Han, Sol. Energy, 2024, **282**, 112939.
30. W. Li, J. Ma, J. Qiu and S. Wang, Mater. Today Energy, 2022, **27**, 101032.
31. Y. Ding, P. Cai and Z. Wen, Chem. Soc. Rev., 2021, **50**, 1495–1511.

32. Z. M. Bhat, D. Pandit, S. Ardo, R. Thimmappa, A. R. Kottaichamy, N. Christudas Dargily, M. C. Devendrachari and M. Ottakam Thotiyl, Joule, 2020, **4**, 1730–1742.
33. R. Mondal, R. Thimmappa, B. Nayak, A. Dewan, M. C. Devendrachari, Q. Chen, Z. Wen and M. O. Thotiyl, Energy Environ. Sci., 2023, **16**, 3860–3872.
34. L. Fan, Y. Ji, G. Wang, J. Chen, K. Chen, X. Liu and Z. Wen, J. Am. Chem. Soc., 2022, **144**, 7224–7235.
35. R. Mondal, B. Nayak and M. Ottakam Thotiyl, J. Phys. Chem. Lett., 2024, **15**, 6866–6871.

Chapter 3

A Spontaneous Electrochemical Fuel Purifier under Ambient Weather Conditions

Abstract

The hydrogen economy is an ideal energy vector to offer a carbon-neutral energy pathway. However, the contamination of produced hydrogen with carbonaceous and non-carbonaceous impurities beyond the tolerance level of a fuel cell always demands exceptionally endergonic fuel separation modules requiring multiple steps and extreme temperatures and pressures (- 85°C to -15°C and 7 to 30 bar). These contribute to a severe energy imbalance between the key steps of hydrogen production and hydrogen utilization. By directly harvesting the water-formation energy, a spontaneous fuel purification is demonstrated under truly ambient weather conditions, including an open-air environment, wherein contaminated hydrogen streams can be purified to nearly 99.9 % purity in a single step at the expenditure of ~24 kJ/mol_{H2} with an electrical energy output of ~90 kJ/mol_{H2}. As a major leap in the hydrogen economy, a laboratory-level prototype can spontaneously generate ~99.4 % pure hydrogen in a single step even from a quaternary mixture of impurities, including hydrocarbons, CO_2 and N_2.

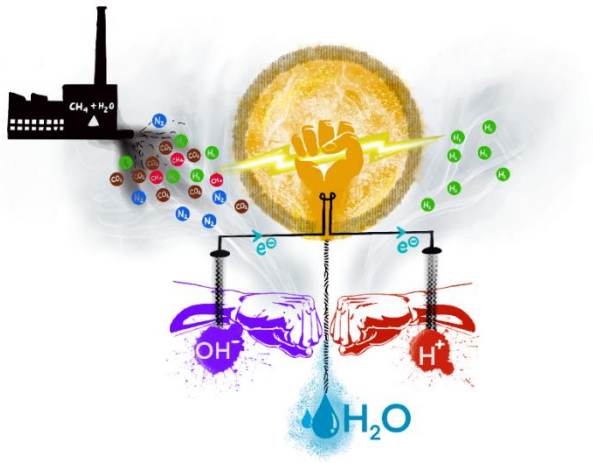

This work has been published in the following journal:

Ritwik Mondal et al. *Energy Environ. Sci.* **2023**, *16* (9), 3860–3872.

Introduction

The hydrogen economy is being touted as an ideal energy vector across the globe as its combustion for energy generation occurs with a near zero-carbon footprint,[1-4] which in turn has the potential to rejuvenate the life on this planet by stabilizing the global mean temperatures.[5-8] However, the implementation of the hydrogen economy is thwarted by the physicochemical properties of gaseous hydrogen which has led to hydrogen storage molecules as safer hydrogen carrier molecules.[9-11]Among the hydrogen storage molecules, lower aliphatic alcohols such as methanol are considered attractive candidates for storing hydrogen as they are in the liquid state at room temperature with a reasonable weight percent of hydrogen.[12] Nevertheless, state-of-the-art steam reforming of alcohols to release hydrogen is technologically incompetent as it requires significant energy input such as high temperature >200°C and high pressure >25 bar.[13] The hydrogen fuel produced by these techniques is carbonized with impurities such as CO, CO_2, and hydrocarbons, along with other impurities like N_2, NH_3, sulphur, O_2, H_2O vapor, etc., which are often beyond the tolerance level of a proton exchange membrane fuel cell.[14-16] Therefore, the impure fuel streams must be purified before feeding it into a fuel cell, and state-of-the-art fuel separation techniques such as cryogenic distillation (-85°C to -15°C, 7 to 30 bar), pressure swing adsorption (100°C to 400°C, 5 to 25 bar), and membrane-based methods (0.5 to 1 bar, 200°C to 400°C), etc., are highly endergonic and require expensive, and sophisticated instrumentations.[17-19] These techniques often require numerous steps to achieve a certain purity level, which further demands additional energy expenses.[20,21] The fact that higher energy investment is required for H_2 production and purification than that can be recovered by its utilization in a fuel cell eventually contributes to a serious energy imbalance between energy storage and energy conversion pathways.

Differing from the existing approach, an exergonic pathway for hydrogen fuel purification technique is shown, wherein a newly designed device that can directly harvest the water formation energy from H^+/OH^- dual ions can purify carbonized and contaminated hydrogen fuel streams at room temperature and pressure during electricity production. Thermodynamic calculation (Calculation 3.1) shows that water formation

from the H^+/OH^- dual-ion gradient has an inbuilt energy that can be converted to electrical energy.

Calculation 3.1

Water formation Reaction from H^+ and OH^- dual ions

$H^+ + OH^- \leftrightarrow H_2O$

Enthalpy changes for the reaction.

$\Delta H^0 = H^0 (H_2O) - H^0 (H^+) - H^0 (OH^-)$

$= -285.8 - 0 - (-230)$

$= \mathbf{-55.8\ kJ/mol}$

Entropy changes for the reaction

$\Delta S^0 = S^0 (H_2O) - S^0 (H^+) - S^0 (OH^-)$

$= 69.91 - 0 - (-10.75)$

$= \mathbf{0.08066\ kJ/K\ mol}$

Gibbs free energy of the reaction

$\Delta G^0 = \Delta H^0 - T\Delta S^0$

$= -55.8 - (298 * 0.08066)$

$= \mathbf{-79.875\ kJ/mol}$

$\Delta G^0 = -nFE^0$

$E^0 = -\Delta G^0 / nF$

$E^0 = -(-79875)/1*96484$

$E^0 = \mathbf{0.82\ V}$

0.82 V of electromotive force can be harvested from the water formation energy.

Quite recently, the energy of water formation from H^+/OH^- dual ions has been explored to increase the electrical efficiency of various devices such as fuel cells, batteries,

supercapacitors, and electrolytic devices.[22-26] Here, an unprecedented application of spontaneous hydrogen fuel purification is explored via harvesting the energy of water formation in a single step under ambient conditions, interestingly with electric power production. The device can even purify hydrogen from a quaternary mixture of contaminants, including hydrocarbons, CO_2, and N_2 commonly encountered in the exhaust of a steam reformer in a single step, and the purified H_2 can be directly fed to a commercial proton exchange membrane fuel cell (PEMFC) for further energy conversion. Previous literatures[27,28] related to electrochemical fuel purification are electrolytic approaches in a thermodynamically uphill pathway. However, the spontaneous fuel purifier is galvanic in nature, wherein the fuel purification is achieved in a thermodynamically downhill pathway. Therefore, this H_2 purifier paves the way for a robust hydrogen economy because electric power is harnessed during hydrogen fuel separation as well as its utilization.

3.1 Results and Discussion

The overall fuel-purifying architecture contains an anodic alkaline half-cell and a cathodic acidic half-cell separated by a cation conducting Nafion 117 membrane, Scheme 3.1. Pt supported on carbon (Pt/C) was employed as the electrocatalyst in the anodic alkaline half-cell, and electrodeposited platinum on Ti mesh (by applying a constant current of 4 mA/cm^2 for 5 min) was used as the electrocatalyst for the cathodic acidic half-cell. The energy of water formation can be harvested by employing hydrogen redox in the pH gradient electrochemical cell. Hydrogen is oxidized at the alkaline anode with the concomitant degree of hydrogen evolution in the acidic cathode, which suggests that hydrogen is the only electroactive portion in the system. This suggests that when an impure hydrogen fuel stream is bubbled into the anodic half-cell wherein the impurities cannot be oxidized further, only hydrogen will get oxidized, and corresponding to this degree of oxidation, there should be exclusive hydrogen evolution in the cathodic half-cell. This offers opportunities for hydrogen fuel purification during electricity production. or spontaneous fuel purification at room temperature and pressure.

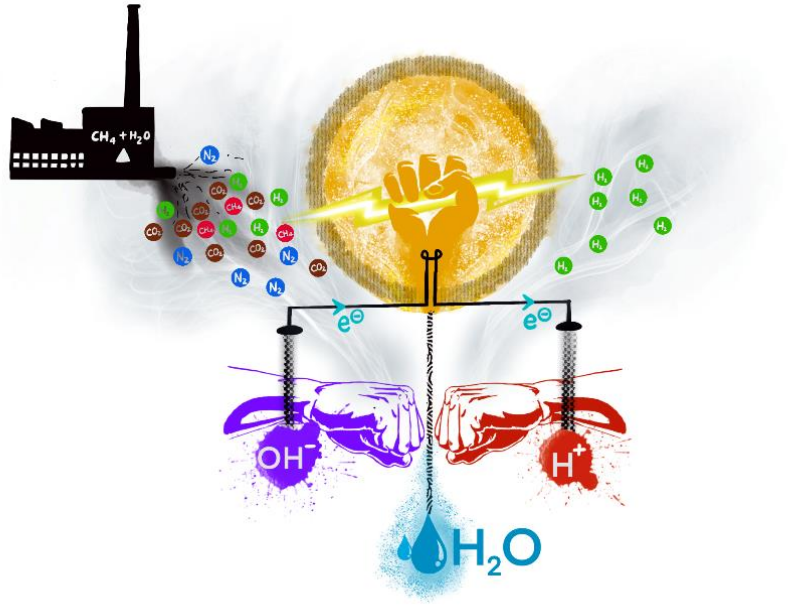

Scheme 3.1. Schematics of the spontaneous hydrogen fuel purifier.

3.1.1 Spontaneous Fuel Purification of Binary Fuel Mixtures

The common contaminants of hydrogen fuel steam during steam reforming are CO_2, N_2, CO, H_2S, CH_4, etc.[14] In order to understand how impurity affects electrochemistry, we resorted to voltammetric analysis with the binary mixtures. The outlined data suggests the decrease in limiting current and shift in the hydrogen oxidation potential can be attributed to the decrease in the hydrogen partial pressure, Figure 3.1a, 3.1b. Linear sweep voltammogram has been recorded at a scan rate of 5 mV/s with a Pt-based electrode at a rotation of 1600 rpm for impure gas mixtures in 1 M NaOH solution. In the

Table 3.1: Comparison table of limiting current densities and overpotential (at 3 mA/cm^2) for various gas mixtures (corresponds to figure 3.1a, 3.1b).

Impure Mixtures	Limiting Current (mA/cm^2)	Overpotential (mV) (at 3 mA/cm^2)
Pure H_2	7.9	0
H_2-N_2 (20%)	6.9	61
H_2-CO_2 (20%)	6	157

case of the H_2-N_2 mixture (20 %), a shift in the oxidation potential with a decrease in the limiting current density compared to pure H_2 is majorly attributed to the decrease in the partial pressure of hydrogen in the mixture (Figure 3.1a and Table 3.1). However, for the H_2-CO_2 mixture (20 %), the impurity (CO_2) can chemically react with the hydroxyl ions, eventually decreasing the pH of the solution.[29] The noticeable positive shift in the H_2 oxidation potential in the H_2-CO_2 mixture compared to pure H_2 can be attributed to this chemical consumption of OH^- by CO_2 (Figure 3.1b, Table 3.1).

Further, the prospects of fuel purification from binary gas mixtures in the spontaneous fuel purifier have been evaluated. When a 1:1 mixture of H_2 and N_2 is fed (10 mL/min) to the anodic half-cell at room temperature and pressure, the performance metrics were nearly 25 mW/cm^2 at ~52 mA/cm^2, which were almost half of the that with pure H_2 (10 mL/min), (Figure 3.1c). With CO_2 as the impurity instead of N_2, performance

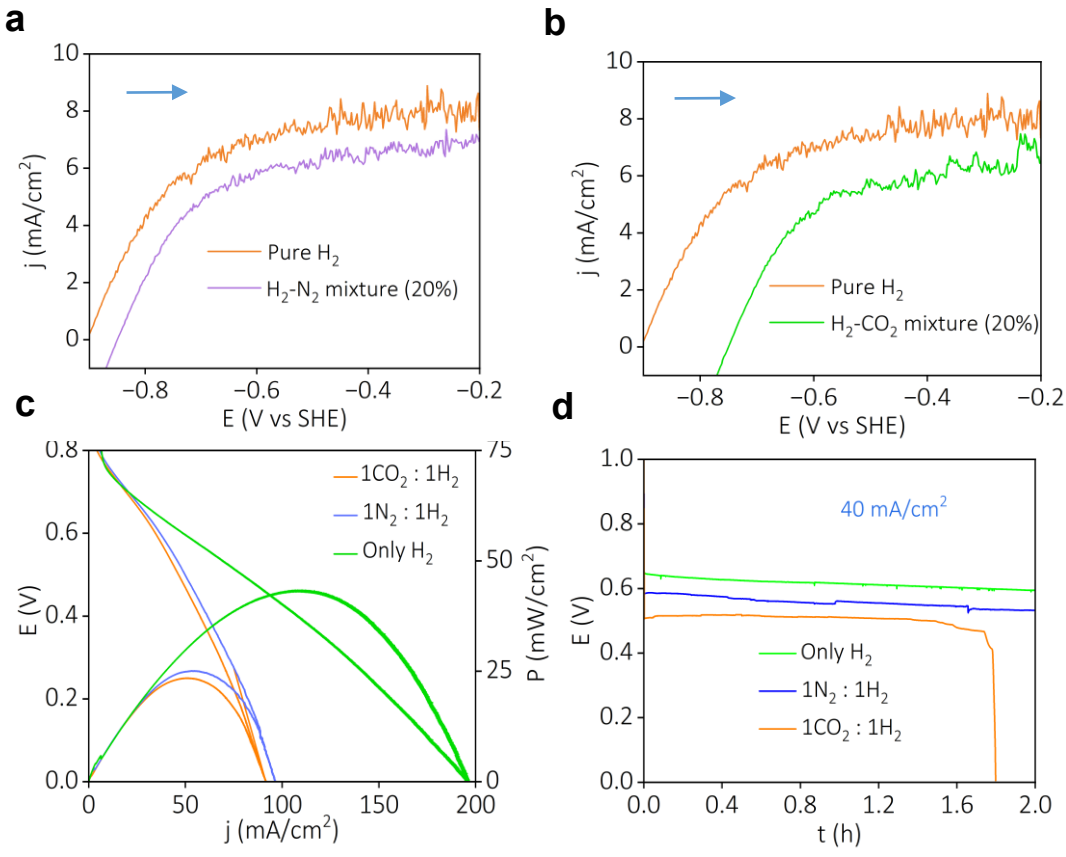

Figure 3.1: Rotating disk electrode measurements during hydrogen oxidation reaction at 1600 rpm at a scan rate of 5 mV/s on a Pt/C electrode for a) H_2-N_2 (80:20) binary mixture and (b) H_2-CO_2 (80:20) binary mixture. c) Polarization curves for H_2 purifier with pure and impure H_2 gas feed streams (10 mL/min). d) Galvanostatic polarizations at a constant current density of 40 mA/cm^2 with pure and impure H_2 gas feed streams. The impure gas streams were H_2-CO_2 (1:1) gas mixture and H_2-N_2 (1:1) gas mixture.

metrics were lower, which we attribute to the direct reaction of CO_2 with OH^- ions forming carbonates and bicarbonates.[30] When diluted HCl (0.1 M) was added to the anolyte after purging with an H_2-CO_2 mixture, there was an evolution of CO_2 bubbles due to the decomposition of carbonates. In the case of the H_2-N_2 mixture, CO_2 dissolved in the alkaline anolyte can react with hydroxyl ions to form carbonate, which is also a well-known issue in all alkali-based fuel cells. Notably, we did not see any carbonate salt forming at the anode, possibly due to the continuous bubbling of H_2, implying the issue of CO_2 in the air can be somehow mitigated by H_2 blowing.

Nevertheless, the data suggests hydrogen in the binary gas mixture is the electroactive segment. With a 1:1 impure hydrogen gas stream as the feed (10 mL/min) at the same current density as the pure hydrogen stream, the galvanostatic polarization occurred at a lower operating voltage (Figure 3.1d). Noticeably, at the same current

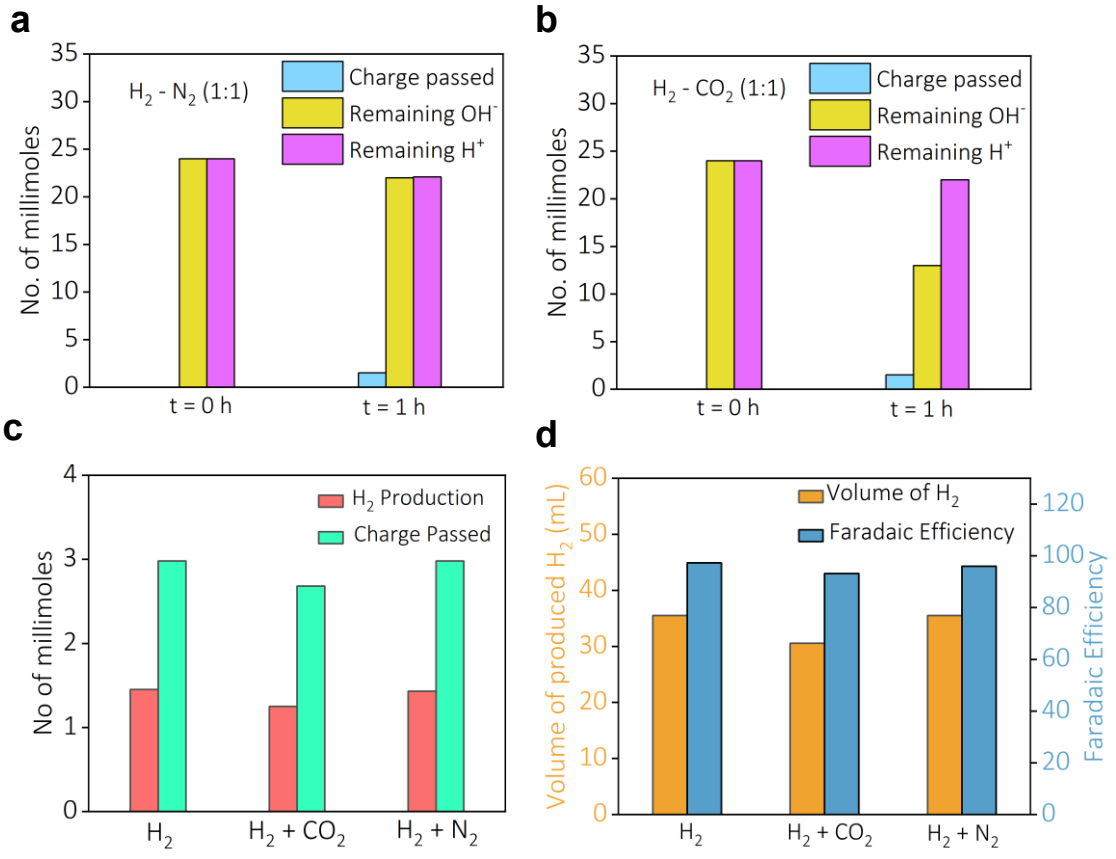

Figure 3.2: Pre- and post-purification H^+/OH^- dual ion concentrations and the charge passed during galvanostatic polarization at 40 mA/cm^2 for 1 hour with a) H_2-N_2 (1:1) and b) H_2-CO_2 (1:1) binary mixtures. c) Quantification of H_2 gas evolved in the cathodic half-cell with the amount of charge passed. (d) Volume of H_2 and Faradaic efficiency with pure and impure hydrogen gas feed streams.

density, the operating voltage was a bit lower with the CO_2 mixture in the beginning and in the middle regions; however, with a serious concentration polarization towards the end of polarization (Figure 3.1d). This we attribute to the chemical consumption of OH^- by CO_2 in forming bicarbonates and carbonates as CO_2 can gradually accumulate in the system as explained above.

To further prove this chemical consumption of hydroxyl ions, the amount of acid in the catholyte and alkali in the anolyte is determined at the end of the purification of the H_2-CO_2 binary mixture. The consumption of hydroxyl ion is higher than the charge passed and proton consumption in the H_2-CO_2 mixture; however, a linear correlation was observed between charge passed and H^+/OH^- dual ion consumption in the H_2-N_2 binary mixture (Figure 3.2a, 3.2b). This proves the involvement of the parasitic reaction between hydroxyl ions and CO_2 during the fuel purification of the H_2-CO_2 binary mixture, Figure 3.2b. Galvanostatic polarizations at 40 mA/cm^2 further suggest that with pure hydrogen and impure hydrogen, the cathodic outlet provides pure hydrogen (Figure 3.2c and Figure 3.2d). Nearly 18 mL of hydrogen per hour is generated in the cathodic half-cell with nearly 100 % Faradaic efficiency, (Figure 3.2d). With impure mixtures as feed gas stream, the Faradaic efficiency is similar with an almost equal amount of pure H_2 gas at the cathodic end of the fuel purifier, (Figure 3.2c, Figure 3.2d, and Calculation 3.2). The slight deviation of Faradaic efficiency from the expected 100 % value could be due to the trapping of residual hydrogen in the tubing and piping connected to the water displacement apparatus.

Calculation 3.2

Quantification of Hydrogen (Figure 3.1d)

Charge passed during 40 mA constant current test for 2 hours = $(2 * 3600 * 40 * 10^{-3})$ C

= 288 C

Moles corresponding to the charge passed = (288/96484) = 0.002985 mol

= 2.985 mmol

To evolve one H_2 molecule, there is a requirement of 2 electrons.

So, theoretically the amount of evolved H_2 = (2.985/2) = 1.4925 mmol

At room temperature (298 K) 1 mol of gas is equivalent to 24.45 L.

So, the theoretical amount of evolved H_2 gas **=** (24.45 * 1.4925 * 10^{-3}) = 36.49 mL

Faradaic Efficiency Calculation

1) Only H_2 gas as feed gas mixture –

Experimentally, the volume of evolved H_2 gas = 35.5 mL

Faradaic Efficiency = (35.50/36.49) * 100 = 97.29 %

2) 1:1 H_2 and N_2 mixture as feed gas –

Experimentally, the volume of evolved H_2 gas = 34.70 mL

Faradaic Efficiency = (34.70/36.49) * 100 = 95.1 %

3) 1:1 H_2 and CO_2 mixture as feed gas –

Experimentally, the volume of evolved H_2 gas = 30.5 mL

Faradaic Efficiency = (30/32.78) * 100 = 93 %

To understand the extent of fuel purification, we have carried out in situ electrochemical mass spectrometry with galvanometric polarization at 40 mA/cm^2 (Figure 3.3a, and Figure 3.3b) for the anodic and cathodic half-cells with impure H_2 gas streams. With a 1:1 mixture of N_2 and H_2 fed to the anode, the anodic half-cell demonstrates a drop in partial pressure of hydrogen (purple trace in Figure 3.3c) with a commensurate increase in partial pressure of hydrogen in the cathodic half-cell (Green trace in Figure 3.3c) when the cell is ON. It should be noted that, in the electrochemical mass spectra of the anodic half-cell (Figure 3.3c), the relative pressure of nitrogen (red trace in Figure 3.3c) is increased due to a decrement in the partial pressure of hydrogen (purple trace in Figure 3.3c). In the case of a 1:1 H_2 and CO_2 mixture, there is a fall of H_2 pressure in the anodic half (Green trace in Figure 3.3d) and a rise in relative pressure of H_2 for the cathodic half (black trace in Figure 3.3d) when the device is ON. It is to be noted that the relative pressure of CO_2 in the in situ electrochemical mass spectra of the anodic half-cell is very low due to the accumulation of CO_2 in the anolyte (blue trace in Figure 3.3d); however, the process is accompanied by electric power production and fuel purification. From the in situ electrochemical mass spectra of the anodic half-cell, it is

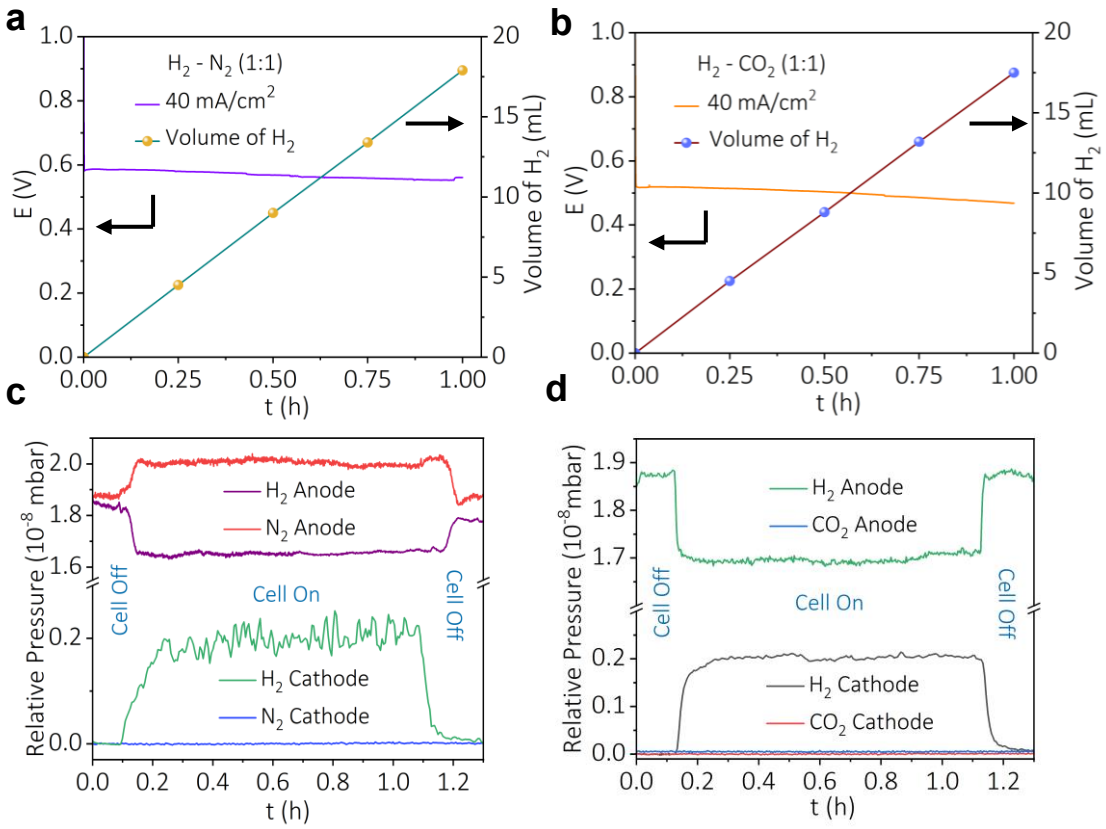

Figure 3.3: Galvanostatic polarization at 40 mA/cm^2 and quantification of H_2 in the cathodic half-cell of the fuel purifier with H_2-N_2 (1:1) gas mixture as feed. (b) Galvanostatic polarization at 40 mA/cm^2 and quantification of H_2 in the cathodic half-cell of the fuel purifier with H_2-CO_2 (1:1) gas mixture as feed. (c) In situ electrochemical mass spectra for the anodic half-cell and the cathodic half-cell of the fuel purifier with H_2-N_2 (1:1) gas mixture as feed. (d) In situ electrochemical mass spectra for the anodic half-cell and the cathodic half-cell of the fuel purifying cell with H_2-CO_2 (1:1) gas mixture as feed.

confirmed that only H_2 is consumed at the anode when the cell is ON. On the other hand, the electrochemical mass spectra of the cathodic half reveal no rise in the relative pressure of impurities except the rise in hydrogen partial pressure when the cell is ON. These demonstrate that pure hydrogen fuel is obtained at the cost of the impure hydrogen gas streams, (Figure 3.3c and 3.3d) during electric power production.

3.1.2 Spontaneous Fuel Purification of Quaternary Fuel Mixture

The regular contaminants during steam reforming are CO_2, hydrocarbons, and N_2 as mentioned before. To demonstrate the practical viability of this exergonic fuel purification at room temperature and pressure, we have attempted the separation of hydrogen from quaternary gas mixtures consisting of CO_2, CH_4, N_2, and H_2 in the ratio of (20: 1: 4: 75) corresponding to crude fuel stream from industrial methanol reformation.[14] It is well

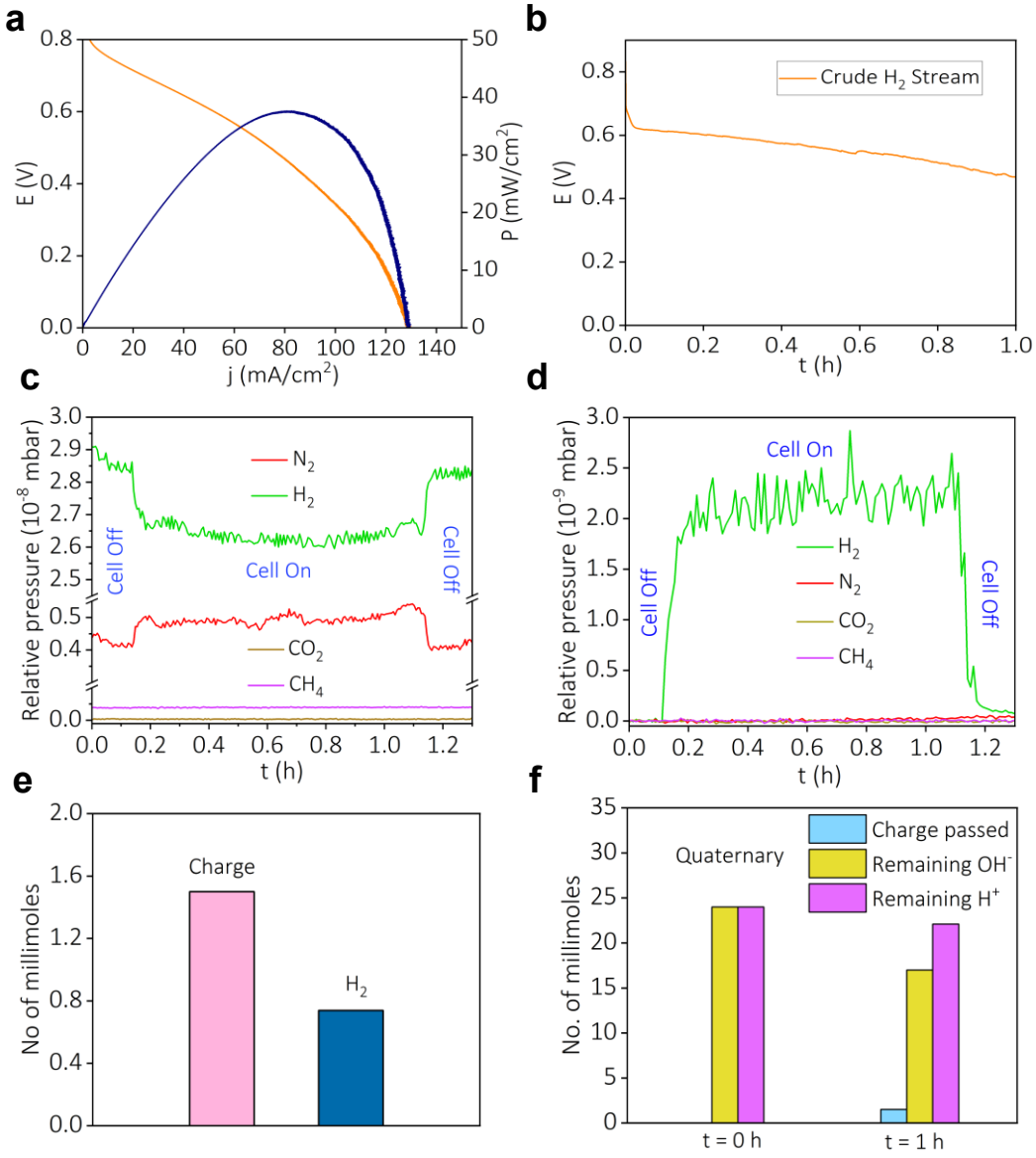

Figure 3.4: a) Polarization curve for H_2 purifier and b) galvanostatic polarization at 40 mA/cm^2 with crude H_2 gas stream as anodic feed gas stream (CO_2: CH_4: N_2: H_2 = 20: 1: 4: 75) at 10 mL/min. In-situ electrochemical mass spectra for c) the anodic half-cell and d) the cathodic half-cell with crude H_2 gas mixture as anodic feed gas stream. e) Correlation of charge passed vs. pure H_2 fuel evolved in the cathodic half-cell of the fuel purifier. f) Pre- and post-purification H^+/OH^- dual ion concentration and the charge passed during galvanostatic polarization at 40 mA/cm^2 for 1 hour with quaternary gas mixture as an anodic feed gas stream.

known that the absence of methane oxidation could be due to the higher temperature requirement for its oxidation on Pt-based electrodes, as reported in the literature.[31,32] When a crude quaternary mixture is fed (10 mL/min) to the anodic half-cell of the spontaneous fuel purifier at room temperature and pressure, the peak performance metrics were 36 mW/cm^2 of power at 75 mA/cm^2 of current, (Figure 3.4a) which is

dependent upon the proportion of H_2 in feed gas mixture. During galvanostatic polarization at 40 mA/cm^2 (Figure 3.4b), in situ electrochemical mass spectrometry of the anodic part of the fuel purifier (Figure 3.4c) is recorded, and it indicates that only hydrogen is consumed at the anode as only its pressure is decreased. The electrochemical mass spectra of the cathodic half-cell show major H_2 evolution at the cathode (Figure 3.4d). The quantification of evolved H_2 gas in the cathodic half-cell shows nearly 18 mL of H_2 gas in one hour with almost 100 % Faradaic efficiency, (Figure 3.4e). H^+/OH^- dual ion concentration measurement after fuel purification shows the chemical consumption of hydroxyl ion by CO_2 present in impure quaternary feed gas stream, (Figure 3.4f). Nevertheless, the data outlined in Figure 3.4 suggest the capability of the device to purify hydrogen from complex mixtures in a single step during electric power production.

Taken together, when an impure gas stream is fed to the anodic half-cell, only the hydrogen undergoes oxidation (equation 3.1), and commensurate to that, there is hydrogen evolution from the cathodic half-cell (equation 3.2). Therefore, the total cell reaction is the hydrogen fuel purification from the complex gas mixtures by utilizing the

Fuel purifier's reactions

Anodic Half Cell Reaction

$$(H_2 + N_2 + CO_2 + CH_4) + 2OH^- \leftrightarrow 2H_2O + 2e^- \qquad \textbf{(equation 3.1)}$$

Cathodic Half Cell Reaction

$$2H^+ + 2e^- \leftrightarrow H_2 \qquad \textbf{(equation 3.2)}$$

Overall Cell Reaction

$$(H_2 + N_2 + CO_2 + CH_4) + 2H^+ + 2OH^- \leftrightarrow 2H_2O + H_2 \qquad \textbf{(equation 3.3)}$$

water formation energy (equation 3.3). To further demonstrate the practical viability of the device to generate pure hydrogen while purifying quaternary rises and on utilization of this hydrogen, the operating voltage of the fuel cell decreases. This process can be repeated multiple times, suggesting that electric power can be harnessed during fuel purification as well as its utilization (Figure 3.5). This further demonstrates that the fuel purifier during electric power production can directly serve as the fuel reservoir for an H_2-air fuel cell.

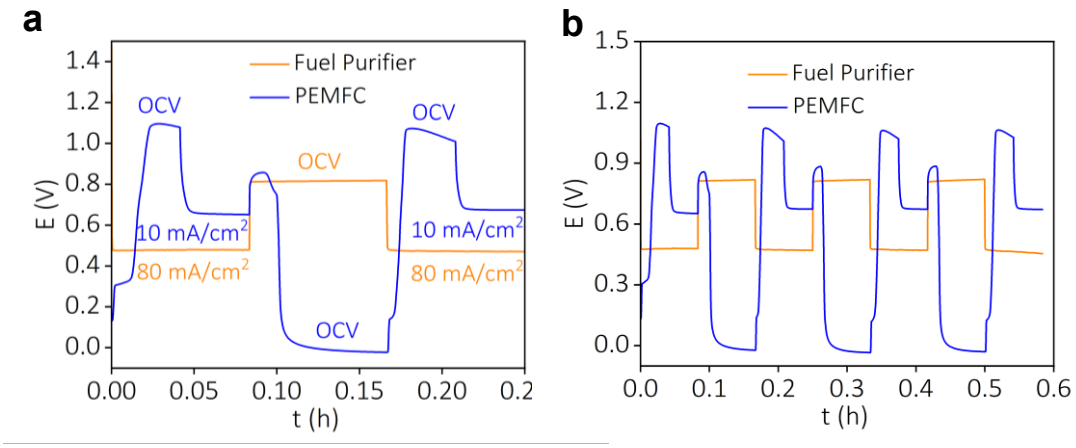

Figure 3.5: a. b) Fuel purifying device directly serving as a fuel reservoir for a PEMFC in a tandem configuration.

3.1.3 Energy Balance and Purity

The energy consumption during H_2 purification is the spotlight parameter for any purification technique. To derive the value of energy consumption of our device, we have performed long-term discharge at a constant current of 40 mA/cm^2 with pure H_2 and impure H_2 ($1H_2$:$1N_2$) as gas feed streams (Figure 3.6a, Calculation 3.3). The shaded area in Figure 3.6a depicts the energy lost due to the impurity present in the anodic feed stream or the energy required to obtain pure H_2 from the cathodic outlet. It is to be noted that in the proposed device, the water formation energy is harvested as an electrical driving force by utilizing H_2 redox. However, the presence of impurity lowers the extent to which this interconversion happens. Simultaneously, pure hydrogen is produced at the cathodic half-cell at the expense of this energy loss. So, the loss in the amount of electrical energy output due to the impurity can be correlated to the energy required to generate pure hydrogen on the cathodic side. If this purified hydrogen stream from the cathodic outlet is fed to the anodic half-cell of another spontaneous fuel purifier (at the same set of conditions as in the case of the impure stream), the voltage output should be similar in magnitude to that of pure hydrogen. However, the time of operation should be lower. The difference should be the energy expended for fuel purification, which should be similar to the loss of electrical energy due to the impurity. To further prove that the decrease in the electrical energy output is not simply due to the decrease in the concentration of hydrogen, we have calculated the energy consumption for the H_2-CO_2 (1:1) mixture and the quaternary mixture, wherein the impurity (CO_2) can chemically consume the OH^-. It

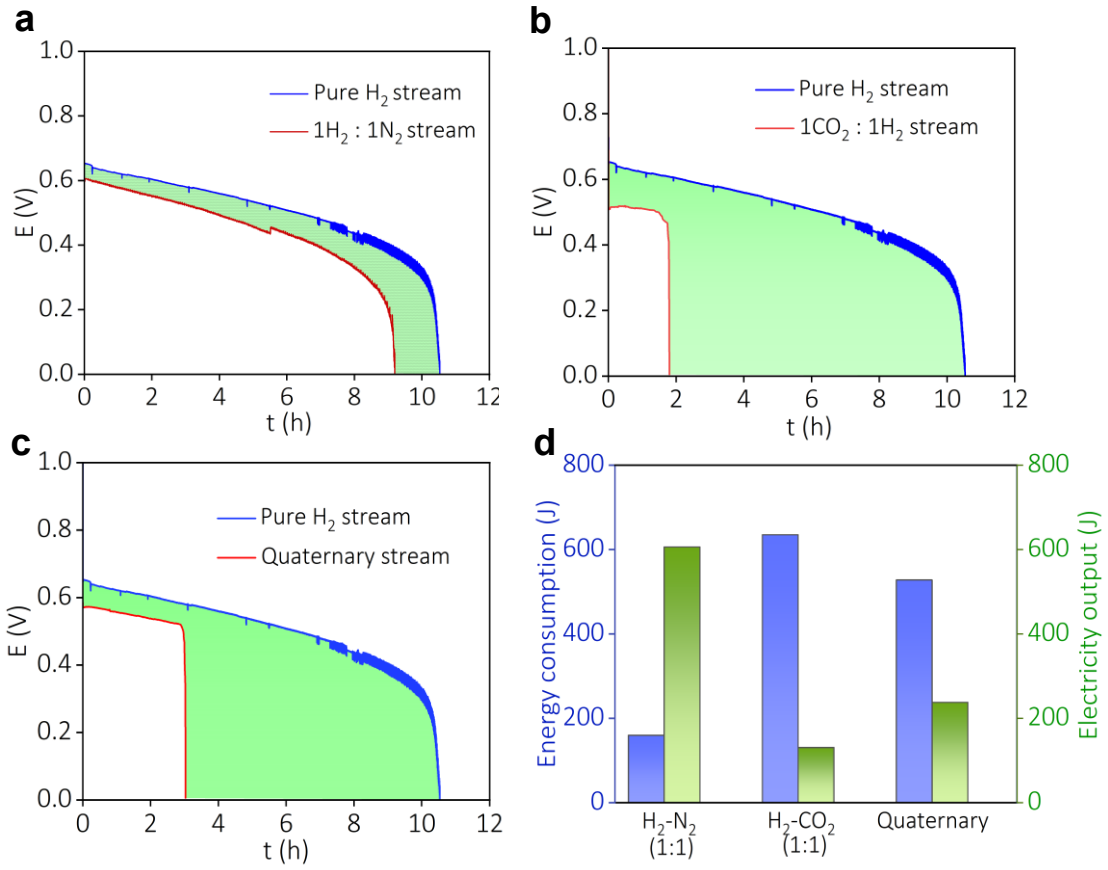

Figure 3.6: Galvanostatic polarization at a current density of 40 mA/cm^2 for (a) H_2-N_2 (1:1) binary mixture, (b) H_2-CO_2 (1:1) binary mixture, and (c) quaternary mixture (CO_2: CH_4: N_2: H_2 = 20: 1: 4: 75). (d) Energy consumption and electrical energy output for the gas mixtures.

is found that the energy consumption during fuel purification is high for H_2-CO_2 (1:1) mixture and quaternary mixture (CO_2: CH_4: N_2: H_2 = 20: 1: 4: 75) compared to H_2-N_2 (1:1) mixture, Figure 3.6. In such a case, the energy required for purification is much higher than what is predicted by the Nernst equation (by the decrease in H_2 partial pressure) and the impurity can independently affect the overall electrical energy output, (Figure 3.6d). In the same way, the energy for H_2-CO_2 (1:1) and quaternary mixture are determined (Figure 3.6, Calculation 3.3 and Calculation 3.4). The energy consumption for H_2-CO_2 (1:1) binary mixture and quaternary mixture is pretty high due to the chemical consumption of hydroxyl ions during the process. Nevertheless, the spontaneous fuel purifier offers an approach for simultaneous fuel purification and CO_2 capture (as carbonate) during electricity production. The energy spent for hydrogen separation from this binary mixture at room temperature and pressure in a single step is calculated from the shaded area in Figure 3.6a, which is ~24 kJ for 1 mole of pure hydrogen (Calculation 3.3, Calculation 3.4).

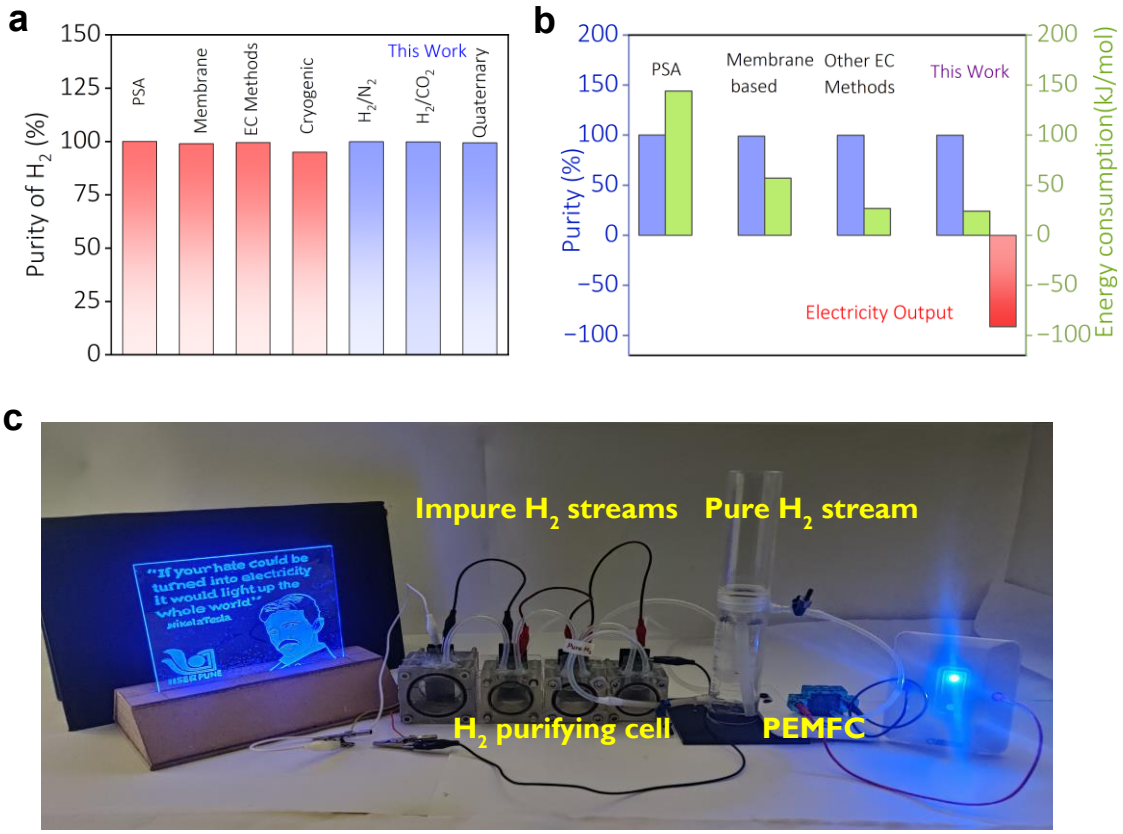

Figure 3.7: a) The purity, and b) energy consumption and the purity of produced H_2 for the spontaneous fuel purifier compared with the state-of-the-art fuel purification processes like pressure swing adsorption (PSA), membrane-based methods, electrochemical techniques (EC), etc. c) Photograph demonstrating spontaneous fuel purifier directly serving as a fuel reservoir for a commercial PEMFC

The electricity output during the process is calculated from the area under the maroon trace in Figure 3.6a, which is found to be ~90 kJ for 1 mole of pure hydrogen gas (Calculation 3.4, Calculation 3.5). This energy consumption value is compared with state-of-the-art fuel separation techniques such as pressure swing adsorption (PSA), membrane-based separation, and other electrochemical separations (Figure 3.7a, 3.7b), and the value obtained for our method is on par with the literature.[20,21,33,34] The energy consumption and electricity output are also calculated for a 1:1 binary mixture of H_2 and CO_2 and a crude quaternary mixture (Figure 3.6). It is to be noted that the estimated purity of the produced hydrogen from the spontaneous fuel purifier (by electrochemical mass spectrometric analysis), as shown in Figure 3.3c, Figure 3.3d, Figure 3.4d, are comparable with PSA and membrane-based methods (Figure 3.7b). However, it should be noted that the purity level we have reported is based on a single step of the fuel purification process,

(Figure 3.7a).[14,21,35-38] The purity is found to be ~99.90 % (1:1 binary mixture of H_2 and N_2), ~99.8 % (1:1 binary mixture of H_2 and CO_2) and ~99.4 % (crude quaternary mixture).

To demonstrate the practical utility of the proposed fuel purifier, a laboratory-level spontaneous fuel purifier is fabricated and connected it in tandem with a commercial air-breathing PEMFC (Figure 3.7c). The demonstration confirms that the spontaneous H_2 purifier can directly function as a fuel reservoir for PEMFC when the former produces electricity output. For the long-term operation of the purifying device, the best way is to set up a flow cell so that the anolyte and the catholyte can be refreshed continuously. But it is also possible to operate our flood cell for a longer time when the concentration of H^+/OH^- dual ions is increased. When the concentration of H^+/OH^- dual ions is increased to 3 M, the purifier could run for nearly 55 hours when a constant current of 10 mA/cm^2 was drawn from the device (red trace in Figure 3.8). When the concentration is further increased to 5 M, the purifier could run for nearly 85 hours at the same current rating (violet trace in Figure 3.8). These suggest that the duration of device operation can be further enhanced by increasing the H^+/OH^- dual ions concentrations in the respective half-cells, which indicates their role in device sustenance. The proposed spontaneous fuel purifier holds promise in these directions. Firstly, it allows neutralization to happen during electric power production, and secondly, it allows fuel purification at room temperature and pressure.

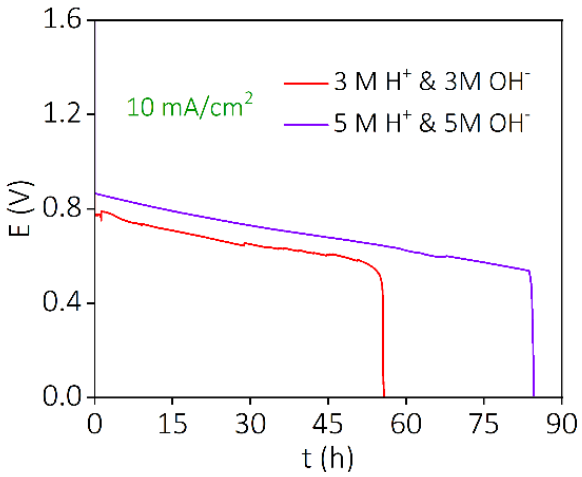

Figure 3.8: Long term performance of the fuel purifier when a constant current of 10 mA/cm^2 is drawn from the device, with 3 M (red trace) and 5 M (violet trace) H^+/OH^- dual ion concentration.

Calculation 3.3

Energy consumption for purification

A) Case 1: $1H_2$:$1N_2$ binary mixture

From Figure 3.6a

Area of the green shaded portion = Area under the curve with pure H_2 stream as anodic feed (blue trace in Figure 3.6a) – Area under the curve with a binary mixture of $1H_2$: $1N_2$ as anodic feed (maroon trace in Figure 3.6a)

= 19155.2 – 15156.6 V. s

= 3998.6 V. s

Energy = 3998.6 * 40 * 10^{-3} A. V. s

= 159.94 A. V. s

= 159.94 W. s

= **159.94 J**

B) Case 2: $1H_2$:$1CO_2$ binary mixture

From Figure 3.6b

Area of the green shaded portion = Area under the curve with pure H_2 stream as anodic feed (blue trace in Figure 3.6b) – Area under the curve with a binary mixture of $1H_2$: $1CO_2$ as anodic feed (maroon trace in Figure 3.6b)

=19155.2 – 3256.8 V. s

=15898.4 V. s

Energy = 15898.4 * 40 * 10^{-3} A. V. s

= 635.93 W. s

= **635.93 J**

C) Case 3: Quaternary mixture

From Figure 3.6c

Area of the green shaded portion = Area under the curve with pure H_2 stream as anodic feed (blue trace in Figure 3.6c) – Area under the curve with quaternary mixture as anodic feed (red trace in Figure 3.6c)

= 19155.2 – 5940 V. s

= 13215.2 V. s

Energy = 13215.2 * 40 * 10^{-3} A. V. s

= 528.6 W, s

= **528.6 J**

Calculation 3.4

Normalized energy output

Amount of pure H_2 produced during the purification of $1H_2$:$1N_2$ binary mixture = **163.5 mL**

The energy consumption for purification per 1 mole of pure H_2 = (159.94*24450)/163.5

= **23.92 kJ/mol**

Electricity energy output per 1 mole of pure H_2 = (606.264*24450)/163.5

= **90.66 kJ/mol**

Calculation 3.5

Electricity energy output

A) Case 1: $1H_2$:$1N_2$ binary mixture

Area under the curve with binary mixture of $1H_2$: $1N_2$ as anodic feed (maroon trace in Figure 3.6a)

= 15156.6 V. s

Energy = 15156.6 * 40 * 10^{-3} A. V. s

= 606.264 W. s

= **606.264 J**

B) Case 2: $1H_2$:$1CO_2$ binary mixture

Area under the curve with binary mixture of $1H_2$: $1CO_2$ as anodic feed (maroon trace in Figure 3.6b)

= 3256.8 V. s

Energy = 3256.8 * 40 * 10^{-3} A. V. s

= 130.27 W. s

= **130.27 J**

C) Case 3: Quaternary mixture

Area under the curve with quaternary mixture as anodic feed (red trace in Figure 3.6c)

= 5940 V. s

Energy = 5940 * 40 * 10^{-3} A. V. s

= 237.6 W. s

= **237.6 J**

3.2 Conclusion

A spontaneous hydrogen fuel purifier is demonstrated wherein carbonized and contaminated hydrogen streams can be directly purified in a single stage at room temperature and pressure with simultaneous electric power production by harvesting the energy of water formation. The fuel purifying device converts chemical energy to electrical energy during fuel purification in a thermodynamically downhill pathway, which is contrary to the thermodynamically uphill pathways adopted in state-of-the-art electrolytic approaches. A comparison with state-of-the-art purification processes such as pressure swing adsorption, membrane-based methods, and electrochemical methods suggests that the spontaneous hydrogen fuel purifier achieves nearly 99.9 % purity in a single step at the expenditure of 24 kJ/mol_{H2}, with an electrical energy output of ~90

kJ/mol_{H2}. A laboratory-level prototype purifier can purify hydrogen even from a quaternary mixture of contaminants, including hydrocarbons, CO_2, and N_2 commonly encountered in the exhaust of a steam reformer in a single step, and the purified H_2 can be directly fed to a commercial proton exchange membrane fuel cell (PEMFC) for further energy conversion. Though carbonate accumulation is present in this device during the impurity removal from CO_2-contaminated streams, this is the first approach where CO_2 is captured, and pure hydrogen is released during concomitant electric power production. It is to be noted that in a perfectly sealed anodic half-cell, CO_2 contamination from atmospheric air can be controlled reasonably. The methods to address carbonate accumulations are to set up a flow cell or to raise the operation temperature because the solubility of CO_2 in the alkaline medium is lower at higher temperature.[39] Nevertheless, this spontaneous fuel purifier serves as the first example wherein electric power can be harnessed during fuel purification as well as fuel utilization, thereby demonstrating a major leap in the hydrogen economy.

3.3 Experimental Section

3.3.1 Materials

H_2SO_4 (98%), NaOH (97%), oxalic acid (98%), AgCl (98 %), KCl (99%), H_2O_2 and phenolphthalein were obtained from Sigma Aldrich. Pt supported on carbon catalyst (0.5 mg/cm^2 Pt/C), and Nafion-117 membrane were obtained from Fuel Cell Store (USA).

3.3.2 Electrochemical Study (Single Compartment)

Electrochemical measurements were performed using a Biologic (VMP-300) electrochemical workstation. Cyclic voltammetry experiments were conducted using a three-electrode system. Platinum (0.031 cm^2) was used as the working electrode, and a larger area of platinum mesh was used as the counter electrode. Ag/AgCl (3.5M KCl) was used as the reference electrode. 15 mL of electrolyte was used for each measurement.

3.3.3 In-situ Electrochemical Mass Spectrometry

In-situ electrochemical mass spectrometry was conducted with an HPR-40 (Hiden Analytical) quadruple mass analyzer using a standard QIC inlet. The study was carried out with the help of a 'T' shaped connector where three sides are a mass spectrometer inlet, cell outlet, and exhaust to the surroundings. For the cathodic half-cell experiments,

Argon (Ar) was used as the carrier gas, and in the case of the anodic half-cell, the impure mixture (anodic feed gas mixture) was fed directly to the mass spec. The generated gas flow from the cell was channeled to mass the spectrometer inlet via the 'T' connector.

3.3.4 Electrochemical Study (Double compartment)

A laboratory prototype in a two-compartment configuration was fabricated out of poly-acrylic sheets for spontaneous H_2 purification. Nafion-117 membrane was used to separate the two half-cells of the device. Nafion-117 membrane was pretreated with acidic H_2O_2 solution at 80°C before using in the cell. To avoid intercompartment leakage, the membrane was placed between two silicone washer gaskets. The volume of the acid and alkali used was 12 mL in both the half-cells. The anodic electrocatalysts were Pt/C coated on Toray carbon paper, and the cathodic electrocatalysts were electrodeposited Pt on Ti mesh (obtained by applying 5 mA/cm^2 constant current for 10 mins in chloro-platinic acid solution). The loading of respective catalysts is provided in Table 3.2.

Table 3.2: Catalyst loading used at the anodic and cathodic half-cells of the spontaneous fuel purifier.

	Cathode	Anode
Catalyst	Pt on Ti mesh	Pt/C (Pt:C = 2:3)
Amount	1.5 mg/cm^2	1 mg/cm^2

All the electrochemical experiments were performed under room temperature and pressure. Quantification of generated hydrogen was carried out by water displacement technique. The concentration of anolyte and catholyte was measured by acid-base titration with a phenolphthalein indicator. Oxalic acid was used as the primary standard. Firstly, the prepared NaOH was standardized with oxalic acid. Then, the catholyte from the cell is titrated with the standardized NaOH, and the concentration of the catholyte is determined. The concentration of anolyte is determined by titration with the oxalic acid.

3.4 References

1. P. Zhang, Y.-J. Guo, J. Chen, Y.-R. Zhao, J. Chang, H. Junge, M. Beller and Y. Li, Nat. Catal., 2018, **1**, 332–338.
2. D. Hauglustaine, F. Paulot, W. Collins, R. Derwent, M. Sand and O. Boucher, Commun. Earth Environ., 2022, **3**, 1–14.
3. J. O. M. Bockris, Int. J. Hydrogen Energy, 2013, **38**, 2579–2588.
4. A. M. Oliveira, R. R. Beswick and Y. Yan, Curr. Opin. Chem. Eng., 2021, **33**, 100701.
5. G. Marbán and T. Valdés-Solís, Int. J. Hydrogen Energy, 2007, **32**, 1625–1637.
6. P. M. Falcone, M. Hiete and A. Sapio, Curr. Opin. Green Sustain. Chem., 2021, **31**, 100506.
7. M. van der Spek, C. Banet, C. Bauer, P. Gabrielli, W. Goldthorpe, M. Mazzotti, S. T. Munkejord, N. A. Røkke, N. Shah, N. Sunny, D. Sutter, J. M. Trusler and M. Gazzani, Energy Environ. Sci., 2022, **15**, 1034–1077.
8. J. N. Tiwari, N. K. Dang, S. Sultan, P. Thangavel, H. Y. Jeong and K. S. Kim, Nat. Sustain., 2020, **3**, 556–563.
9. N. Heinemann, J. Alcalde, J. M. Miocic, S. J. T. Hangx, J. Kallmeyer, C. Ostertag-Henning, A. Hassanpouryouzband, E. M. Thaysen, G. J. Strobel, C. Schmidt-Hattenberger, K. Edlmann, M. Wilkinson, M. Bentham, R. Stuart Haszeldine, R. Carbonell and A. Rudloff, Energy Environ. Sci., 2021, **14**, 853–864.
10. M. H. McCay and S. Shafiee, Futur. Energy Improv. Sustain. Clean Options Our Planet, 2020, 475–493.
11. K. Mazloomi and C. Gomes, Renew. Sustain. Energy Rev., 2012, **16**, 3024–3033.
12. J. Zheng, H. Zhou, C. G. Wang, E. Ye, J. W. Xu, X. J. Loh and Z. Li, Energy Storage Mater., 2021, **35**, 695–722.
13. M. Nielsen, E. Alberico, W. Baumann, H. J. Drexler, H. Junge, S. Gladiali and M. Beller, Nature, 2013, **495**, 85–89.
14. Z. Du, C. Liu, J. Zhai, X. Guo, Y. Xiong, W. Su and G. He, Catalysts, 2021, **11**, 1–19.
15. K. M. K. Yu, W. Tong, A. West, K. Cheung, T. Li, G. Smith, Y. Guo and S. C. E. Tsang, Nat. Commun., 2012, **3**, 1-7.
16. M. Onozaki, K. Watanabe, T. Hashimoto, H. Saegusa and Y. Katayama, Fuel, 2006, **85**, 143–149.
17. S. Sircar and T. C. Golden, Sep. Sci. Technol., 2000, **35**, 667–687.
18. Y. Wang, S. B. Peh and D. Zhao, Small, 2019, **15**, 1–38.
19. H. Li, Z. Song, X. Zhang, Y. Huang, S. Li, Y. Mao, H. J. Ploehn, Y. Bao and M. Yu, Science., 2013, **342**, 95–98.
20. X. Zhu, S. Li, Y. Shi and N. Cai, Prog. Energy Combust. Sci. 2019, **75**, 100784.
21. M. Nordio, S. A. Wassie, M. Van Sint Annaland, D. A. Pacheco Tanaka, J. L. Viviente Sole and F. Gallucci, Int. J. Hydrogen Energy, 2021, **46**, 23417–23435.
22. Y. Ding, P. Cai and Z. Wen, Chem. Soc. Rev., 2021, **50**, 1495–1511.

23. P. Cai, K. Chen, Z. Lu, R. Mondal, M. O. Thotiyl and Z. Wen, ChemSusChem, 2022, n/a, e202201034.
24. Z. M. Bhat, D. Pandit, S. Ardo, R. Thimmappa, A. R. Kottaichamy, N. Christudas Dargily, M. C. Devendrachari and M. Ottakam Thotiyl, Joule, 2020, **4**, 1730–1742.
25. S. Sur, R. Mondal, R. Thimmappa, S. Mukhopadhyay and M. O. Thotiyl, J. Colloid Interface Sci., 2023, **630**, 477–483.
26. Z. Manzoor Bhat, R. Thimmappa, M. C. Devendrachari, A. R. Kottaichamy, S. P. Shafi, S. Varhade, M. Gautam and M. O. Thotiyl, J. Phys. Chem. Lett., 2018, **9**, 388–392.
27. G. N. B. Durmus, C. O. Colpan and Y. Devrim, J. Power Sources, 2021, **494**, 229743.
28. D. Marciuš, A. Kovač and M. Firak, Int. J. Hydrogen Energy, 2022, **47**, 24179–24193.
29. S. H. Han, Y. Jun and J. H. Kim, Constr. Build. Mater., 2022, **342**, 127977.
30. M. Yoo, S. J. Han and J. H. Wee, J. Environ. Manage., 2013, **114,** 512–519.
31. M. J. Boyd, A. A. Latimer, C. F. Dickens, A. C. Nielander, C. Hahn, J. K. Nrskov, D. C. Higgins and T. F. Jaramillo, ACS Catal., 2019, **9**, 7578–7587.
32. A. Tomita, J. Nakajima, and T. Hibino, Angew. Chemie - Int. Ed., 2008, **47**, 1462–1464.
33. L. Schorer, S. Schmitz and A. Weber, Int. J. Hydrogen Energy, 2019, **44**, 12708–12714.
34. M. Mondal and A. Datta, Int. J. energy Res., 2017, **41**, 448–458.
35. N. Sazali, Int. J. Hydrogen Energy, 2020, **45**, 18753–18771.
36. P. L. Mores, A. M. Arias, N. J. Scenna, J. A. Caballero, S. F. Mussati and M. C. Mussati, Processes, 2018, **6**, 221.
37. L. Vermaak, H. W. J. P. Neomagus and D. G. Bessarabov, Membranes (Basel)., 2021, **11**, 1–32.
38. G. Venugopalan, D. Bhattacharya, E. Andrews, L. Briceno-Mena, J. Romagnoli, J. Flake and C. G. Arges, ACS Energy Lett., 2022, **7**, 1322–1329.
39. F. Lucile, J. Serin, D. Houssin and P. Arpentinier, J. Chem. Eng. data, 2012, **57**, 784–789.

Chapter 4

Spontaneous Electrochemical Hydrogen Fuel Purification from Catalyst Poisoning impurities

Abstract

Electrocatalyst poisoning impurities, even in trace quantities, severely damage fuel cell catalysts, clog active sites and drastically diminish the efficiency and performance of hydrogen-based technologies. Current purification methods face issues like huge energy demand, high costs, and extreme conditions, threatening the feasibility of a sustainable hydrogen economy. Differing from existing approaches, a hydrogen fuel purification pathway during electricity production is demonstrated by harvesting the energy of water formation to selectively remove catalyst poisoning impurities such as CO and H_2S in a single step under ambient weather conditions. Using a non-precious and poison-resistant electrocatalytic architecture, the system becomes durable and produces purified hydrogen for direct utilization in a proton exchange membrane fuel cell (PEMFC). Unlike traditional uphill electrolytic methods, this spontaneous galvanic process combines efficient purification with power generation, advancing the hydrogen economy's sustainability.

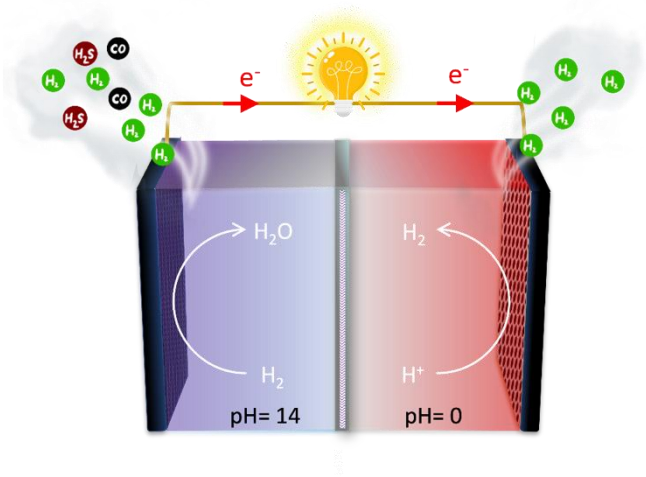

This work has been published in the following journal:

Ritwik Mondal et al. *Energy Environ. Sci.* **2023**, *16* (9), 3860–3872.

4.1 Introduction

The global shift towards sustainable energy systems has intensified the need for green hydrogen as a versatile and eco-friendly energy carrier.[1-3] Hydrogen's high gravimetric energy density and its potential to decarbonize multiple sectors make it a potential future fuel for the transition to a net-zero carbon energy future.[4,5] However, the widespread adoption of hydrogen depends on the successful implementation of the major branches of the hydrogen economy such as hydrogen production, and hydrogen utilization.[6,7] Current hydrogen production methods, such as steam methane reforming (SMR), biomass gasification, and partial oxidation, often yield hydrogen mixed with impurities like carbon monoxide (CO), sulfur compounds, and other trace gases.[8-14] These impurities not only lower the proportion of hydrogen in the stream but also severely poison the fuel cell catalysts during the fuel utilization stage and that in turn drastically reduce the efficiency of hydrogen-based systems.[15-17] The impurities bind with the platinum-based electrocatalysts and clog up the active catalytical sites for hydrogen redox.[18,19] This will reduce the rate of the hydrogen oxidation reaction within the fuel cell, severely impacting its performance and long-term efficiency.[18-21] Even trace concentrations of these impurities as low as a few parts per million (ppm) can substantially degrade the efficiency of a hydrogen fuel cell.[15,21,22] These factors demand an intermediate step of hydrogen fuel purification between the production and utilization stages of hydrogen fuel.[12,23] Traditional hydrogen purification methods, including pressure swing adsorption (PSA), cryogenic distillation, and membrane-based separation, are well-established but have significant technological and financial limitations.[24-26] PSA and cryogenic techniques, while effective for large-scale operations, are highly energy-intensive and often require extreme pressures and temperatures.[24,25,27] Membrane-based systems, particularly those using palladium-based materials, offer high selectivity and efficiency but are limited by their high cost, susceptibility to fouling, and degradation under harsh conditions.[24,28-30] Taken together, these energy-demanding hydrogen production techniques, completely derail the hydrogen economy from its sustainable future.[8,10,24-27]

Taking a detour from the traditional purification methods, spontaneous hydrogen fuel purification via harnessing water formation energy from a mixture of poisonous contaminants is explored. Under ambient conditions, impure fuel mixtures with

poisonous contaminants can be refined in a single step with the added benefit of electric power generation. By employing a poison-resisting electrocatalyst in the fuel purifier, the electrode poisoning is decently suppressed even in the presence of impurities like CO and H_2S. The purified hydrogen can then be directly supplied to a commercial proton exchange membrane fuel cell (PEMFC) for further energy conversion. Unlike previous studies on electrochemical fuel purification, which rely on electrolytic methods following a thermodynamically uphill pathway, this spontaneous fuel purifier operates as a galvanic system, achieving purification via a thermodynamically downhill process. This innovative H_2 purifier represents a significant advancement toward a sustainable hydrogen economy by combining hydrogen separation with simultaneous electric power generation.

4.2 Results and Discussion

The fuel purification system consists of an anodic alkaline half-cell and a cathodic acidic half-cell, separated by a cation-conducting Nafion-117 membrane (Scheme 4.1). Platinum supported on carbon (Pt/C) serves as the electrocatalyst in the anodic alkaline half-cell, while the cathodic acidic half-cell uses platinum electrodeposited on a titanium mesh (applied at a constant current of 4 mA/cm² for 5 minutes) as the electrocatalyst.

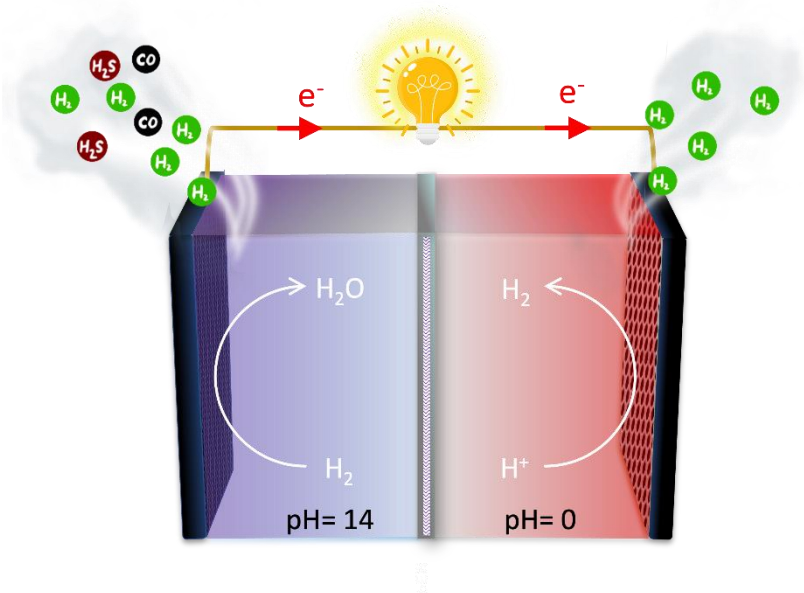

Scheme 4.1: Schematics of spontaneous hydrogen fuel purifier to purify hydrogen from catalyst poisoning impurities under ambient weather conditions.

To prove the prospects of the device for applications, fuel purification experiments were carried out with catalyst poisoning feed gas streams, including CO and H_2S. It is well known that CO and H_2S beyond a few ppm can poison the electrocatalytic domains. To understand how poisonous impurity affects electrochemistry, we verified the fuel purifier's performance with binary fuel mixtures when Pt/C is employed as an anodic electrocatalyst. From Figures 4.1a and 4.1b, it is very clear that even 1000 ppm of toxic impurity diminishes the performance matrix of the fuel purifier. The power delivery (Figure 4.1a) and the voltage output (Figure 4.1b) during the purifications of these impurities decreased even half of the magnitude as compared to the pure hydrogen case. To get rid of the poisoning, the bi-metallic electrocatalyst of Pt-Ru is employed instead of only Pt-based electrocatalyst as it is renowned that the poisoning can be arrested noticeably by employing bifunctional electrocatalysts like Pt-Ru.[31,32] Linear sweep

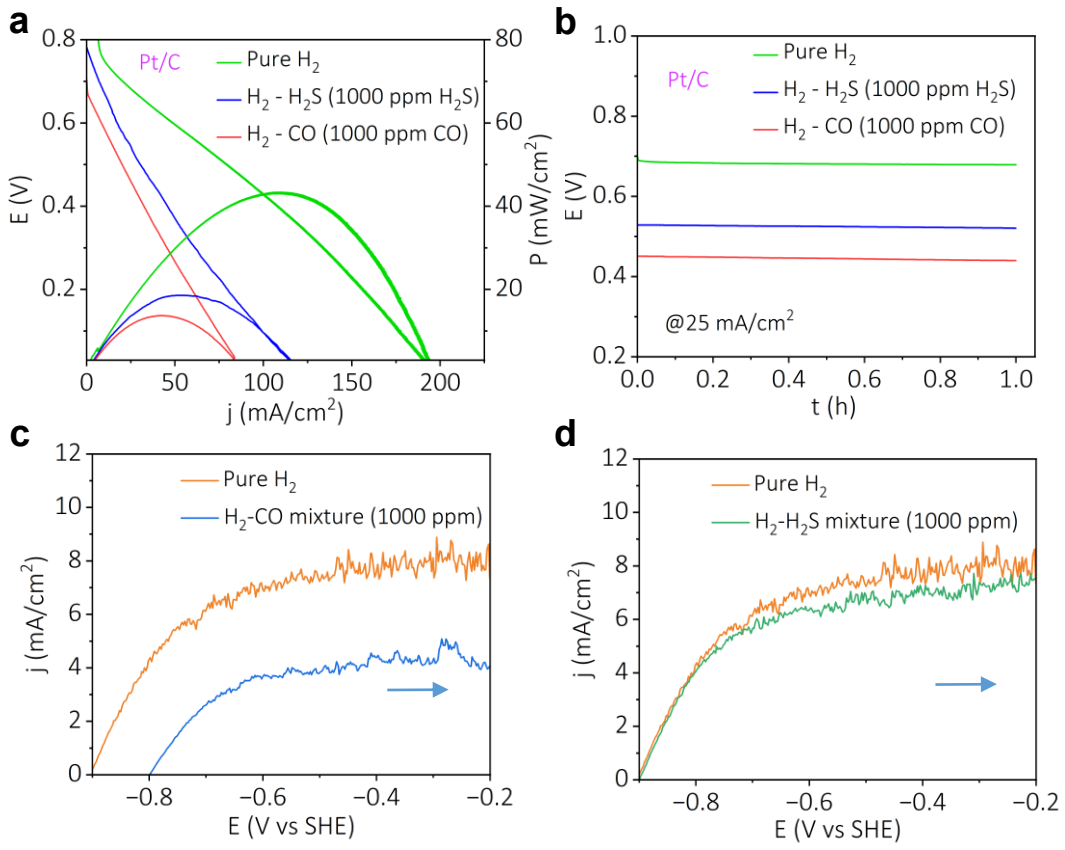

Figure 4.1: a) Polarization curves and b) galvanostatic polarizations at a constant current density of 25 mA/cm² for the fuel purifier with Pt/C as anodic electrocatalyst. Pure H_2, H_2-H_2S (1000 ppm H_2S), and H_2-CO (1000 ppm CO) binary mixtures are used as anodic feed gas streams. c) Rotating disk electrode measurements during hydrogen oxidation reaction at 1600 rpm at a scan rate of 5 mV/s on a Pt-Ru/C electrode for c) H_2-CO (1000 ppm CO) and d) H_2-H_2S (1000 ppm H_2S) binary mixtures.

voltammograms have been performed at a scan rate of 5 mV/s with Pt-Ru/C electrode at a rotation of 1600 rpm for impure gas mixtures in 1 M NaOH solution. In the case of an H_2-CO mixture (1000 ppm), the limiting current density is comparatively lower, and the oxidation potential is positively shifted, which is attributed to the adsorption of CO onto Pt domains[33,34] (Figure 4.1c, Table 4.1); however, a very stable limiting current demonstrates the capability of Pt-Ru electrode to resist CO poisoning in a bifunctional pathway well reported in the literature.[32] When the H_2-H_2S mixture (1000 ppm H_2S) was purged into the electrolyte, a slight decrease in limiting current density compared to pure hydrogen was observed, which may be due to the slow adsorption of sulfur onto the electrode surface[35] (Figure 4.1d, Table 4.1).

Table 4.1: Comparison table of limiting current densities and overpotential (at 3 mA/cm^2) for various gas mixtures on a Pt-Ru/C electrode.

Impure Mixtures	Limiting Current (mA/cm^2)	Overpotential (mV). (at 3 mA/cm^2)
Pure H_2	7.9	0
H_2-CO (1000 ppm CO)	4.3	162
H_2-H_2S (1000 ppm H_2S)	7.3	6

Therefore, a Pt-Ru-based anodic electrocatalyst is utilized in the spontaneous fuel purifier for the purification of binary mixtures of CO and H_2 (1000 ppm CO). With Pt-Ru/C, a peak power density of nearly 20 mW/cm^2 at a peak current density of 60 mA/cm^2 is observed in the polarization curve (purple trace in Figure 4.2a), and the performance metrics are noticeably higher compared to pure Pt/C, red trace in Figure 4.1a. The chronopotentiometry at a constant current density of 25 mA/cm^2 (Figure 4.2b) also reflects the superior performance of Pt-Ru/C as compared to Pt/C, which confirms the employment of a Pt-Ru catalyst as a poison-resistant anodic electrocatalyst. In line with this, during the purification of H_2-CO binary mixture (1000 ppm CO) with a Pt-Ru/C electrode, in-situ electrochemical mass spectrometry suggests the drop in partial pressure of H_2 in the anodic half-cell (red trace in Figure 4.2c) is commensurate to the rise in partial

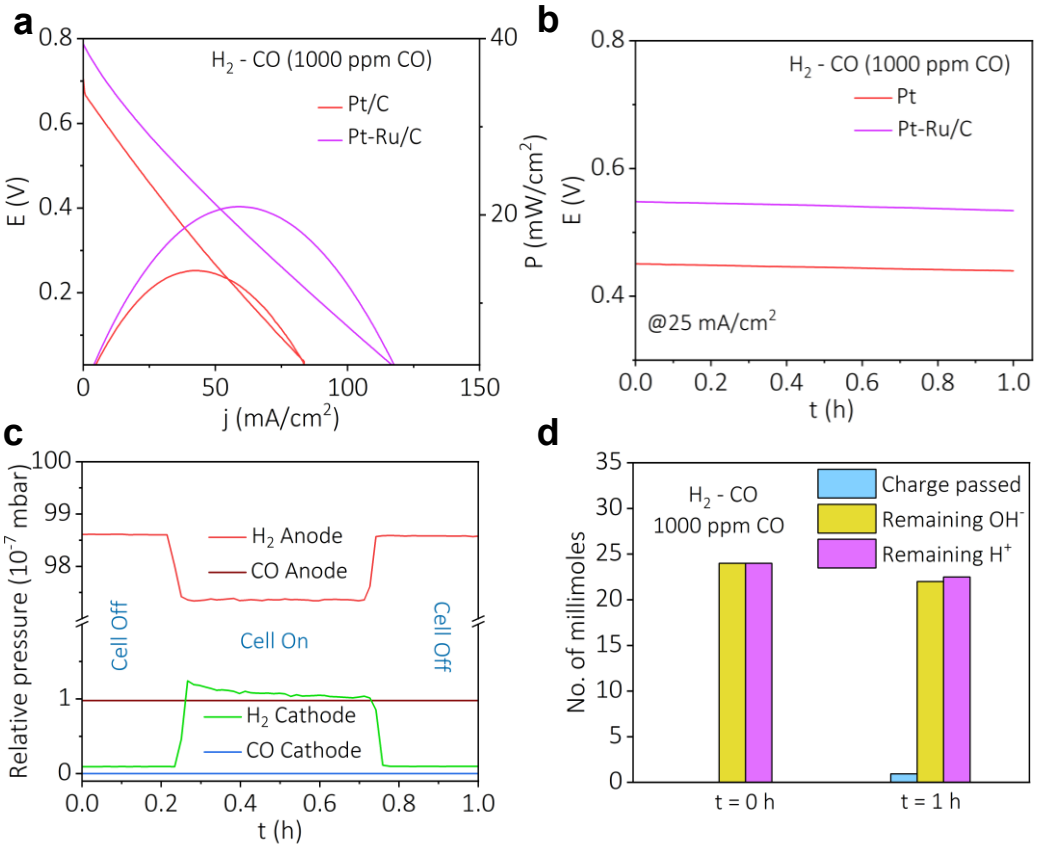

Figure 4.2: a) Polarization curves and b) galvanostatic polarizations at a constant current density of 25 mA/cm^2 for the fuel purifier with Pt/C and Pt-Ru/C as anodic electrocatalysts. Pure H_2 and H_2-CO (1000 ppm CO) binary mixtures are used as anodic feed gas streams**.** c) In-situ electrochemical mass spectra during fuel purification for the anodic half-cell and the cathodic half-cell of the fuel purifier with H_2-CO (1000 ppm CO) gas mixture as anodic feed gas stream. d) Pre- and post-purification H^+/OH^- dual ion concentrations and the charge passed during galvanostatic polarization at 25 mA/cm^2 in 1 hour with H_2-CO (1000 ppm CO) binary gas mixture.

pressure of H_2 in the cathodic half-cell (green trace in Figure 4.2c). In the cathodic half-cell, the presence of CO is almost negligible (blue trace in Figure 4.2c), and extremely pure H_2 gas with impurity CO levels, lower by 99.92% compared to the anodic CO levels is achieved. Following the purification of the H_2-CO (1000 ppm CO) binary gas mixture, the concentration of H^+/OH^- dual ions was measured (Figure 4.2d), revealing a linear relationship between the charge passed and the consumption of H^+/OH^- ions.

Similarly, with an H_2-H_2S gas mixture (1000 ppm H_2S), the Pt-based purifier demonstrated a decrement in the power and current density (blue traces in Figure 4.1a), which is further clear from the galvanostatic polarization (at 25 mA/cm^2), blue trace in Figure 4.1b. This may be due to the slow adsorption of sulfur on the electrode surface.[36,37]

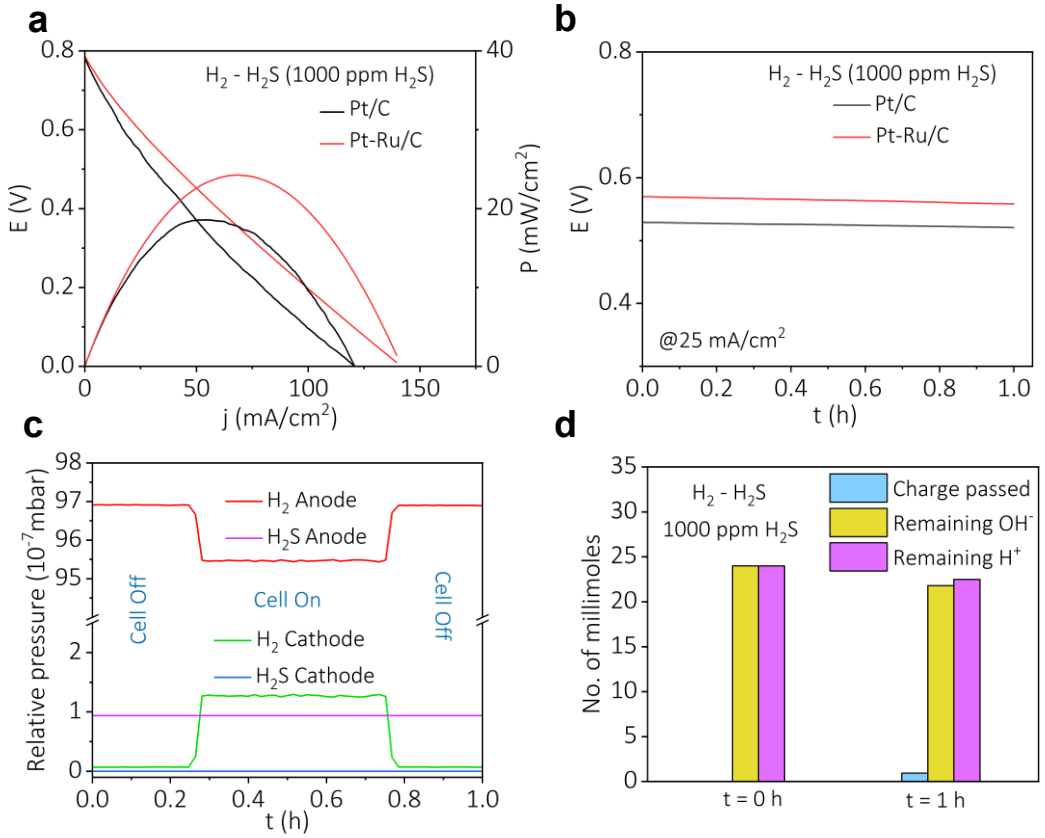

Figure 4.3: a) Polarization curves and b) galvanostatic polarizations at a constant current density of 25 mA/cm² for the fuel purifier with Pt/C and Pt-Ru/C as anodic electrocatalysts. Pure H_2 and H_2-H_2S (1000 ppm H_2S) binary mixtures are used as anodic feed gas streams. c) In-situ electrochemical mass spectra during fuel purification for the anodic half-cell and the cathodic half-cell of the fuel purifier with H_2-H_2S (1000 ppm H_2S) gas mixture as anodic feed gas stream. d) Pre- and post-purification H^+/OH^- dual ion concentrations and the charge passed during galvanostatic polarization at 25 mA/cm² in 1 hour with H_2-H_2S (1000 ppm H_2S) binary gas mixture.

With Pt-Ru/C, the polarization curve with H_2S (1000 ppm H_2S) exhibited a peak power density of nearly 25 mW/cm² at a peak current density of nearly 70 mA/cm² (red trace in Figure 4.3a), which is higher than the performance metrics with Pt/C, (black trace in Figure 4.3a). Chronopotentiometry at a constant current density of 25 mA/cm² (Figure 4.3b) demonstrates the superior performance of Pt-Ru/C compared to Pt/C, confirming the effectiveness of the Pt-Ru catalyst as a poison-resistant anodic electrocatalyst. The in-situ electrochemical mass spectrometry during spontaneous fuel purification of H_2-H_2S mixture (1000 ppm H_2S) shows that there is consumption of H_2 in the anodic half-cell (red trace in Figure 4.3c) and generation of pure H_2 streams in the cathodic half-cell (green trace Figure 4.3c) with impurity H_2S levels lower by 99.90% compared to the anodic H_2S

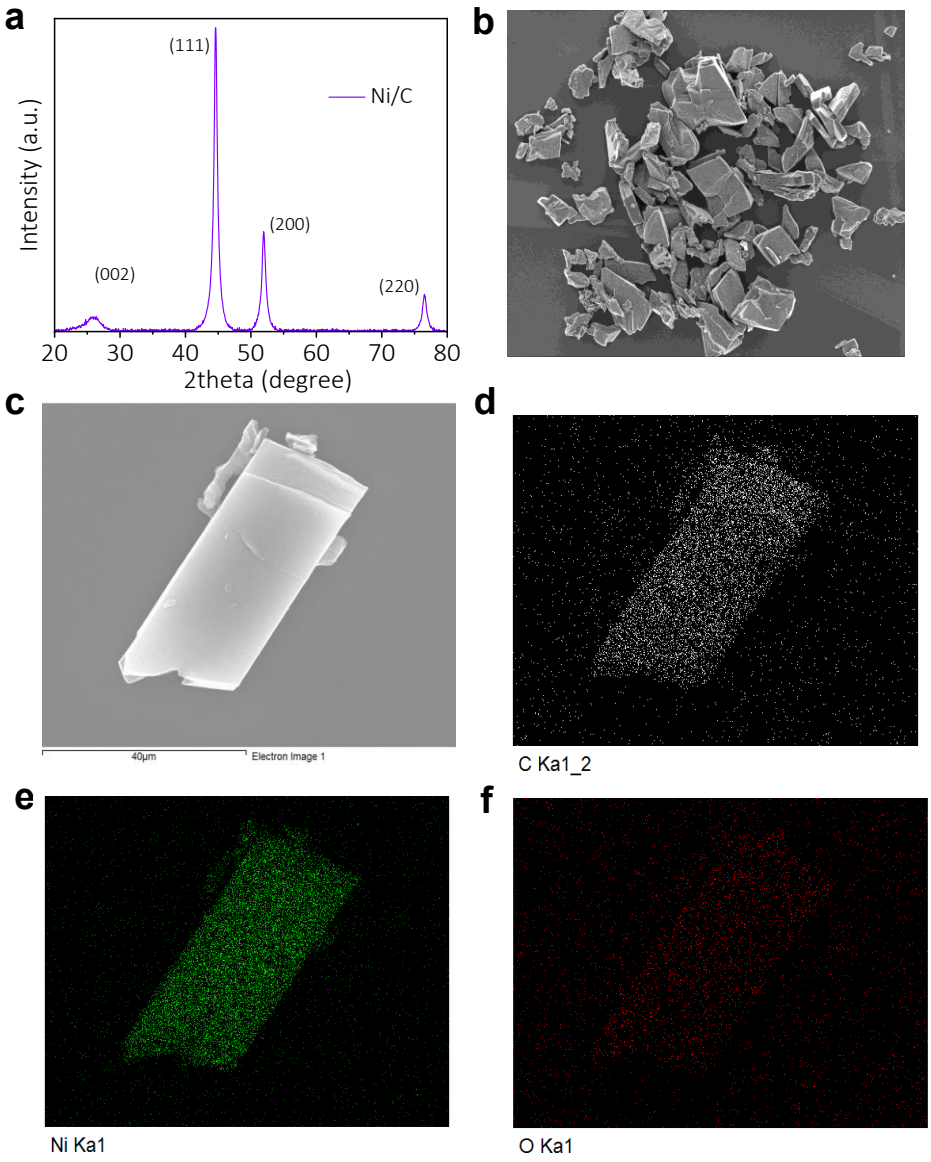

Figure 4.4: a) XRD pattern b) FESEM image and (c) region of EDAX elemental mapping. Elemental mapping images for (d) carbon, (e) nickel, and (f) oxygen of C-embedded Ni nanoparticles.

levels. After the purification of the H_2-H_2S (1000 ppm H_2S) binary gas mixture, the concentration of H^+/OH^- dual ion was measured, Figure 4.3d, and a linear correspondence was obtained between the charge passed and H^+/OH^- dual ion consumption. It is to be noted that H_2S can react with NaOH to form NaHS.[38] However, the amount of H_2S usually present in anodic feed gas streams is very low in concentration, and hence, hydroxyl consumption by H_2S may not pose a threat to device operation under normal circumstances.

Since Pt-Ru/C is a precious metal-based electrocatalyst, to further reduce the cost

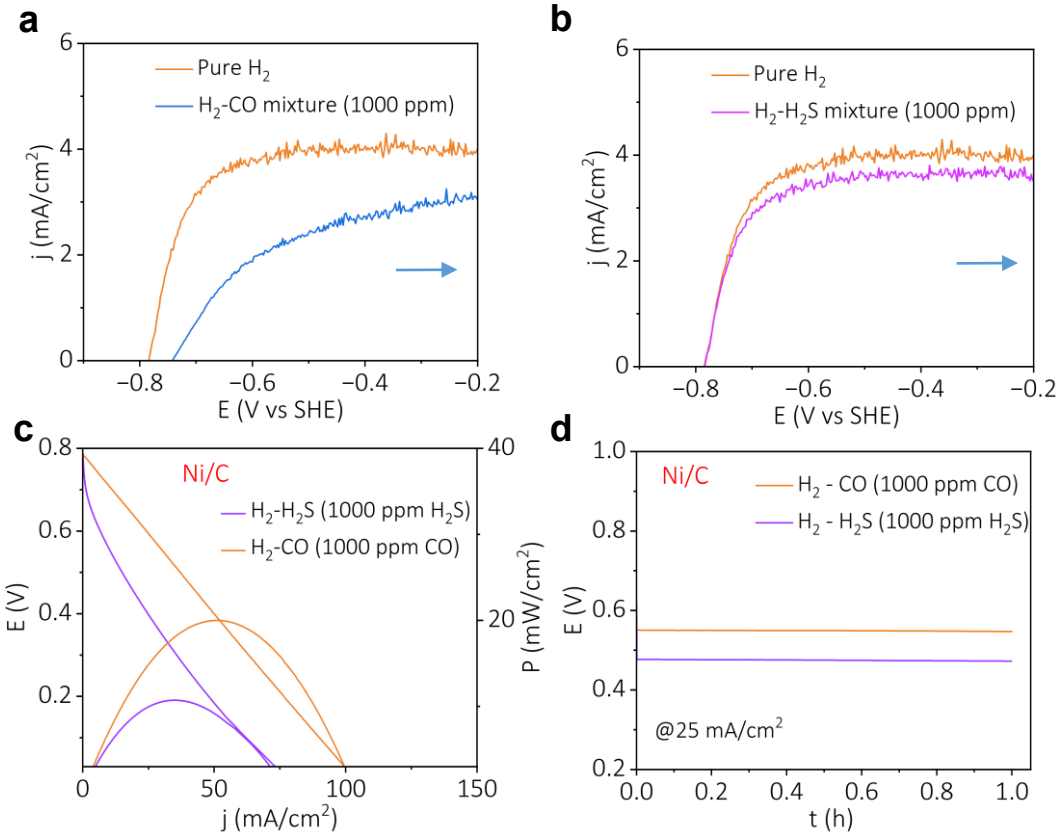

Figure 4.5: a) Rotating disk electrode measurements during hydrogen oxidation reaction at 1600 rpm at a scan rate of 5 mV/s on a Ni-based electrode for (a) H_2-CO binary mixture (1000 ppm CO), and b) H_2-H_2S binary mixture (1000 ppm H_2S) in 1 M NaOH solution. c) Polarization curves and d) galvanostatic polarizations at a constant current density of 25 mA/cm^2 for the device with H_2-CO (1000 ppm CO) binary mixture and H_2-H_2S (1000 ppm H_2S) binary mixture as feed gas streams with Ni/C as anodic electrocatalysts.

of fuel purification, Ni-based electrocatalyst is employed as a poison tolerant alternative[39-41]. Ni/C has been synthesized[42] and characterized Ni/C (Figure 4.4), confirming its successful formation. With Ni/C as the catalyst, the hydrogen oxidation reaction has been carried out with binary poisonous mixtures, Figure 4.5a, 4.5b, and Table 4.2. The outlined data shows that Ni/C poisoning can be reasonably addressed (Figures 4.5a and 4.5b). In device mode, it can achieve a peak power density of 20 mW/cm^2 at the peak current density of 55 mA/cm^2 with an H_2-CO binary mixture (1000 ppm CO), orange trace in Figure 4.5c. It should be noted that Pt-Ru/C has superior H_2S tolerance than Pt/C and Ni/C which is due to slower adsorption kinetics towards S^{2-} species.[37] Galvanostatic polarization at a constant current density of 25 mA/cm^2 exhibits stable performances

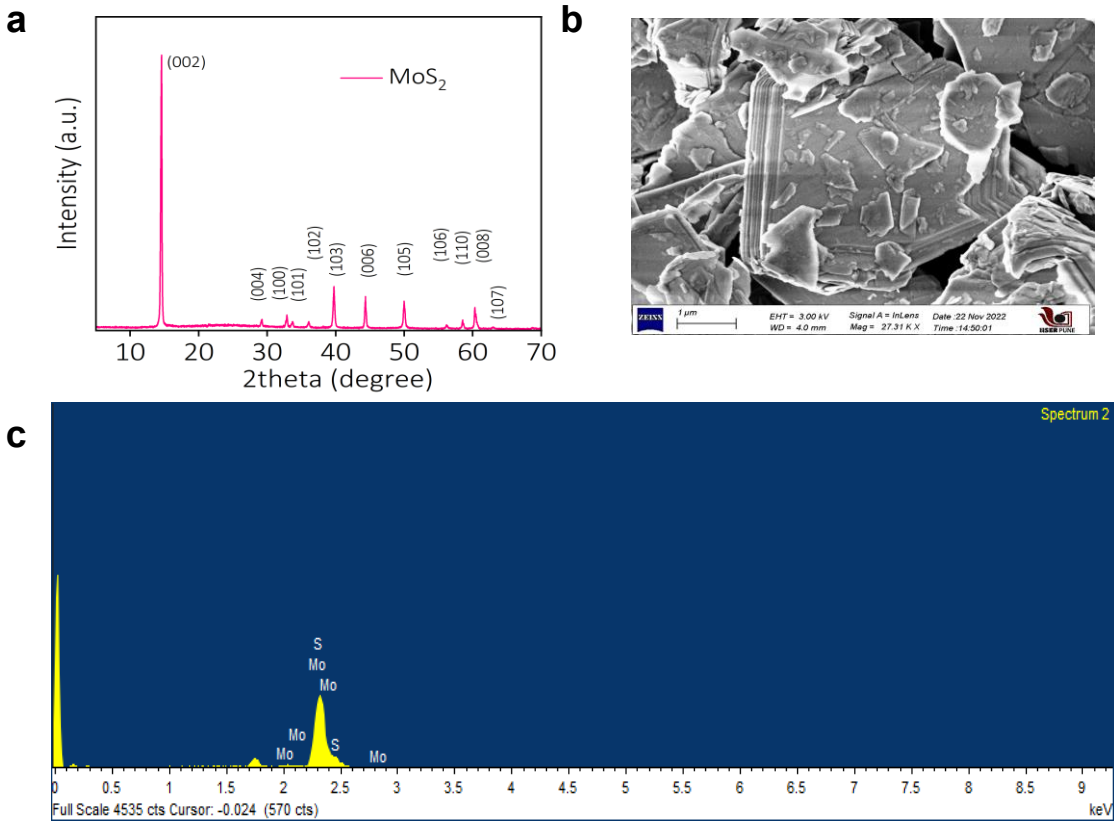

Figure 4.6: a) XRD, b) SEM image and c) EDX spectrum of as synthesized MoS_2.

during the purification of poisonous impurities, Figure 4.5d. All these reveal that a spontaneous fuel purifier driven by the water formation energy can be employed to purify catalyst poisoning impurities by proper engineering of electrocatalytic domains.

Table 4.2: Comparison table of limiting current densities and overpotential (at 3 mA/cm^2) for various gas mixtures on a Ni/C electrode.

Impure Mixtures	Limiting Current (mA/cm^2)	Overpotential (mV) (at 2 mA/cm^2)
Pure H_2	4	115.7
H_2-CO (1000 ppm CO)	2.85	269
H_2-H_2S (1000 ppm H_2S)	3.55	123

One of the important challenges of electrochemical fuel purification is the generation of highly pure H_2 in the cathodic half-cell even in the presence of ambient air, as Pt-based cathodic electrocatalysts can participate in proton-consuming oxygen

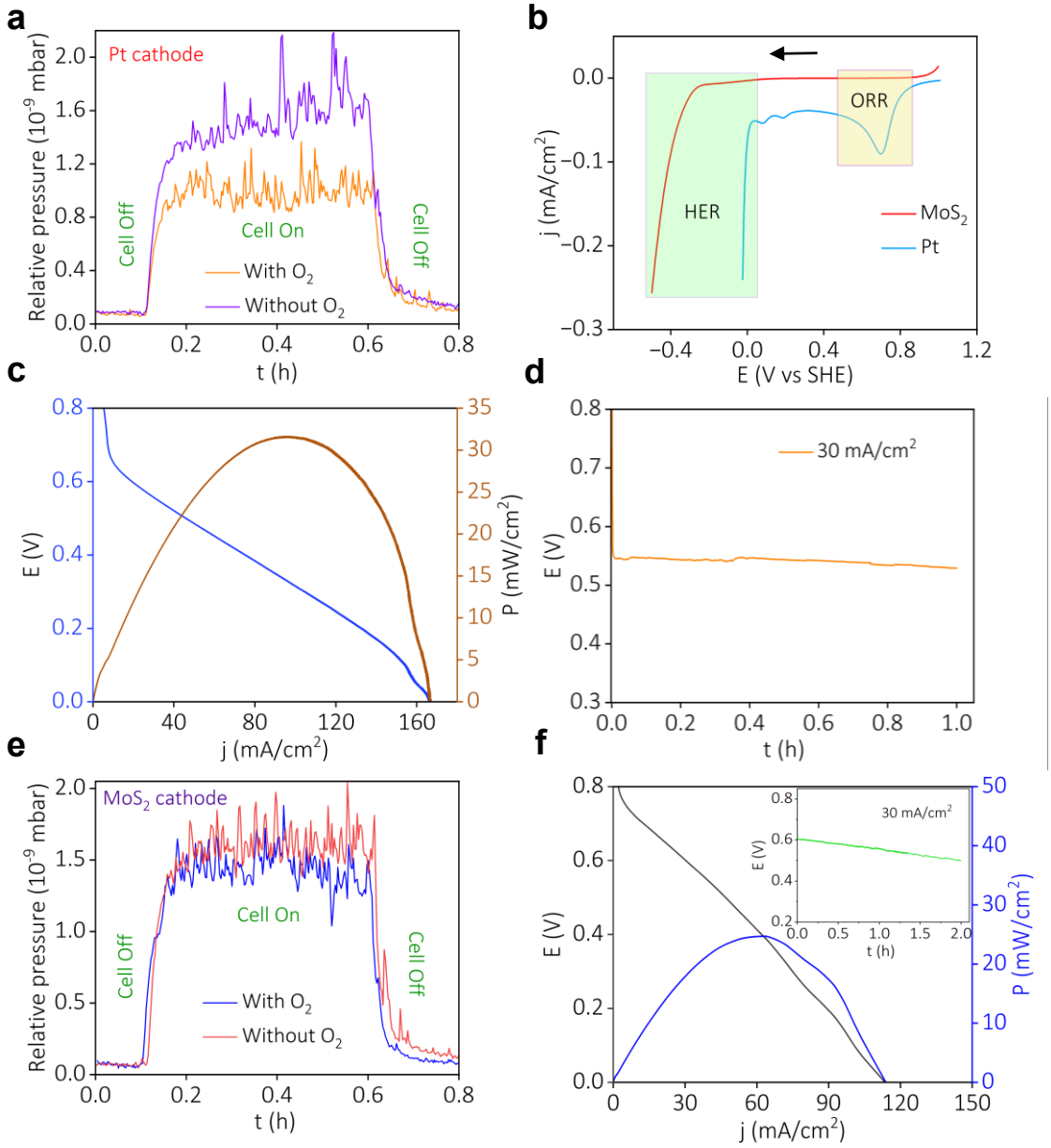

Figure 4.7: a) In-situ electrochemical mass spectrometry of the cathodic half-cell of the fuel purifier with Pt as the cathodic electrocatalyst in the presence and absence of oxygen. b) Linear sweep voltammograms of Pt and MoS_2 electrodes in the presence of oxygen in 0.5 M H_2SO_4 at a scan rate of 20 mV/s. c) Polarization curve and d) galvanostatic polarization (at 30 mA/cm^2) of the purifying device equipped with MoS_2-based cathodic electrocatalyst. e) In-situ electrochemical mass spectrometry of the cathodic half-cell of the fuel purifier with MoS_2 as the cathodic electrocatalyst in the presence and absence of oxygen. f) Polarization curve of the Pt-free fuel purifier equipped with Ni/C as anodic electrocatalyst and MoS_2/rGO as the cathodic electrocatalyst. Inset shows the galvanostatic polarization when a current of 30 mA/cm^2 is drawn from the Pt-free fuel purifier.

reduction reactions.[43] To enable spontaneous fuel purification even in the presence of ambient air (dissolved oxygen in the electrolyte), we have employed MoS_2 based

electrocatalyst (synthesis is carried out as per literature[44-47]), as a selective hydrogen evolution reaction catalyst. Detailed characterization, including XRD, SEM, and EDS, reveals the formation of the MoS_2 electrocatalyst (Figure 4.6). Firstly, in-situ electrochemical mass spectrometry of the cathodic half is performed in the presence and absence of oxygen with a Pt/C cathode, Figure 4.7a). With Pt/C as the cathodic electrocatalyst, the partial pressure of evolved hydrogen in the presence of oxygen (orange trace in Figure 4.7a) is lower as compared to the absence of oxygen, violet trace in Figure 4.7a. The quantity of generated H_2 is decreased in the presence of oxygen,

Figure 4.7a with the platinum as cathodic electrocatalyst. To address the issue, the linear sweep voltammogram was carried out with Pt and MoS_2 electrocatalysts, and it demonstrates that MoS_2 selectively catalyzes hydrogen evolution reaction even in the presence of oxygen, unlike a Pt electrode (Figure 4.7b). When the cathode of the spontaneous fuel purifier (with a Pt/C-based anode) is replaced by a MoS_2-based electrode, a peak power density of nearly 30 mW/cm^2 at a peak current density of nearly 90 mA/cm^2 is obtained with pure H_2 as anodic feed gas (Figure 4.7c). Galvanostatic polarization at a constant current density of 30 mA/cm^2, (Figure 4.7d) shows a stable voltage output for a sufficiently longer duration. In-situ electrochemical mass spectrometry with MoS_2-based cathode shows the feasibility of fuel purification even in the presence of dissolved oxygen. With MoS_2 as a cathodic electrocatalyst, the presence of oxygen does not affect the fuel purification, Figure 4.7e. Taken together, by employing selective HER catalysts, fuel purification can be achieved even under an open-air atmosphere. In addition, it is shown that engineering of catalytic domains can assist in finding non-precious electrocatalysts for this fuel purifier because both HER in acid and HOR in alkali are relatively easily catalysable electrochemical reactions. So, it is attempted to fabricate a Pt-free fuel purifier by exploiting the hydrogen oxidation capability and poison tolerance of Ni/C (Figure 4.5) and hydrogen evolution capability of MoS_2/rGO (Figure 4.7) as demonstrated before. The Pt-free fuel purifier demonstrated a peak power density of 25 mW/cm^2 at a current density of 55 mA/cm^2 (Figure 4.7f and its inset), which attests to the prospects for further decreasing the cost for fuel purification by using this spontaneous fuel purifier. The system employs a poison-resistant electrocatalyst to minimize electrode poisoning and deliver purified hydrogen for direct use in commercial proton exchange membrane fuel cells (PEMFCs). Under open-air

conditions, this thermodynamically downhill process integrates efficient hydrogen fuel purification with power generation in a single step, contributing to a more sustainable hydrogen economy.

4.3 Conclusion

The transition to sustainable energy systems has underscored the critical role of green hydrogen as a clean and versatile energy carrier for achieving a net-zero future. Conventional hydrogen production methods, such as steam methane reforming, biomass gasification, and water electrolysis, often produce hydrogen mixed with impurities like carbon monoxide (CO) and sulfur compounds, which poison platinum-based fuel cells even at trace levels. Energy-intensive and expensive purification methods pose barriers to the hydrogen economy's sustainability. In the proposed approach, a new pathway for hydrogen fuel purification has been developed, by harvesting the energy of water formation to remove poisonous contaminants spontaneously while simultaneously generating electric power. With Pt-Ru/C or Ni/C as anodic electrocatalysts for the fuel purifier, electrode poisoning caused by impurities like CO and H_2S was suppressed, and very pure hydrogen was generated at the cathodic exhaust of the fuel purifier. Even under ambient open-air conditions, it achieves purification through a thermodynamically downhill process with the help of a selective hydrogen evolution reaction electrocatalyst. It offers a cost-effective, an energy-efficient, and a sustainable alternative to traditional methods, paving the way for a broader adoption of green hydrogen as a cornerstone of future energy systems.

4.4 Experimental Section

4.4.1 Materials

H_2SO_4 (98%), NaOH (97%), oxalic acid (98%), Ammonium molybdate tetrahydrate $(NH_4)_6Mo_7O_{24}.\ 4H_2O$, sulfocarbamide $(CS(NH_2)_2)$, KCl (99%), H_2O_2 and phenolphthalein were procured from Sigma Aldrich. Pt supported on carbon catalyst (0.5 mg/cm^2 Pt/C), and Nafion117 membrane were collected from Fuel Cell Store (USA).

4.4.2 Electrochemical Study (Single compartment)

Electrochemical measurements were carried out using a Biologic VMP-300 electrochemical workstation. Cyclic voltammetry experiments employed a three-

electrode setup, with a platinum electrode (0.031 cm^2) as the working electrode and a larger platinum mesh serving as the counter electrode. An Ag/AgCl (3.5 M KCl) electrode was used as the reference. Each measurement utilized 15 mL of electrolyte.

4.4.3 In-situ Electrochemical Mass Spectrometry

In-situ electrochemical mass spectrometry was performed using an HPR-40 quadrupole mass analyser (Hiden Analytical) with a standard QIC inlet. The setup included a 'T'-shaped connector with three ports: one for the mass spectrometer inlet, one for the cell outlet, and one for exhaust to the surroundings. For cathodic half-cell experiments, argon (Ar) served as the carrier gas, while for anodic half-cell experiments, the impure anodic feed gas mixture was fed directly into the mass spectrometer. The gas generated from the cell was directed to the mass spectrometer inlet through the 'T' connector.

4.4.4 Electrochemical Study (Double compartment)

A laboratory prototype for spontaneous H_2 purification was constructed using a two-compartment design made from poly-acrylic sheets. The compartments were separated by a Nafion 117 membrane, which was pretreated in an acidic H_2O_2 solution at 80°C before assembly. To prevent intercompartment leakage, the membrane was secured between two silicone washer gaskets. Each half-cell contained 12 mL of acid and alkali solutions. The anodic electrocatalysts—Pt/C, Pt-Ru/C, and Ni/C—were coated onto Toray carbon sheet, while the cathodic electrocatalysts included electrodeposited Pt on Ti mesh (achieved by applying a constant current of 5 mA/cm^2 for 10 minutes in a chloro-platinic acid solution) and MoS_2/rGO coated on Toray carbon paper. The respective catalyst loadings are detailed in Table 4.3.

Table 4.3: Catalyst loading used at the anodic and cathodic half-cells of the fuel purifier.

	Cathode		Anode		
Catalyst	MoS_2/rGO (MoS_2: rGO = (1: 4)	Pt on Ti mesh	Pt-Ru/C (Pt: Ru: C =2: 3) (Pt: Ru = 2: 1)	Ni/C (Ni: C = 3: 2)	Pt/C (Pt: C = 2: 3)

Amount	2 mg/cm^2	1.5 mg/cm^2	1 mg/cm^2	1 mg/cm^2	1 mg/cm^2

The concentrations of the anolyte and catholyte were determined through acid-base titration with phenolphthalein as an indicator. Initially, the prepared NaOH solution was standardized against oxalic acid, which is the primary standard. Subsequently, the catholyte from the cell was titrated with the standardized NaOH to determine its concentration. Similarly, the anolyte concentration was determined by titration with oxalic acid. Hydrogen generation was quantified using the water displacement technique. All electrochemical experiments were conducted at room temperature and pressure.

4.5 References

1. K. de Kleijne, M. A. J. Huijbregts, F. Knobloch, R. van Zelm, J. P. Hilbers, H. de Coninck and S. V. Hanssen, Nat. Energy, 2024, **9**, 1139-1152
2. S. Li, M. Tabatabaei, F. Li and S. H. Ho, Int. J. Hydrogen Energy, 2024, **54**, 218–238.
3. C. Zhang, J. Low and Y. Xiong, Precis. Chem., 2024, **2**, 229–238.
4. M. D. Allendorf, V. Stavila, J. L. Snider, M. Witman, M. E. Bowden, K. Brooks, B. L. Tran and T. Autrey, Nat. Chem., 2022, **14**, 1214–1223.
5. M. Chatenet, B. G. Pollet, D. R. Dekel, F. Dionigi, J. Deseure, P. Millet, R. D. Braatz, M. Z. Bazant, M. Eikerling, I. Staffell, P. Balcombe, Y. Shao-Horn and H. Schäfer, Chem. Soc. Rev., 2022, **51**, 4583–4762.
6. D. Guan, B. Wang, J. Zhang, R. Shi, K. Jiao, L. Li, Y. Wang, B. Xie, Q. Zhang, J. Yu, Y. Zhu, Z. Shao and M. Ni, Energy Environ. Sci., 2023, **16**, 4926–4943.
7. N. Sazali, Int. J. Hydrogen Energy, 2020, **45**, 18753–18771.
8. A. M, M. K. V, V. S. Hariharan, T. Narahari, A. K. P, M. K, P. K. G and R. Prabakaran, Renew. Sustain. Energy Rev., 2023, **188**, 113791.
9. S. R. Arsad, P. J. Ker, M. A. Hannan, S. G. H. Tang, N. R S, C. F. Chau and T. M. I. Mahlia, Int. J. Hydrogen Energy, 2024, **50**, 447–472.
10. S. K. Dash, S. Chakraborty and D. Elangovan, Energies, 2023. **16**, 1141-1158.
11. M. Younas, S. Shafique, A. Hafeez, F. Javed and F. Rehman, Fuel, 2022, **316**, 123317.
12. Z. Du, C. Liu, J. Zhai, X. Guo, Y. Xiong, W. Su and G. He, Catalysts, 2021, **11**, 1–19.
13. S. Masoudi Soltani, A. Lahiri, H. Bahzad, P. Clough, M. Gorbounov and Y. Yan, Carbon Capture Sci. Technol., 2021, **1**, 100003.
14. A. Midilli, H. Kucuk, M. E. Topal, U. Akbulut and I. Dincer, Int. J. Hydrogen Energy, 2021, **46**, 25385–25412.

15. S. Delgado, T. Lagarteira and A. Mendes, Int. J. Electrochem. Sci., 2020, **15**, 613–627.
16. J. J. Baschuk and X. Li, Int. J. Energy Res., 2001, **25**, 695–713.
17. F. Wang, H. Kishimoto, T. Ishiyama, K. Develos-Bagarinao, K. Yamaji, T. Horita and H. Yokokawa, J. Power Sources, 2020, **478**, 228763.
18. J. H. Kim, M. Liu, Y. Chen, R. Murphy, Y. M. Choi, Y. Liu and M. Liu, ACS Catal., 2021, **11**, 13556–13566.
19. S. K. Das, A. Reis and K. J. Berry, J. Power Sources, 2009, **193**, 691–698.
20. C. Jackson, L. F. J. M. Raymakers, M. J. J. Mulder and A. R. J. Kucernak, J. Power Sources, 2020, **472**, 228476.
21. M. Wang, P. Pei, Y. Xu, P. Ren and H. Wang, Appl. Energy, 2024, **375**, 124021.
22. Y. Qin, C. Sun, S. Ke, R. Wen, Y. Wang, J. Ji and M. Dou, Clean Energy, 2023, **7**, 139–147.
23. G. Bernardo, T. Araújo, T. da Silva Lopes, J. Sousa and A. Mendes, Int. J. Hydrogen Energy, 2020, **45**, 7313–7338.
24. M. Yáñez, F. Relvas, A. Ortiz, D. Gorri, A. Mendes and I. Ortiz, Sep. Purif. Technol., 2020, **240**, 116334.
25. Y. Wang, S. B. Peh and D. Zhao, Small, 2019, **15**, 1–38.
26. H. Li, Z. Song, X. Zhang, Y. Huang, S. Li, Y. Mao, H. J. Ploehn, Y. Bao and M. Yu, Science., 2013, **342**, 95–98.
27. S. Sircar and T. C. Golden, Sep. Sci. Technol., 2000, **35**, 667–687.
28. M. R. Rahimpour, F. Samimi, A. Babapoor, T. Tohidian and S. Mohebi, Chem. Eng. Process. Process Intensif., 2017, **121**, 24–49.
29. L. Schorer, S. Schmitz and A. Weber, Int. J. Hydrogen Energy, 2019, **44**, 12708–12714.
30. E. Fernandez, A. Helmi, J. A. Medrano, K. Coenen, A. Arratibel, J. Melendez, N. C. A. de Nooijer, V. Spallina, J. L. Viviente, J. Zuñiga, M. van Sint Annaland, D. A. Pacheco Tanaka and F. Gallucci, Int. J. Hydrogen Energy, 2017, **42**, 13763–13776.
31. M. J. Lee, J. S. Kang, Y. S. Kang, D. Y. Chung, H. Shin, C. Y. Ahn, S. Park, M. J. Kim, S. Kim, K. S. Lee and Y. E. Sung, ACS Catal., 2016, **6**, 2398–2407.
32. T. Yajima, H. Uchida and M. Watanabe, J. Phys. Chem. B, 2004, **108**, 2654–2659.
33. Q. Li, R. He, J.-A. Gao, J. O. Jensen and N. J. Bjerrum, J. Electrochem. Soc., 2003, **150**, A1599.
34. J. Y. Tilquin, R. Côté, D. Guay, J. P. Dodelet and G. Denès, J. Power Sources, 1996, **61**, 193–200.
35. W. Dong, C. Xu, W. Zhao, M. Xin, Y. Xiang, A. Zheng, M. Dou, S. Ke, J. Dong, L. Qiu and G. Xu, ACS Appl. Energy Mater., 2022, **5**, 12640–12650.
36. H. Chen, F. Wang, W. Wang, D. Chen, S. D. Li and Z. Shao, Appl. Energy, 2016, **179**, 765–777.
37. S. Ke, B. Cui, C. Sun, Y. Qin, J. Zhang and M. Dou, ACS Appl. Mater. Interfaces, 2022, **14**, 47765–47774.
38. A. Bagreev and T. J. Bandosz, Ind. Eng. Chem. Res., 2002, **41**, 672–679.

39. Y. Gao, Y. Yang, R. Schimmenti, E. Murray, H. Peng, Y. Wang, C. Ge, W. Jiang, G. Wang, F. J. DiSalvo, D. A. Muller, M. Mavrikakis, L. Xiao, H. D. Abruña and L. Zhuang, Proc. Natl. Acad. Sci. U. S. A., 2022, **119**, 1–9.
40. F. Song, W. Li, J. Yang, G. Han, P. Liao and Y. Sun, Nat. Commun., 2018, **9**, 1-10.
41. S. Qin, Y. Duan, X. L. Zhang, L. R. Zheng, F. Y. Gao, P. P. Yang, Z. Z. Niu, R. Liu, Y. Yang, X. S. Zheng, J. F. Zhu and M. R. Gao, Nat. Commun., 2021, **12**, 1–10.
42. H. Liang, R. Li, C. Li, C. Hou, Y. Li, Q. Zhang and H. Wang, Mater. Horizons, 2019, **6**, 571–579.
43. L. Huang, S. Zaman, X. Tian, Z. Wang, W. Fang and B. Y. Xia, Acc. Chem. Res., 2021, **54**, 311–322.
44. S. Wang, C. An and J. Yuan, Materials (Basel)., 2010, **3**, 401–433.
45. Y. Kim, D. H. K. Jackson, D. Lee, M. Choi, T. W. Kim, S. Y. Jeong, H. J. Chae, H. W. Kim, N. Park, H. Chang, T. F. Kuech and H. J. Kim, Adv. Funct. Mater., 2017, **27**, 1701825.
46. C. Feng, J. Ma, H. Li, R. Zeng, Z. Guo and H. Liu, Mater. Res. Bull., 2009, **44**, 1811–1815.
47. U. Krishnan, M. Kaur, K. Singh, M. Kumar and A. Kumar, Superlattices Microstruct., 2019, **128**, 274–297.

Chapter 5

A Spontaneous Heavy Hydrogen Generator via Electrochemical Heavy Water Formation

Abstract

The extreme significance of heavy hydrogen (D_2) in medicinal, nuclear, and chemical sectors, despite its scarce natural abundance, underscores the vital imperative for inventing novel chemistries for its production. A spontaneous heavy hydrogen generator is demonstrated during commensurate electrical energy production by decoupling the direct chemistry of OD^-/D^+ dual ions via a pH-dependent protium redox. This exergonic electrochemistry yields ~357 mL of D_2 in nearly 85 hours of continuous electrolysis, with a commensurate electrical energy output of 122 kJ/per mole of D_2. This laboratory-level demonstration of spontaneous heavy hydrogen production presents a novel chemistry for the scalable manufacture of non-primordial D_2.

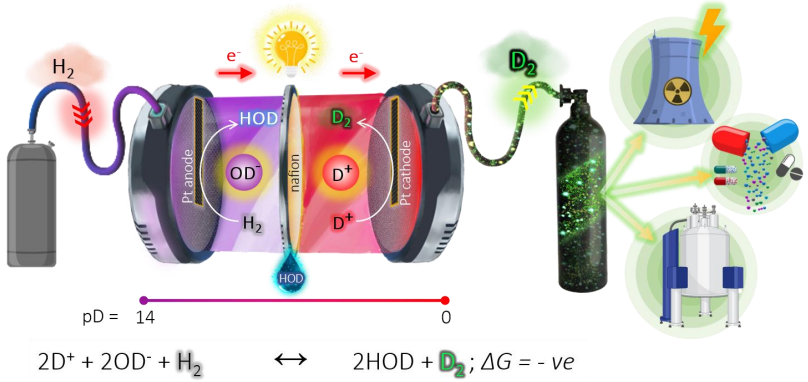

This work has been published in the following journal:

Ritwik Mondal et al. *J. Phys. Chem. Lett.* **2024**, *15* (26), 6866–6871.

5.1 Introduction

Despite being the third most abundant element in the universe, deuterium's natural abundance on Earth is a mere 0.01%.[1-3] Heavy hydrogen has extensive applications in various sectors, including nuclear magnetic resonance, drug development, medicinal chemistry, biochemical tracer, deuterated industrial chemical synthesis, and neutron moderator in nuclear reactors.[4-9] Having an excess neutron in the nucleus, deuterium (D_2) is electrochemically distinct from protium (H_2).[10] With regard to its low zero point energy, small ion product, and significant dehydration energy of heavy water (D_2O), deuterium exhibits the electrochemical isotopic effect (EEI).[11-15] The sole non-primordial D_2 production mechanisms are cryogenic, photocatalytic, and electrochemical processes.[2,16-20] There are few pieces of evidence to show that electrolysis of heavy alkaline (NaOD in D_2O) or heavy acidic water (D_2SO_4 in D_2O) can lead to deuterium (D_2) production. Still, it demands a high applied voltage of nearly 1.6 V to initiate the electrochemical production of heavy hydrogen.[20-22] However, the severe conditions render the process economically unfeasible and mostly inconvenient.[16,20-25]

In contrast to the endergonic processes for deuterium synthesis, a spontaneous deuterium generator is demonstrated operating along a thermodynamically downhill pathway during concurrent electrical power delivery under natural weather conditions. The foundation of this spontaneous deuterium generator relies on the instantaneous interconversion of the redox energy of OD^-/D^+ dual ions by hydrogen redox. A laboratory-level deuterium-generating prototype produces ~357 ml of heavy hydrogen in nearly 85 hours of continuous electrolysis under ambient conditions with a commensurate electric power output of 122 kJ/per mole of D_2.

5.2 Results and Discussion

This spontaneous heavy hydrogen generator comprises two half-cells separated by a Nafion 117 membrane, as illustrated in Scheme 5.1. The anolyte is a sodium deuteroxide (NaOD) solution in heavy water (D_2O) with a platinum-based electrocatalyst as the anodic electrocatalyst.

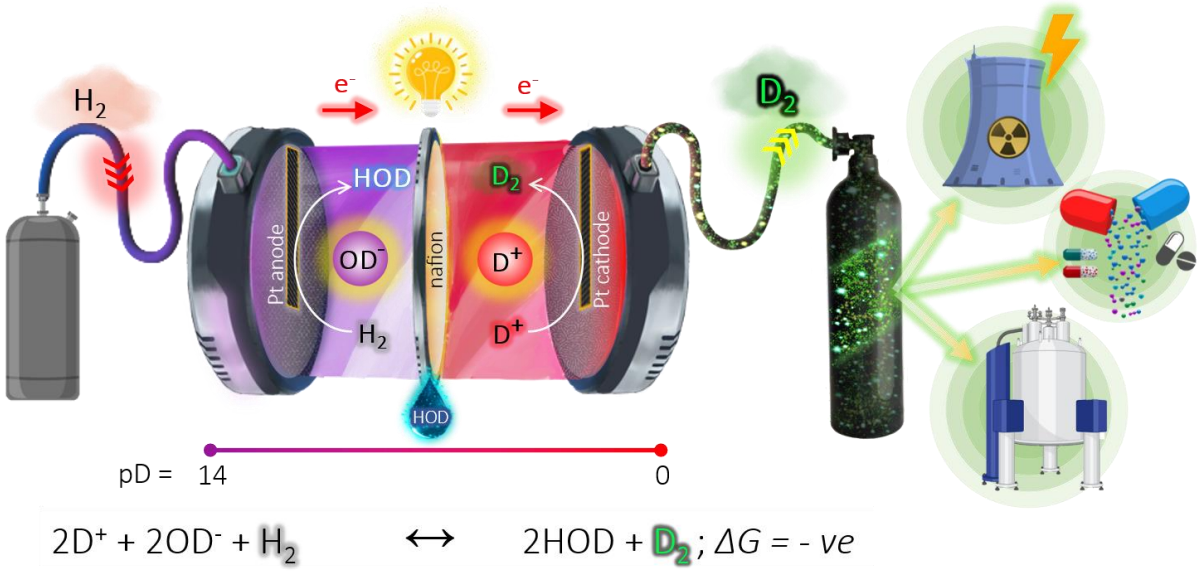

Scheme 5.1 Schematics of spontaneous electrochemical deuterium generator under ambient weather conditions.

Dideuterosulphuric acid (D_2SO_4) solution in heavy water (D_2O) serves as the catholyte, with a platinum-based electrode as the cathodic electrocatalyst. The Nafion 117 membrane was treated with D_2SO_4/D_2O solution for 12 hours for activation. In this architectural design, the direct acid (pD = 0) alkali (pD = 14) chemistry is decoupled, and an inbuilt electromotive force of ~0.85 V (ΔG^0 = -83.5 kJ/mol) will be developed between the two half-cells (Calculation 5.1).

Calculation 5.1

Net cell reaction for heavy hydrogen system

$H^+ + OD^- \leftrightarrow HOD$

Enthalpy change for the reaction

$\Delta H^0 = H^0(HOD) - H^0(H^+) - H^0(OD^-)$

$= -289.3 - 0 - (-231.9)$

$= \mathbf{-57.4\ kJ/mol}$

Entropy change for the reaction

$\Delta S^0 = S^0(HOD) - S^0(H^+) - S^0(OD^-)$

= 79.3 – 0 – (– 8.3)

= 87.6 J/ K mol = **0.0876 kJ/K mol**

Gibbs free energy of the reaction

$\Delta G^0 = \Delta H^0 - T\Delta S^0$

= – 57.4 – (298 * 0.0876)

= **– 83.5 kJ/mol**

$\Delta G^0 = - nFE^0$

$E^0 = - \Delta G^0 / nF$

$E^0 = - (- 83500)/1*96500$

E^0 = **0.85 V**

0.85 V of electromotive force can be harvested from the heavy hydrogen system.

Nevertheless, because of the non-redox nature of the recombination reaction of OD^-/D^+ dual ions, it cannot be harvested directly as an electrical driving force. To make this direct interconversion possible, hydrogen redox is employed because the acid-base reaction is just the difference between the hydrogen redox in the alkaline electrolyte and the acidic electrolyte (equations 5.1 and 5.2). These suggest that hydrogen is consumed in the alkaline anolyte with concomitant hydrogen evolution in the acidic catholyte. Hence, the overall reaction chemistry does not involve any net consumption of hydrogen fuel (equation 5.3). On replacing the acidic half-cell with D_2SO_4 instead of H_2SO_4, this chemistry should evolve D_2 instead of H_2 at the expense of hydrogen fuel in the anodic half-cell, equations 5.4 to 5.6.

In the case of the hydrogen system,

Anodic half-cell reaction:

$2H_2O + 2e^- \leftrightarrow H_2 + 2OH^-$ **(equation 5.1)**

Cathodic half-cell reaction:

$2H^+ + 2e^- \leftrightarrow H_2$ **(equation 5.2)**

Overall cell reaction:

$2H^+ + 2OH^- \leftrightarrow 2H_2O$ **(equation 5.3)**

In the case of the deuterium system,

Anodic half-cell reaction:

$2HOD + 2e^- \leftrightarrow H_2 + 2OD^-$ **(equation 5.4)**

Cathodic half-cell reaction:

$2D^+ + 2e^- \leftrightarrow D_2$ **(equation 5.5)**

Overall cell reaction:

$2D^+ + 2OD^- + H_2 \leftrightarrow 2HOD + D_2$ **(equation 5.6)**

To check its feasibility, deuterium and hydrogen redox reactions were probed in the acidic and alkaline media. In the cyclic voltammograms, the anodic peak corresponds to the deuterium/hydrogen oxidation reaction (DOR/HOR), and the cathodic currents are due to the deuterium/hydrogen evolution reaction (DER/HER). In deuterated sulphuric acid solution (D_2SO_4), the deuterium evolution reaction is negatively shifted as compared to H_2SO_4, with a similar shift in corresponding alkaline solutions, Figure 5.1a, Figure 5.1b and Table 5.1.

Table 5.1. Cathodic and anodic currents extracted from Figures 5.1a and 5.1b.

Electrolyte	Anodic peak current (HOR/DOR)	Cathodic current at η = 0.035 V (HER/DER)
H_2SO_4	0.049 mA/cm^2	-0.55 mA/cm^2
D_2SO_4	0.050 mA/cm^2	-0.50 mA/cm^2
NaOH	0.033 mA/cm^2	-0.23 mA/cm^2
NaOD	0.026 mA/cm^2	-0.16 mA/cm^2

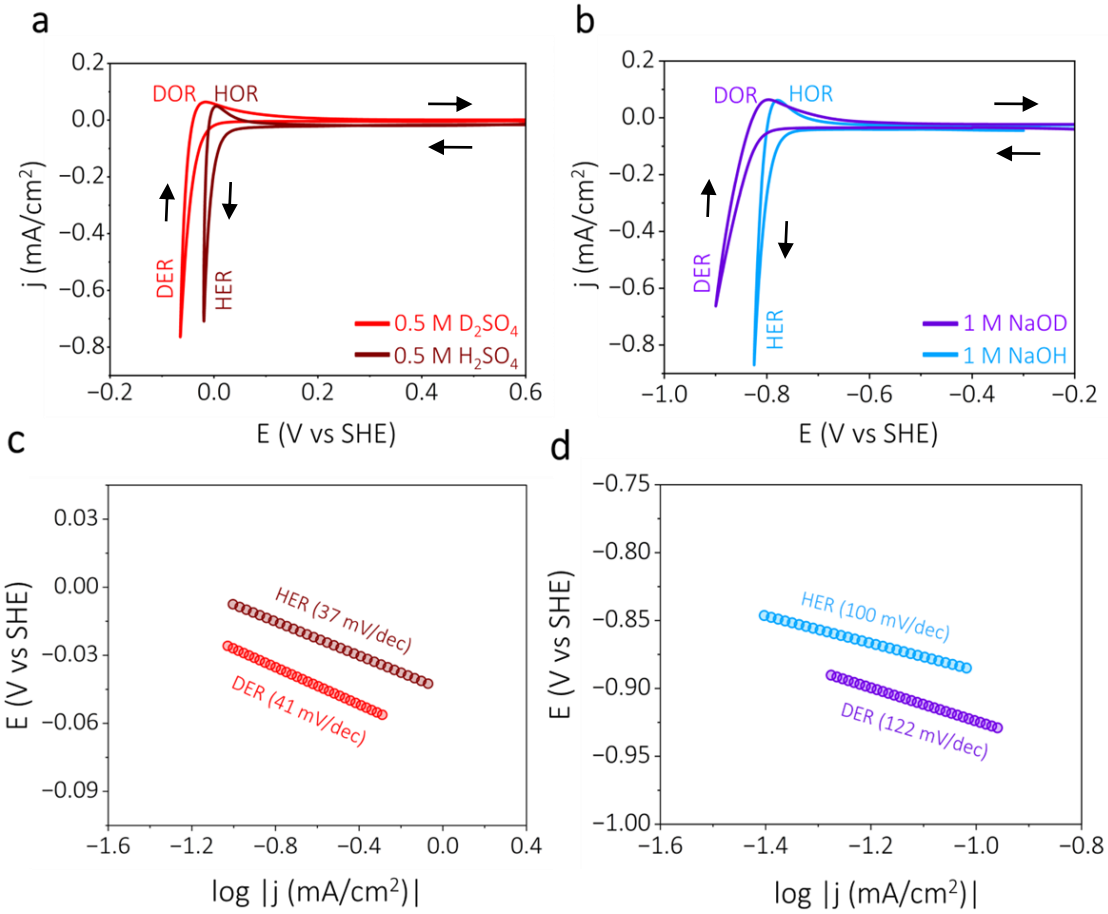

Figure 5.1: a) Hydrogen redox in acidic (wine red trace) and deuterium redox in heavy acidic (red trace) electrolytes. b) Hydrogen redox in alkaline (sky blue trace) and deuterium redox in heavy alkaline (violet trace) electrolytes. c) Tafel plots for HER in acidic (wine red trace) and DER in heavy acidic (red trace) electrolytes. d) Tafel plots for HER in alkaline (sky blue trace) and DER in heavy alkaline (violet trace) electrolytes.

This is attributed to the electrochemical isotopic effect (EEI) caused by deuterium's lower zero-point energy coupled with heavy water's high dehydration energy.[11-13, 26-28] For D_2O, the elevated activation energy, stemming from its lower zero-point energy, leads to a relatively high overpotential for the deuterium evolution reaction.[11] The smaller ionic product of D_2O ($K_{w(H2O)} = 10^{-14}\,mol^2\,L^{-2}$, $K_{w(D2O)} = 0.25\times10^{-14}\,mol^2\,L^{-2}$) also translates to a lower concentration of D^+ ions in the solution, consequently resulting in a decreased rate of the deuterium evolution reaction.[11,13] The disparity in zero-point energy (ZPE) between D and H leads to a difference in the solvation or hydration energy between D_2O and H_2O. Due to the mass increment from H to D, the nuclear-electron vibration becomes weaker for D systems, resulting in higher solvation energy in the case of D_2O.[11] The higher dehydration energy of D_2O also renders the deuterium evolution reaction (DER) less

electrochemically favorable compared to the hydrogen evolution reaction (HER) in H_2O.[11,14] As the entropy change of the D system is relatively more positive than the H system, the energy harvesting from the surroundings will be higher for the former as compared to the latter (Calculations 5.1 and 5.2). This leads to a slightly higher thermodynamic efficiency for the D system (1.45) (Calculation 5.1) compared to the H system 1.43 (Calculation 5.2). To investigate the kinetic behavior, we have derived the Tafel slope values for hydrogen and heavy hydrogen evolution reaction (HER/DER) in acidic and alkaline media. It has been observed that HER has a lower Tafel slope compared to DER in both the media, Figure 5.1c and 5.1d, resulting in a relatively faster reaction kinetics for HER than DER. This may be attributed to the relatively lower zero-point energy of the D_2O and its smaller ionic product compared to H-based systems.[10-14]

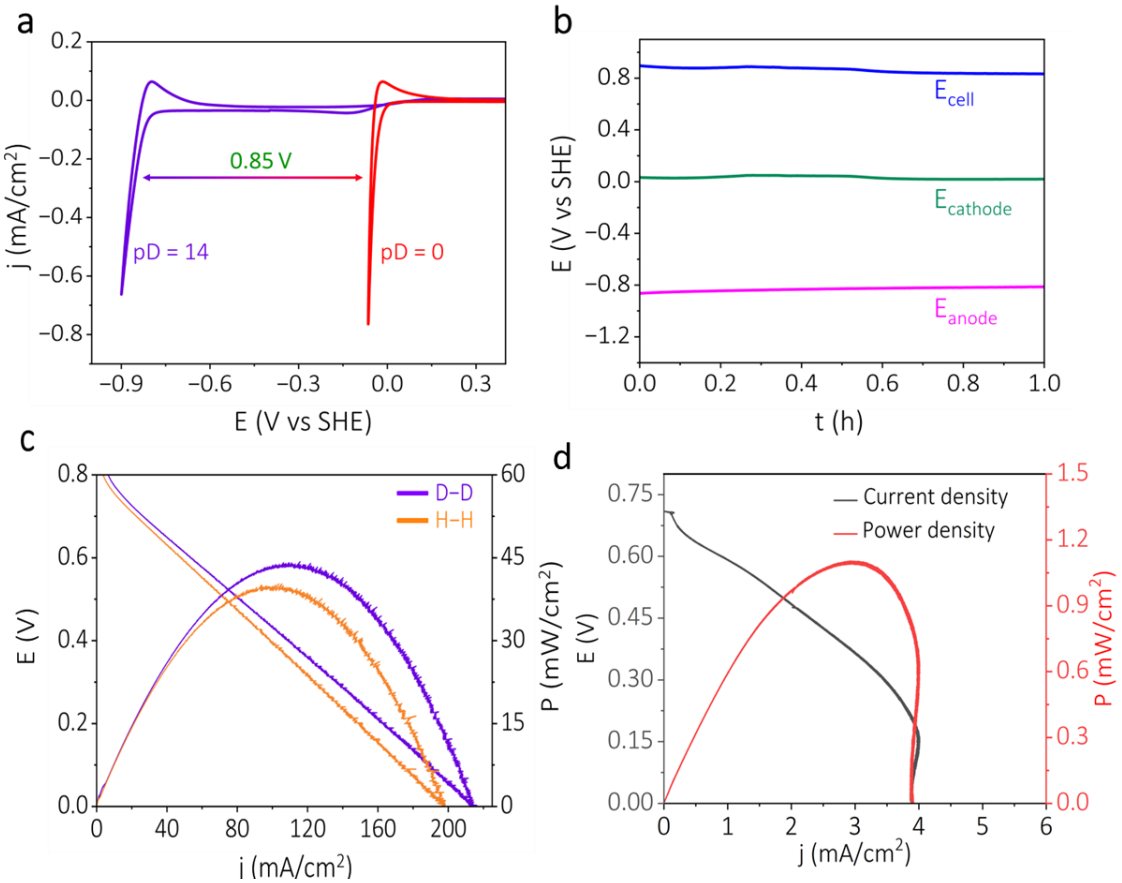

Figure 5.2: a) The accessible potential difference available based on the gradients in dual ions concentration (pD gradients) between the electrolytes. b) Single electrode potentials of the half cells of the two-electrode device with pD gradients of 14 (anodic) and 0 (cathodic). c) Polarisation curves for the two-compartment device with NaOH-H_2SO_4 (orange trace) and NaOD-D_2SO_4 (violet trace) dual electrolyte systems. d) Polarisation curve for electrochemical heavy hydrogen generator without H_2 feed at the anodic half-cell with NaOD/D_2O as anolyte and D_2SO_4/D_2O as catholyte.

In summary, these characteristics of D_2O lead to a distinct electrochemical disparity in its activity compared to H_2O. In line with these, a positive potential difference of around 0.85 V (Calculation 5.2) is observed between the hydrogen redox in an alkaline medium (pD = 14, 1 M NaOD) and the deuterium redox in the acidic medium (pD = 0, 0.5 M D_2SO_4), Figure 5.2a. Single electrode potentials Figure 5.2b suggests that hydrogen-fed alkaline half-cell exhibits more negative potential than the deuterium evolving acidic half-cell in the device configurations, resulting in an overall positive cell potential, Figure 5.2b.

Calculation 5.2

Net cell reaction for hydrogen system

$H^+ + OH^- \leftrightarrow H_2O$

Enthalpy change for the reaction

$\Delta H^0 = H^0 (H_2O) - H^0 (H^+) - H^0 (OH^-)$

$= -285.8 - 0 - (-230)$

$=$ **-55.8 kJ/mol**

Entropy change for the reaction

$\Delta S^0 = S^0 (H_2O) - S^0 (H^+) - S^0 (OH^-)$

$= 69.91 - 0 - (-10.75)$

$= 80.66$ J/ K mol = **0.08066 kJ/K mol**

Gibbs free energy of the reaction

$\Delta G^0 = \Delta H^0 - T\Delta S^0$

$= -55.8 - (298 * 0.08066)$

$=$ **-79.875 kJ/mol**

$\Delta G^0 = -nFE^0$

$E^0 = -\Delta G^0 / nF$

$E^0 = -(-79875)/1*96500$

E^0 = **0.82 V**

0.82 V of electromotive force can be harvested from the hydrogen system.

Consequently, the heavy alkaline (NaOD) anodic half-cell should experience oxidation upon feeding hydrogen (H_2) and release electrons (equation 5.4). Upon acquiring these electrons, a corresponding deuterium evolution reaction (equation 5.5) should occur at the cathodic half-cell with the heavy acidic electrolyte (D_2SO_4). Since heavy hydrogen (D_2) is produced at the expense of light hydrogen (H_2) during electric power delivery (equation 5.6); this device is named a spontaneous heavy hydrogen generator. The polarization curve for this deuterium generator exhibits a peak power density of ~45 mW/cm^2 at a current density of nearly 115 mA/cm^2 (violet trace in Figure 5.2c). The performance comparison when D_2 evolution is replaced by H_2 evolution is almost identical, (orange trace in Figure 5.2c). It should be noted that no appreciable power density was observed in the absence of hydrogen as the anodic feed, suggesting that H_2 is the fuel for this deuterium generator, Figure 5.2d. Galvanostatic polarization at a constant current density of 40 $mA/\ cm^2$ shows a decent voltage output with spontaneous deuterium evolution (violet trace in Figure 5.3a). Over time, the potential output was observed to gradually decline due to the continuous decline in H^+/D^+ and OH^-/OD^- dual-ion gradients in the respective half cells, Calculation 5.3. A similar behavior is observed when deuterium evolution is replaced by hydrogen evolution, orange trace in Figure 5.3a.

Calculation 5.3

The total cell reaction for the deuterium generator is:

$$\tfrac{1}{2}\ H_2\ (g) + D^+\ (aq) + OD^-\ (aq) \rightarrow HOD\ (l) + \tfrac{1}{2}\ D_2\ (g)$$

The free energy change for that reaction can be written as follows:

$$\Delta G = \Delta G^o + RT \ln \left(^{product}/_{reactant}\right)$$

$$\Delta G = \Delta G^o + RT \ln \left(^{[HOD]}/_{[D^+][OD^-]}\right)$$

$$\Delta G = \Delta G^o - RT \ln [D^+] - RT \ln [OD^-]$$

$$\Delta G = \Delta G^o - RT\ 2.303\ (\log[D^+] + \log [OD^-])$$

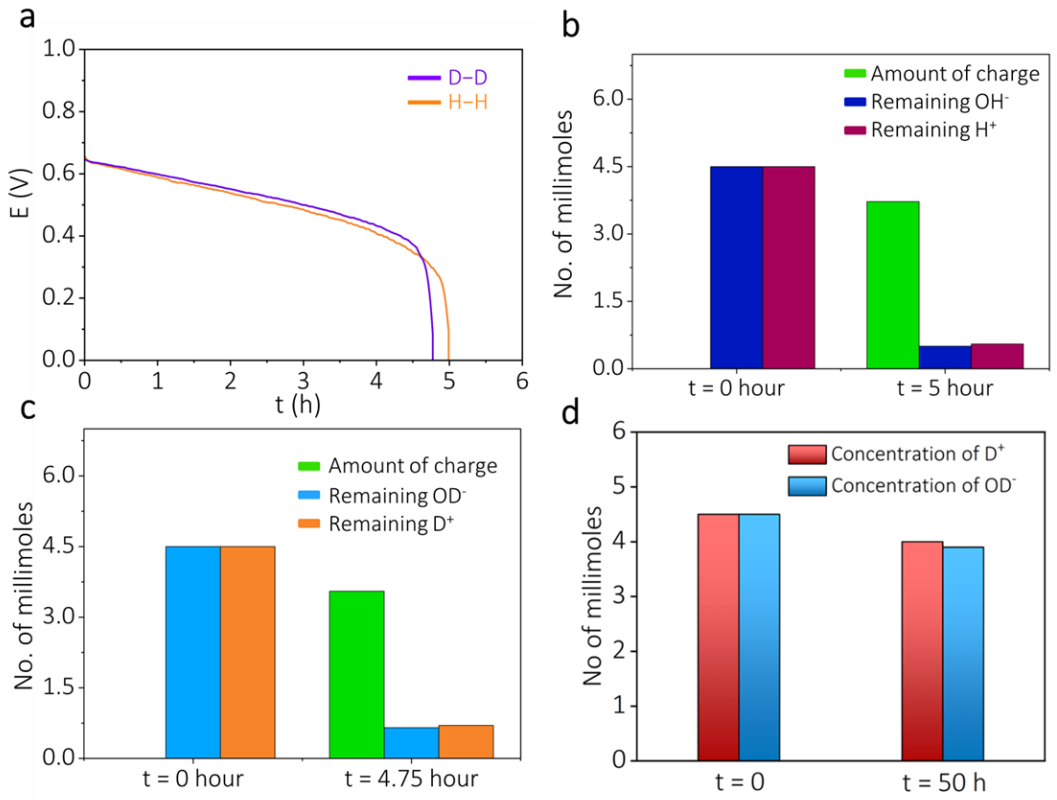

Figure 5.3: a) Galvanostatic polarisation at a constant current density of 40 mA/cm^2 for both devices. The correlation between the charge passed and the changes in the H^+/D^+ concentrations in the catholyte and OH^-/OD^- in the anolyte during the galvanostatic polarizations for b) NaOH-H_2SO_4 electrolyte and c) NaOD-D_2SO_4 electrolytes. d) Amount of D^+ in the catholyte and OD^- in the anolyte before and after keeping the system under open circuit condition for 50 hours.

$\Delta G = \Delta G^o - RT\ 2.303\ (-pD - pOD)$

$\Delta G = \Delta G^o + RT\ 2.303\ (pD + pOD)$

$\Delta G = \Delta G^o + RT\ 2.303\ (pD_A + 14 - pD_B)$,

where pD_A = pD of acidic electrolyte and pD_B = pD of alkaline electrolyte

$\Delta G = \Delta G^o + RT\ 2.303\ (pD_A - pD_B) + RT\ 2.303*14$

$\Delta G = \Delta G^o - RT\ 2.303\ \Delta pD + RT\ 2.303*14 \qquad (pD_B > pD_A)$

$\Delta G = -79.8 - 5.7\Delta pD + 79.8$

$\Delta G = -5.7\ \Delta pD$

$E = {}^{-\Delta G}/_{nF} = 0.059\ \Delta pD.$

Equation 5.6 suggests that the lifetime of this cell relies on the OD^-/D^+ dual ion concentration gradient between the two half-cells. The dual ion concentrations are estimated before and after the electrochemical deuterium evolution, and they are found to decrease substantially for both systems after the long-term constant current test, Figure 5.3b and 5.3c. Following the constant current tests, the left-over dual ion concentrations are determined (Figure 5.3b and 5.3c), and the quantity of their consumption is commensurate with the amount of charge passed during the constant current test. When current is drawn from the device for nearly 5 hours (Figure 5.3a), the remaining electrolyte contains only ~15 % of dual ions (H^+/D^+ and OH^-/OD^-). When no current is drawn, there is a minimal fluctuation in the dual-ion concentrations of the device for an extended period of 50 hours, Figure 5.3d. Taken together, these suggest that dual ions are consumed via an electrochemical route during spontaneous heavy hydrogen generation (as shown in equation 5.6).

To investigate the working mechanism of the proposed device, in-situ electrochemical mass spectrometry is performed with the NaOH-H_2SO_4 with H^+/OH^- dual ion gradients, Figure 5.4. In the in-situ electrochemical mass spectra, a decrease in

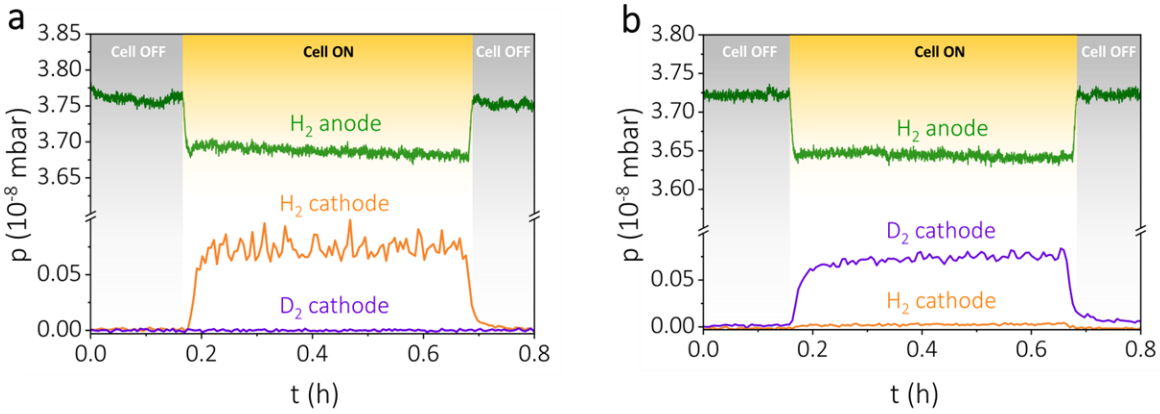

Figure 5.4: In-situ electrochemical mass spectra for the device with a) NaOH-H_2SO_4 dual electrolytes and b) NaOD-D_2SO_4 dual electrolytes.

the partial pressure of hydrogen was noted in the anodic half-cell (indicated by the green trace in Figure 5.4a), accompanied by a simultaneous increase in hydrogen partial pressure in the cathodic half-cell (depicted by the orange trace in Figure 5.4a) during the operation of the cell. This indicates the consumption of H_2 at the alkaline anode and hydrogen evolution in the cathodic half-cell, thereby corroborating equation 5.4. However, in the NaOD-D_2SO_4 system with D^+/OD^- dual ion gradients, it was observed

that when the cell is kept ON, H_2 is consumed at the anodic half-cell (green trace in Figure 5.4b). Simultaneously, D_2 is produced at the cathodic half-cell (violet trace in Figure 5.4b). This suggests that D_2 is evolved at the cost of the H_2 at anode, corroborating equation 5.5. It is to be noted that a small amount of HD also evolved (whose amount was quantified as discussed below), which is attributed to the presence of trace amounts of water as an impurity in deuterated solvents.

To quantify the amount and faradaic efficiency of evolved deuterium, we have correlated the charge passed with respect to the amount of D_2, HD, and H_2 produced. In-situ electrochemical mass spectrometry of the cathodic half-cell of the deuterium-generating device has been carried out, Figure 5.5a. It has exhibited a Faradaic efficiency of nearly 92% for D_2, 6.5% for HD, and 1.5% for H_2 (Figure 5.5b, Calculation 5.4).

Calculation 5.4

From Figure 5.5a

The area under the cell on the portion of the violet trace (D_2) = $3.8545 * 10^{-10}$

The area under the cell on the portion of the green trace (HD) = $2.933 * 10^{-11}$

The area under the cell on the portion of the orange trace (H_2) = $6.402 * 10^{-12}$

$$D_2 = 3.8545 * 10^{-10} / (3.8545 + 0.2933 + 0.06402) * 10^{-10}$$

$$= 92\ \%$$

$$HD = 0.2933 * 10^{-10} / (3.8545 + 0.2933 + 0.06402) * 10^{-10}$$

$$= 6.5\ \%$$

$$H_2 = 0.064 * 10^{-10} / (3.8545 + 0.2933 + 0.06402) * 10^{-10}$$

$$= 1.5\ \%$$

The rate capability at various current densities was carried out, as shown in Figure 5.5c, demonstrating the device's capability to sustain reasonably higher rates. The total

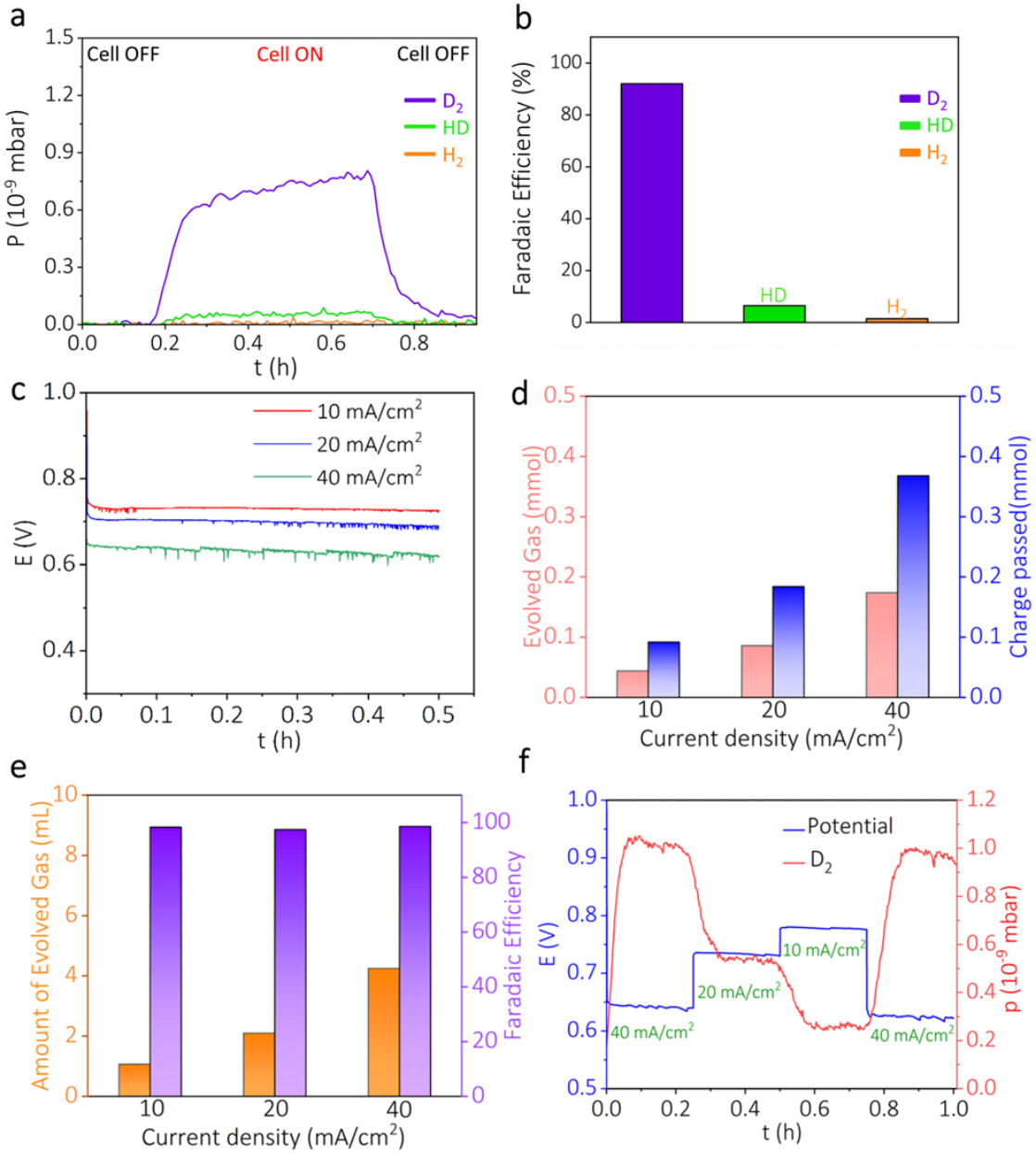

Figure 5.5: a) In-situ electrochemical mass spectra of the cathodic half-cell of the electrochemical deuterium generator with NaOD-D_2SO_4 dual electrolyte system. b) Faradaic efficiency for the electrochemical deuterium evolution. c) Rate capability study of the spontaneous heavy hydrogen generator. d) The correlation between charge passed and quantity of evolved gas during the constant current test at various current densities. e) The quantity of gaseous product and Faradaic efficiency of evolved gas during constant current tests at various current densities. f) In situ electrochemical mass spectrum during chronopotentiometry staircase test of the spontaneous heavy hydrogen generator.

gas evolution, including D_2, H-D, and H_2, is quantified by the water displacement technique, which correlates linearly with the total charge passed, Figure 5.5d. The cumulative Faradaic efficiency for the entire gas evolution is found to be nearly 100% for

all three current densities, Figure 5.5e. Further, the potential output during deuterium evolution is monitored via chronopotentiometry staircase for various current ratings. This behavior is correlated with the corresponding in-situ electrochemical mass spectra of the cathodic half-cell, Figure 5.5f. As evident, an increase in the current rating results in a decline in potential along with a corresponding increase in the rate of D_2 evolution. Interestingly, the device swiftly returns almost to its original voltage plateau on increasing the current rating with a similar trend in the D_2 evolution rate, Figure 5.5f. The durability of this deuterium-generating device has been examined, revealing that it can consistently generate D_2 during prolonged electrolysis for nearly 85 hours under a constant current

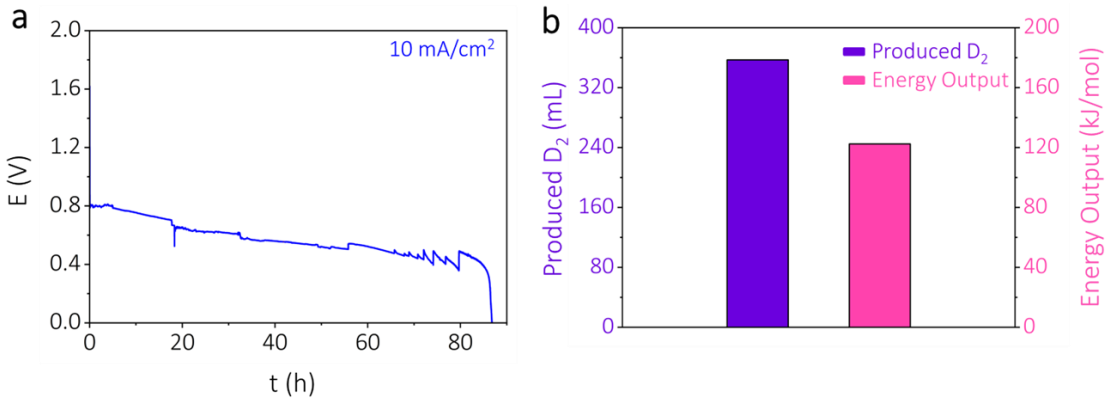

Figure 5.6: a) Long-term durability of the deuterium-generating device for nearly 85 hours at a current rating of 10 mA/cm². b) Quantification of deuterium evolution and electrical energy output for the spontaneous heavy hydrogen generator.

density of 10 mA/cm², Figure 5.6a. The electrical energy output during deuterium evolution has been derived, which turned out to be almost 122.4 kJ per mole D_2, Figure 5.6b, Calculation 5.5.

Calculation 5.5

Electrical energy output calculation from the constant current test at 10 mA

The area under the curve in Figure 5.6a

= 49.6462 V. hour

Energy = Area * current

= 49.6462 * 0.01 A. V. hour

= 49.6462 * 0.01 * 3600 A. V. sec

= 1787.26 W. sec

= 1787.26 J

Amount of evolved D_2 = 14.6 millimoles

Electrical energy output = 122.4 kJ/mol.

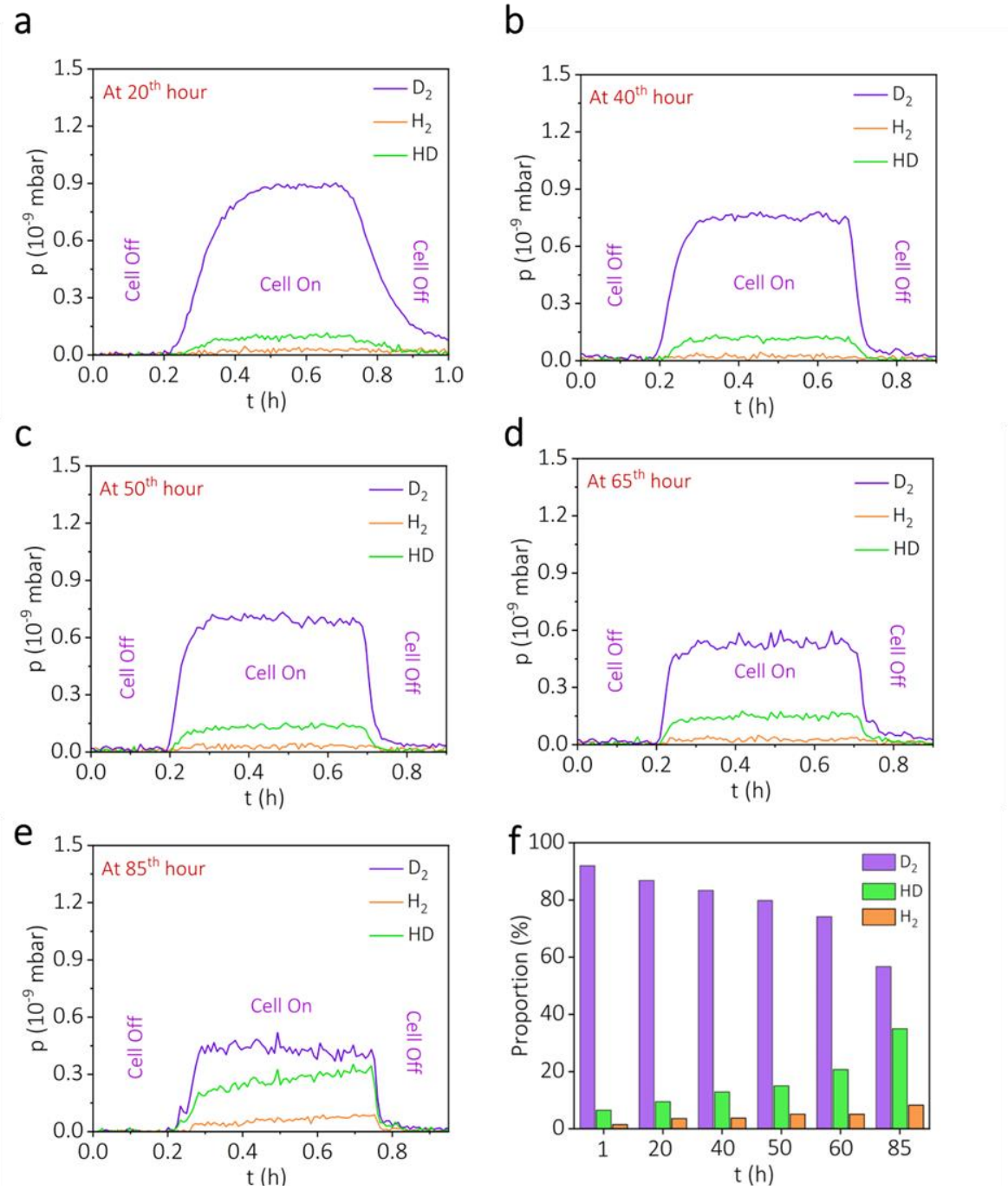

Figure 5.7: In-situ electrochemical mass spectra of the cathodic half-cell in the a) 20th hour, b) 40th hour, c) 50th hour, d) 65th hour, and e) 85th hour of continuous heavy hydrogen generation. (Corresponding to the constant current experiment in Figure 3c) f) The proportions of D_2, HD, H_2 in the cathodic exhaust of the heavy hydrogen generator at various stages of the long-term operation.

The proportion of heavy hydrogen in the cathodic exhaust during the long-term operation was determined by in-situ electrochemical mass spectrometry at various time intervals during the long-term heavy hydrogen evolution, Figure 5.7. The D/H ratio decreases with time as the amount of D_2 decreases with a notable increase in the amount of HD (Figure 5.7f and Calculation 5.6). This may be due to the transport of HOD (both by diffusive and osmotic flux) formed in the anodic half-cell (equation 5.4) to the cathodic half-cell, and its subsequent participation in the cathodic half-cell reaction. This transport will increase during the continuous operation of the device as more and more HOD builds up in the anolyte (equation 5.4). This may explain the increase in the HD content (or decrease in D/H ratio) with respect to time during the long-term heavy hydrogen generation (Figure 5.6a and Figure 5.7f). However, a small amount of HD (nearly 6%) was detected at the very beginning of the long-term experiments (Figure 5.5a and Figure 5.5b), which may be due to slight contamination of the electrolyte with moisture present in the working atmosphere. The cumulative amount of evolved deuterium turned out to be nearly 357 mL. To demonstrate the pragmatic usage of the electrochemical D_2 generator, we have fabricated a laboratory-level spontaneous D_2 generator and connected it in tandem with a D_2 air fuel cell (Figure 5.8). This demonstration validates that the spontaneous electrochemical heavy hydrogen generator can effectively serve as a D_2 reservoir for a D_2 air fuel cell, leveraging its capability to generate electricity during heavy hydrogen generation. In a nutshell, electricity is harnessed along with heavy hydrogen production at the expense of light hydrogen under ambient weather conditions by exploiting the D^+/OD^- dual ion gradient energy.

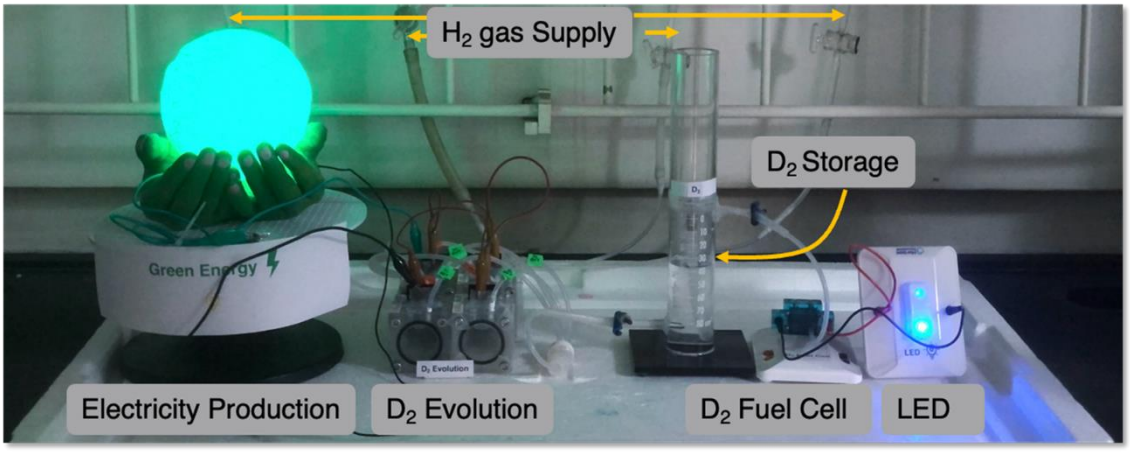

Figure 5.8: Photograph demonstrating the spontaneous electrochemical deuterium generator directly serving as a D_2 reservoir for a D_2 air fuel cell.

Calculation 5.6

From Figure 5.7

At 20th hour, (Figure 5.7a)

The area under the cell on the portion of the violet trace (D_2) = 4.597 * 10^{-10}

The area under the cell on the portion of the green trace (HD) = 5.0325 * 10^{-11}

The area under the cell on the portion of the orange trace (H_2) = 1.913 * 10^{-11}

D_2= 86.86 %

HD = 9.51 %

H_2 = 3.63 %

At 40th hour, (Figure 5.7b)

The area under the cell on the portion of the violet trace (D_2) = 3.648 * 10^{-10}

The area under the cell on the portion of the green trace (HD) = 5.712 * 10^{-11}

The area under the cell on the portion of the orange trace (H_2) = 1.672 * 10^{-11}

D_2 = 83.33 %

HD = 12.91 %

H_2 = 3.76 %

At 50th hour, (Figure 5.7c)

The area under the cell on the portion of the violet trace (D_2) = 3.4835 * 10^{-10}

The area under the cell on the portion of the green trace (HD) = 6.572 * 10^{-11}

The area under the cell on the portion of the orange trace (H_2) = 2.246 * 10^{-11}

D_2 = 79.80 %

HD = 15.05 %

H_2 = 5.15 %

At 65th hour, (Figure 5.7d)

The area under the cell on the portion of the violet trace (D_2) = 2.769 * 10^{-10}

The area under the cell on the portion of the green trace (HD) = 7.744 * 10^{-11}

The area under the cell on the portion of the orange trace (H_2) = 1.913 * 10^{-11}

D_2 = 74.15 %

HD = 20.74 %

H_2 = 5.11 %

At 85th hour, (Figure 5.7e)

The area under the cell on the portion of the violet trace (D_2) = 2.22 * 10^{-10}

The area under the cell on the portion of the green trace (HD) = 1.37 * 10^{-10}

The area under the cell on the portion of the orange trace (H_2) = 3.24 * 10^{-11}

D_2 = 56.8 %

HD = 35 %

H_2 = 8.2 %

5.3 Conclusion

The generation of heavy hydrogen is demonstrated from light hydrogen under ambient weather conditions, accompanied by electrical energy output, by manipulating the OD^-/D^+ dual ion gradient energy. This spontaneous heavy hydrogen generator functions in a thermodynamically downhill manner by decoupling the direct OD^- and D^+ chemistry via an ion-conducting membrane. The laboratory-scale prototype of a heavy hydrogen generator can deliver a peak power density of nearly 45 mW/cm^2 at a current density of nearly 115 mA/cm^2 while generating almost 357 mL of heavy hydrogen with an overall energy output of 122 kJ per mole of D_2 during 85 hours of continuous operation. It is to be noted that continuous device operation leads to the build-up of protium-containing species in the anolyte, which should lead to a decrease in isotope selectivity in the long

run. Therefore, to maintain the purity of heavy hydrogen in the long run, the electrolytes need to be replenished at regular intervals. Nevertheless, the method adopted here presents a unique chemistry for harvesting the energy of the OD^-/D^+ couple as an electrical driving force, even though the OD^- and D^+ combination is a mere non-redox displacement reaction. The energy of this non-redox displacement reaction is harvested as an electrical driving force using a protium redox because the difference between the anodic and cathodic half-cell reaction in a decoupled OD^-/D^+ configuration corresponds to the non-redox reaction taking place in an electrochemical pathway.

5.4 Experimental Section

5.4.1 Materials

Deuterated sulphuric acid (98 % D_2SO_4 in D_2O solution), sodium deuteroxide (40% NaOD in D_2O solution), deuterium oxide (D_2O), sulphuric acid, sodium hydroxide, oxalic acid, and phenolphthalein were procured from Sigma Aldrich. Pt/carbon catalyst (0.5 mg/cm^2 Pt/C) and Nafion117 membrane were bought from Fuel Cell Store (USA).

5.4.2 Electrochemical Study (Single Compartment)

Electrochemical measurements were carried out using a Biologic (VMP-300) electrochemical workstation. The three-electrode system studies were performed via voltammetry experiments in an electrochemical cell of 15 ml. Polycrystalline platinum electrode (0.0176 cm^2) was used as the working electrode, and the platinum disk was used as the counter electrode. Hg/HgO (1 M KOH) reference electrode was used for the experiments in alkaline electrolytes. For acidic electrolytes, the reference electrode was Ag/AgCl (Saturated KCl). We have presented all the experimental results with respect to SHE.

The conversion of Hg/HgO to SHE:

$$E_{SHE} = E_{Hg/HgO} + 0.098\ V$$

The conversion of $Ag/AgCl/Cl^-$ to SHE:

$$E_{SHE} = E_{Ag/AgCl/Cl^-} + 0.197\ V$$

5.4.3 In-situ Electrochemical Mass Spectrometry

In-situ electrochemical mass spectrometry was executed by an HPR-40 (Hiden Analytical) quadruple mass analyzer using a standard QIC inlet. The experiments were performed via a 'T' shaped connector with three sides: a mass spectrometer, an electrochemical cell, and an exhaust to the surroundings, Figure 5.9. Argon (Ar) was the carrier gas for the cathodic half-cell experiments. The generated gas flow from the cell was channeled to mass the spectrometer inlet via the 'T' connector.

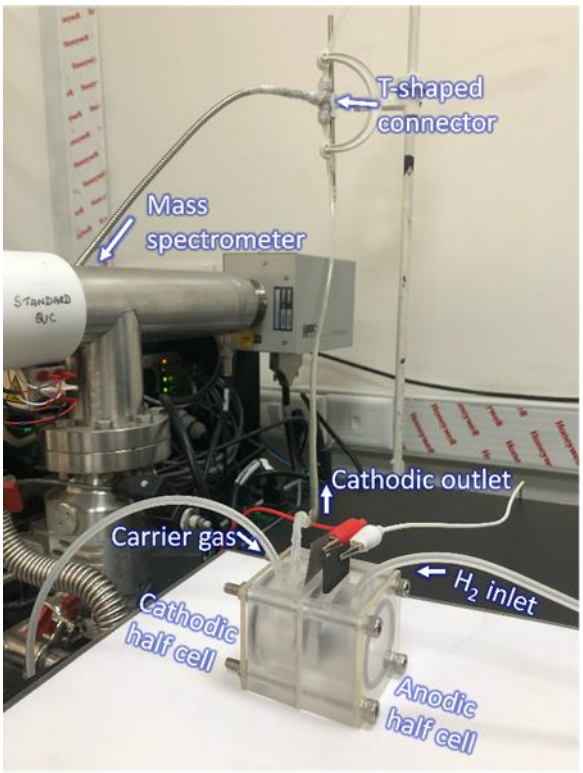

Figure 5.9: Photograph of In situ electrochemical mass spectrometer connected through a T-shaped connector with electrochemical deuterium generator

5.4.4 Electrochemical Study (Double Compartment)

A poly-acrylic sheet-made two-compartment device was forged for electrochemical heavy hydrogen evolution. Nafion 117 membrane was sandwiched between the two half-cells. Before using the membrane, the pretreatment of the Nafion 117 membrane was carried out with a heavy acidic (D_2SO_4/D_2O) solution at 80°C. To eliminate any possible intercompartment leakage, two silicone washer gaskets were placed on the two sides of the membrane. The volume of the acid and alkali used was 3 mL in both the half-cells. The anodic electrocatalysts were Pt/C sheet, and the cathodic electrocatalysts were

electrodeposited Pt on Ti mesh (obtained by applying 5 mA/cm^2 for 10 minutes in chloro-platinic acid solution). All the electrochemical experiments were performed under room temperature and pressure. Quantification of evolved gas was carried out by water displacement technique. Acid-base titration with a phenolphthalein indicator was utilized to estimate the acid and alkali concentrations in the electrolytes. Oxalic acid was used as the primary standard acid. Before and after the electrochemical deuterium evolution, the catholyte and anolyte were collected for exact ion concentration measurement.

5.5 References

(1) Hartogh, P.; Lis, D. C.; Bockelée-Morvan, D.; De Val-Borro, M.; Biver, N.; Küppers, M.; Emprechtinger, M.; Bergin, E. A.; Crovisier, J.; Rengel, M.; Moreno, R.; Szutowicz, S.; Blake, G. A. Nature 2011, **478**, 218–220.

(2) Liu, M.; Zhang, L.; Little, M. A.; Kapil, V.; Ceriotti, M.; Yang, S.; Ding, L.; Holden, D. L.; Balderas-Xicohténcatl, R.; He, D.; Clowes, R.; Chong, S. Y.; Schütz, G.; Chen, L.; Hirscher, M.; Cooper, A. I. Science. 2019, **366**, 613–620.

(3) Miller, A. I. Can. Nucl. Soc. Bull. 2001, **22**, 1–14.

(4) Atzrodt, J.; Derdau, V.; Kerr, W. J.; Reid, M. Angew. Chemie - Int. Ed. 2018, **57**, 3022–3047.

(5) Harbeson, S. L.; Tung, R. D. Elsevier Inc., 2011; Vol. 46.

(6) Ditmire, T.; Zweiback, J.; Yanovsky, V. P.; Cowan, T. E.; Hays, G. Nature 1999, **398**, 489–492.

(7) Di Martino, R. M. C.; Maxwell, B. D.; Pirali, T. Nat. Rev. Drug Discov. 2023, **22**, 562–584.

(8) Lu, L.; Li, H.; Zheng, Y.; Bu, F.; Lei, A. CCS Chem. 2021, **3**, 2669–2675.

(9) Pirali, T.; Serafini, M.; Cargnin, S.; Genazzani, A. A. J. Med. Chem. 2019, **62**, 5276–5297.

(10) Qiu, Y.; Ren, H.; Edwards, M. A.; Gao, R.; Barman, K.; White, H. S. Langmuir 2020, **36**, 6073–6078.

(11) Cai, S.; Bai, T.; Chen, H.; Fang, W.; Xu, Z.; Lai, H.; Huang, T.; Xu, H.; Chu, X.; Ling, J.; Gao, C. J. Phys. Chem. Lett. 2020, **11**, 303–310.

(12) Zhou, X.; Wang, L.; Fan, X.; Wilfong, B.; Liou, S. C.; Wang, Y.; Zheng, H.; Feng, Z.; Wang, C.; Rodriguez, E. E. Chem. Mater. 2020, **32**, 769–775.

(13) Baldwin, J. E.; Gallagher, S. S.; Leber, P. A.; Raghavan, A. S.; Shukla, R. J. Org. Chem. 2004, **69**, 7212–7219.

(14) Krishtalik, L. I. Russ. J. Electrochem. 2000, **36**, 799–80.

(15) Rebollar, L.; Intikhab, S.; Snyder, J. D.; Tang, M. H. J. Phys. Chem. Lett. 2020, **11**, 2308–2313.

(16) Liu, X.; Liu, R.; Qiu, J.; Cheng, X.; Li, G. Angew. Chemie - Int. Ed. 2020, **59**, 13962–13967.

(17) Hagelstein, P. L. J. Condens. Matter Nucl. Sci. 2015, **16**, 46–63.

(18) Zeng, G.; Zeng, H.; Niu, L.; Chen, J.; Song, T.; Zhang, P.; Wu, Y.; Xiao, X.; Zhang, Y.; Huang, S. ChemSusChem 2020, **13**, 2935–2939.

(19) Prodanović, T.; Fields, B. D. Astrophys. J. 2003, **597**, 48–56.

(20) Stilwell, D. E.; Park, K. H.; Miles, M. H. J. Fusion Energy 1990, **9**, 333–336.

(21) Ogawa, R.; Tanii, R.; Dawson, R.; Matsushima, H.; Ueda, M. Energy 2018, **149**, 98–104.

(22) Fleischmann, M.; Pons, S.; Anderson, M. W.; Li, L. J.; Hawkins, M. J. Electroanal. Chem. 1990, **287**, 293–348.

(23) Matsushima, H.; Ogawa, R.; Shibuya, S.; Ueda, M. Materials (Basel). 2017, **10**.

(24) Shibuya, S.; Matsushima, H.; Ueda, M. J. Electrochem. Soc. 2016, **163**, F704–F707.

(25) Junbo, Z.; Kuisheng, W.; Huitang, S.; Shaobo, W. Int. J. Hydrogen Energy 2004, **29**, 1393–1396.

(26) Limbach, H. H.; Klein, O.; Del Amo, J. M. L.; Elguero, J. Zeitschrift fur Phys. Chemie 2004, **218**, 17–49.

(27) Sakaushi, K. J. Electroanal. Chem. 2019, **849**, 113372.

(28) Krishtalik, L. I. Electrochim. Acta 2001, **46**, 2949–2960.

Summary of the thesis entitled "An Electrochemical Neutralization Cell to Harvest the Water Formation Energy"

This chapter provides a summary of thesis and future possibilities of this research. In this thesis, the energy from the water formation reaction is electrochemically captured and utilized as an electromotive force to drive electrochemical processes using an acid-alkali decoupled configuration. Although the water formation reaction is thermodynamically exciting due to its positive entropy change and technologically relevant, the reaction lacks electron transfer because of its non-redox nature. By exploiting the pH-dependent hydrogen redox in an acid-alkali architecture, the water formation energy can be harvested as the electrical driving force. This energy extraction from the water formation reaction can be further enhanced with the introduction of a heat gradient in the water formation cell. The water formation energy is further exploited for a spontaneous hydrogen fuel purification that directly purifies carbonized and contaminated hydrogen streams at room temperature and pressure in a single stage, while simultaneously producing electric power. A laboratory-level prototype successfully purified hydrogen from a quaternary mixture of contaminants, including hydrocarbons, CO_2, and N_2, commonly found in the steam reformer exhaust, with the purified hydrogen directly usable in a commercial proton exchange membrane fuel cell (PEMFC). Conventional hydrogen production methods often yield hydrogen contaminated with impurities like CO and sulfur compounds, which poison fuel cells, while energy-intensive purification methods hinder economic sustainability. The energy of water formation can also enable energy-efficient, single-stepped hydrogen purification to remove poisonous contaminants spontaneously by using poison-resistant electrocatalysts under ambient conditions. In a nutshell, this spontaneous hydrogen fuel purifier in a decoupled acid-alkali architecture showcases a combination of hydrogen generation and utilization in a single device during electricity production with no net loss of hydrogen fuel in the process. In a unique way, the heavy hydrogen can be produced under ambient conditions with simultaneous electrical energy output by utilizing the energy of the heavy water formation energy in a heavy acid-alkali decoupled configuration. This spontaneous heavy hydrogen generator operates in a thermodynamically downhill manner by decoupling OD^- and D^+ chemistry

via an ion-conducting membrane and produces heavy hydrogen at the cost of light hydrogen.

As shown in this thesis, water formation energy has a huge scope in electrochemical energy and conversion devices, however various branches of this promising reaction pathway are still untouched. A water formation harvesting device is an example of a primary battery without a net redox, and its rechargeability still offers an opportunity for a new horizon of secondary batteries.

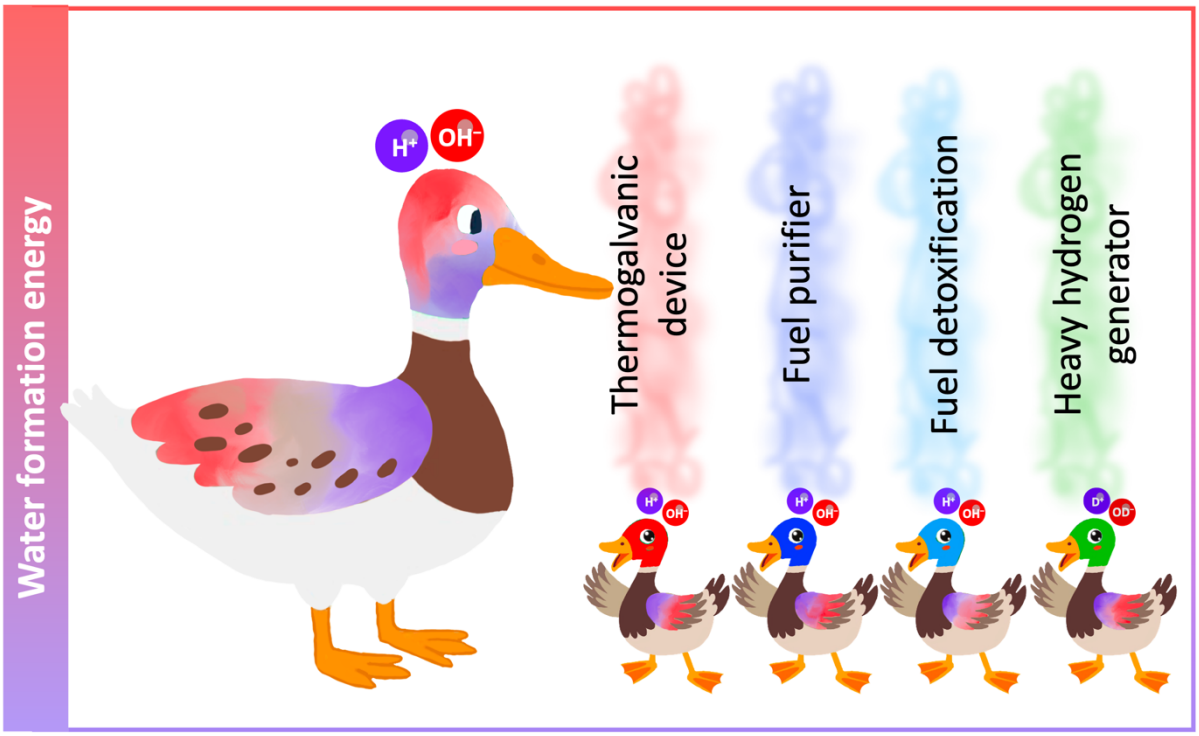

Scheme 6.1: Direct harvesting of water formation energy for hydrogen-based devices.

List of Publications

1. **Mondal, R.**; Thimmappa, R.; Nayak, B.; Dewan, A.; Devendrachari, M. C.; Chen, Q.; Wen, Z.; Thotiyl, M. O. A Spontaneous Hydrogen Fuel Purifier under Truly Ambient Weather Conditions. ***Energy Environ. Sci.*** **2023**, *16* (9), 3860–3872.
2. **Mondal, R.**; Nayak, B.; Ottakam Thotiyl, M. A Spontaneous Heavy Hydrogen Generator via a Protium Redox. ***J. Phys. Chem. Lett.*** **2024**, *15* (26), 6866–6871.
3. Pradhan, H.; **Mondal, R.**; Nayak, B.; Thimmappa, R.; Mendhe, R. M.; Thotiyl, M. O. Unidirectional Competitive Redox Enabled Unsegmented Natural Seawater Splitting for Green Hydrogen Production. ***Green Chem.*** **2025**.
4. Haridas, A.; **Mondal, R**.; Nayak, B.; Ottakam Thotiyl, M. Reductive Inner-Sphere Electrosynthesis of Ammonia via a Nonelectrocatalytic Outer-Sphere Redox. ***Langmuir*** **2024**, *40* (37), 19458-19466.
5. Parmar, M.; Mukhopadhyay, S.; **Mondal, R.**; Nayak, B.; Dargily, N. C.; Nimbegondi Kotresh, H. M.; Vinod, C. P.; Ottakam Thotiyl, M. Synergistic Effects of the Substrate-Ligand Interaction in Metal-Organic Complexes on the de-Electronation Kinetics of a Vitamin C Fuel Cell. ***Dalt. Trans.*** **2024**, *53* (32), 13384–13393.
6. Mendhe, R. M.; **Mondal, R.**; Raja Kottaichamy, A.; Haridas, A.; Kotresh, H. M. N.; Vinod, C. P.; Thimmappa, R.; Ottakam Thotiyl, M. Fuel from Waste: Electrosynthesizing Ammonia Directly from Agricultural Digestate through Ligand Isomerization. ***Green Chem.*** **2024**, *26* (11), 6490–6500.
7. Nayak, B.; **Mondal, R.**; Ottakam Thotiyl, M. Electrostatically Driven Unidirectional Molecular Flux for High Performance Alkaline Flow Batteries. ***Nanoscale*** **2023**, *15* (35), 14468–14475.
8. Sur, S.; **Mondal, R.**; Thimmappa, R.; Mukhopadhyay, S.; Thotiyl, M. O. Aqueous OH−/H+ Dual-Ion Gradient Assisted Electricity Effective Electro-Organic Synthesis of 2,5-Furandicarboxylic Acid Paired with Hydrogen Fuel Generation. ***J. Colloid Interface Sci.*** **2023**, *630*, 477–483.
9. Sur, S.; **Mondal, R.**; Thotiyl, M. O. OH−/H+ Dual-Ion Energy Assisted Electricity Effective Photoelectrochemical Water Splitting. ***J. Photochem. Photobiol.*** **2023**, *16* , 100190.

10. Cai, P.; Chen, K.; Lu, Z.; **Mondal, R.**; Thotiyl, M. O.; Wen, Z. Aqueous OH−/H+ Dual-Ion Zn-Based Batteries. ***ChemSusChem,*** **2022**, e202201034.
11. Amin, I.; Bhat, S. A.; Bhat, M. M.; Sofi, F. A.; Bhat, A. Y.; Ingole, P. P.; **Mondal, R.**; Thotiyl, M. O.; Bhat, M. A. PtxAg100−x Nano-Alloy Decorated N-Doped Reduced Graphene Oxide: A Promising Electrocatalyst for Direct Urea Fuel Cells. ***New J. Chem.*** **2023**, *47* (48), 22146–22156.

Rights and permission

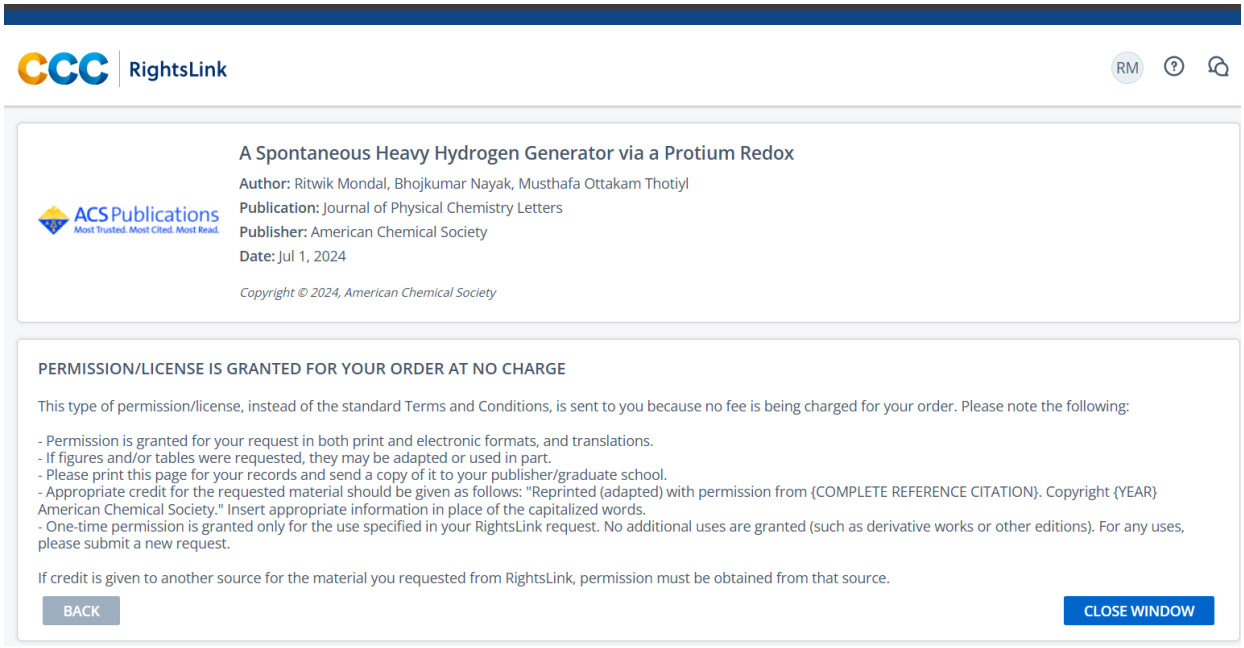

RightsLink

RM

ACS Publications
Most Trusted. Most Cited. Most Read.

A Spontaneous Heavy Hydrogen Generator via a Protium Redox

Author: Ritwik Mondal, Bhojkumar Nayak, Musthafa Ottakam Thotiyl
Publication: Journal of Physical Chemistry Letters
Publisher: American Chemical Society
Date: Jul 1, 2024

Copyright © 2024, American Chemical Society

PERMISSION/LICENSE IS GRANTED FOR YOUR ORDER AT NO CHARGE

This type of permission/license, instead of the standard Terms and Conditions, is sent to you because no fee is being charged for your order. Please note the following:

- Permission is granted for your request in both print and electronic formats, and translations.
- If figures and/or tables were requested, they may be adapted or used in part.
- Please print this page for your records and send a copy of it to your publisher/graduate school.
- Appropriate credit for the requested material should be given as follows: "Reprinted (adapted) with permission from {COMPLETE REFERENCE CITATION}. Copyright {YEAR} American Chemical Society." Insert appropriate information in place of the capitalized words.
- One-time permission is granted only for the use specified in your RightsLink request. No additional uses are granted (such as derivative works or other editions). For any uses, please submit a new request.

If credit is given to another source for the material you requested from RightsLink, permission must be obtained from that source.

BACK

CLOSE WINDOW